State of the Global Climate 2021

WEATHER CLIMATE WATER

WORLD METEOROLOGICAL ORGANIZATION

WMO-No. 1290

WMO-No. 1290

Chair, Publications Board
World Meteorological Organization (WMO)
7 bis, avenue de la Paix
P.O. Box 2300
CH-1211 Geneva 2, Switzerland

Tel.: +41 (0) 22 730 84 03
Fax: +41 (0) 22 730 81 17
Email: publications@wmo.int

ISBN 978-92-63-11290-3

Cover illustration from Adobe Stock: Icebergs (Photo credits: z576); Forest fires, red and orange forest fires at night in the dry season (Photo credits: prirach); Shallow Coral Reef and Island in Raja Ampat (Photo credits: ead72); Flooded terrain in lowlend of Great river (Photo credits: Vladimir Melnikov). iSTOCK: Terre de sécheresse au coucher du soleil. Ciel dramatique de désert. changement climatique (Photo credits: mycola).

Contents

Key messages

The global mean temperature in 2021 was around 1.11 ± 0.13 °C above the 1850–1900 pre-industrial average. This is less warm than some recent years due to the influence of La Niña conditions at the start and end of the year. The most recent seven years, 2015 to 2021, were the seven warmest years on record.

Global mean sea level reached a new record high in 2021, rising an average of 4.5 mm per year over the period 2013–2021.

The Antarctic ozone hole reached a maximum area of 24.8 million km^2 in 2021. This unusually deep and large ozone hole was driven by a strong and stable polar vortex and colder-than-average conditions in the lower stratosphere.

Greenland experienced an exceptional mid-August melt event and the first-ever recorded rainfall at Summit Station, the highest point on the Greenland ice sheet at an altitude of 3 216 m.

Exceptional heatwaves broke records across western North America and the Mediterranean. Death Valley, California reached 54.4 °C on 9 July, equalling a similar 2020 value as the highest recorded in the world since at least the 1930s, and Syracuse in Sicily reached 48.8 °C.

Hurricane *Ida* was the most significant of the North Atlantic season, making landfall in Louisiana on 29 August, equalling the strongest landfall on record for the state, with economic losses in the United States estimated at US$ 75 billion.

Deadly and costly flooding induced economic losses of US$ 17.7 billion in Henan province of China, and Western Europe experienced some of its most severe flooding on record in mid-July. This event was associated with economic losses in Germany exceeding US$ 20 billion.

Drought affected many parts of the world, including areas in Canada, United States, Islamic Republic of Iran, Afghanistan, Pakistan, Turkey and Turkmenistan. In Canada, severe drought led to forecast wheat and canola crop production levels being 35%–40% below 2020 levels, while in the United States, the level of Lake Mead on the Colorado River fell in July to 47 m below full supply level, the lowest level on record.

The compounded effects of conflict, extreme weather events and economic shocks, further exacerbated by the COVID-19 pandemic, undermined decades of progress towards improving food security globally.

Hydro-meteorological hazards continued to contribute to internal displacement. The countries with the highest numbers of displacements recorded as of October 2021 were China (more than 1.4 million), Viet Nam (more than 664 000) and the Philippines (more than 600 000).

Foreword

The release of the World Meteorological Organization *State of the Global Climate 2021* report comes a few months after the release of the Working Group I, II and III contributions to the Sixth Assessment Report of the Intergovernmental Panel on Climate Change (IPCC). The present WMO report provides an update on the annual state of the climate observed in the year 2021, and shows continued trends (also reported in the IPCC reports) in terms of key indicators. These include concentrations of greenhouse gases, global annual mean surface temperature, global mean sea level, ocean heat content, ocean acidification, sea-ice extent and changes in mass of the ice sheets and glaciers. While the key indicators show that climate continues to change, information on socioeconomic impacts highlights the vulnerability of populations to current weather and climate events. Loss and damages of more than US$ 100 billion, as well as severe impacts on food security and humanitarian aspects due to high-impact weather and climate events have been reported.

The increase in atmospheric concentration of CO_2 from 2019 to 2020 was slightly lower than that observed from 2018 to 2019, but higher than the average annual growth rate over the last decade. This is despite a decrease in fossil fuel CO_2 emissions of approximately 5.6% in 2020 due to restrictions related to the COVID-19 pandemic.

Stabilizing global mean temperature at 1.5 °C to 2 °C above pre-industrial (1850–1900) levels by the end of this century will require an ambitious reduction of greenhouse gas emissions, which must accelerate during this decade.

Early warning systems are critically required across sectors for climate adaptation. However, less than half the Members report having early warning systems in place. WMO and its Members are working closely to substantially improve this situation in the near future.

I take this opportunity to congratulate the experts and the lead author, who compiled this report using physical data analyses and impact assessments. I thank all the contributors, particularly WMO Member National Meteorological and Hydrological Services and Regional Climate Centres and United Nations agencies, for their collaboration and input. The present report is intended to help our organizations to update world leaders and citizens on the latest information about the state of the Earth system, the weather and climate conditions in 2021, and the impacts of weather and climate events. WMO remains committed to supporting this publication and communicating it widely for this purpose.

(Prof. Petteri Taalas)
Secretary-General

Global climate indicators

Global climate indicators[1] provide a broad view of climate change at a global scale, encompassing the composition of the atmosphere, energy changes, and the response of the land, ocean and ice. These indicators are closely interrelated. For example, the rise in CO_2 and other greenhouse gases in the atmosphere leads to an imbalance of energy and thus warming of the atmosphere and ocean. Warming of the ocean in turn leads to rising sea levels, to which is added the melting of ice on land in response to increasing atmospheric temperatures. The global indicators draw on a wide range of data sets that are listed at the end of the present report and which are based on multiple observing systems (see Observational basis for climate monitoring). Together, the indicators build a consistent picture of a warming world that touches all parts of the Earth system.

The connections between global climate indicators and the Sustainable Development Goals were highlighted in *Climate Indicators and Sustainable Development: Demonstrating the Interconnections* (WMO-No. 1271). That report traces the links and feedback loops among the key climate indicators as a physical system and the cascading risks to most of the 17 Sustainable Development Goals. Monitoring the global climate indicators, as well as their related risks and impacts, is therefore of critical importance for achieving the Sustainable Development Goals by 2030.

BASELINES

Baselines are specific periods, usually spanning one or more decades, that are used as a fixed period against which current conditions can be compared. A variety of baselines are used in this report, and these are specified in the text and figures where appropriate.

Where possible, the WMO climatological standard normal, 1981–2010, is used as a baseline for consistent reporting.[2] For some indicators, however, it is not possible to use this baseline, due to either a lack of measurement during the whole period, or because a longer period is needed to calculate representative statistics.

There are two notable exceptions. Firstly, for global mean temperature, a baseline of 1850–1900 is used. This is the baseline used in recent IPCC reports (Sixth Assessment Report,[3] Special Report: Global Warming of 1.5 °C[4]) as a reference period for pre-industrial temperatures, and is relevant for understanding progress relative to the goal of the Paris Agreement. Secondly, for greenhouse gases, atmospheric concentrations can be estimated much further back in time, using gas bubbles trapped in ice cores. The year 1750 is therefore used in this report to represent pre-industrial greenhouse gas concentrations.

GREENHOUSE GASES

Atmospheric concentrations of greenhouse gases reflect a balance between emissions from human activities, natural sources, and sinks in the biosphere and ocean. Increasing levels of greenhouse gases in the atmosphere due to human activities have been the major driver of climate change since the mid-twentieth century. Global average mole fractions of greenhouse gases are calculated from in situ observations made at multiple sites in the Global Atmosphere Watch (GAW) Programme of WMO and partner networks.

---

[1] Trewin, B.; Cazenave, A.; Howell, S. et al. Headline Indicators for Global Climate Monitoring, *Bulletin of the American Meteorological Society* **2021**, *102* (1), E20–E37. https://journals.ametsoc.org/view/journals/bams/102/1/BAMS-D-19-0196.1.xml.

[2] 1981–2010 is used in preference to 1991–2020, for consistency with climate reports from WMO Members, not all of whom have yet transitioned to using the more recent period.

[3] Intergovernmental Panel on Climate Change (IPCC), 2021: *AR6 Climate Change 2021: The Physical Science Basis*, https://www.ipcc.ch/report/ar6/wg1/.

[4] Intergovernmental Panel on Climate Change (IPCC), 2018: *IPCC Special Report: Global Warming of 1.5 °C*, https://www.ipcc.ch/sr15/.

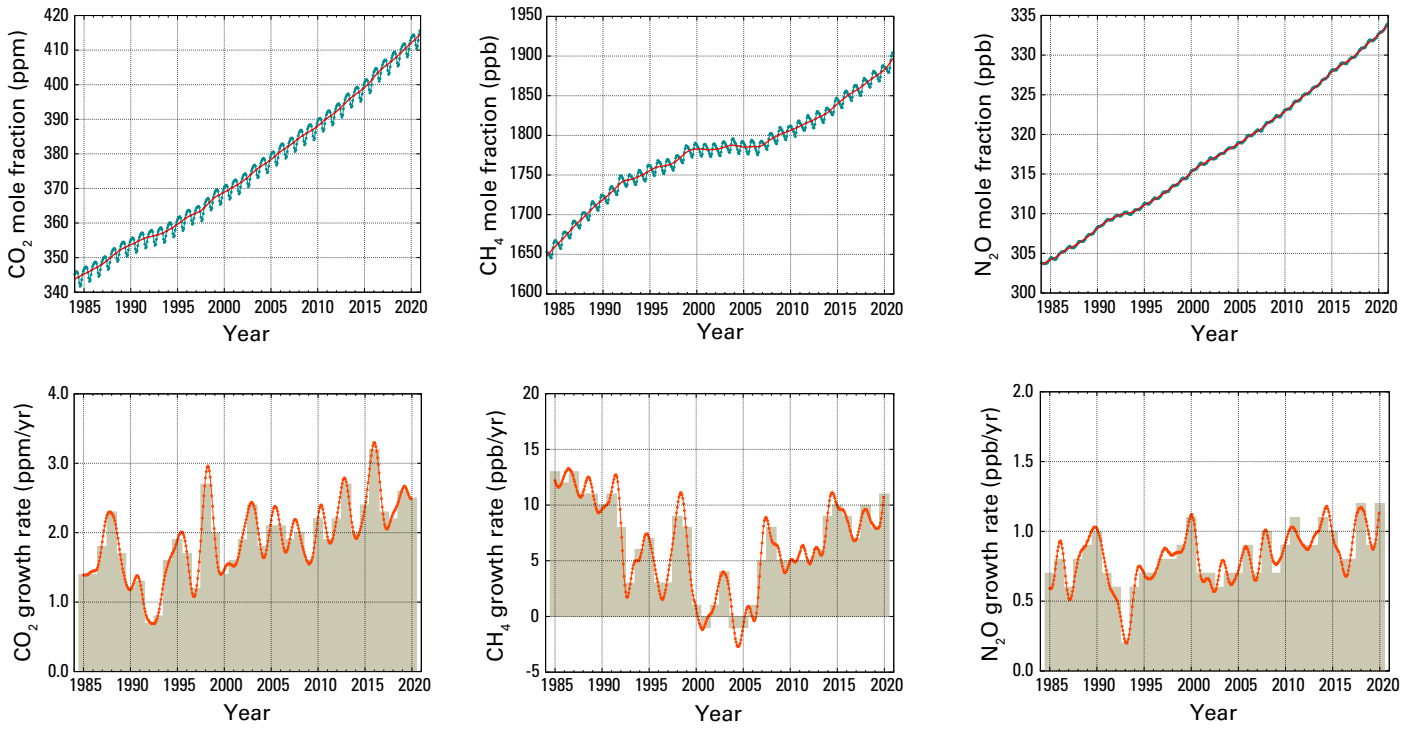

In 2020, greenhouse gas mole fractions reached new highs, with globally averaged surface mole fractions of carbon dioxide (CO_2) at 413.2 ± 0.2 parts per million (ppm), methane (CH_4) at 1889 ± 2 parts per billion (ppb) and nitrous oxide (N_2O) at 333.2 ± 0.1 ppb, respectively 149%, 262% and 123% of pre-industrial (1750) levels (Figure 1). The increase in atmospheric concentration in CO_2 from 2019 to 2020 was slightly lower than that observed from 2018 to 2019, but higher than the average annual growth rate over the last decade. This is despite a decrease in fossil fuel CO_2 emissions of approximately 5.6% in 2020 due to restrictions related to the COVID-19 pandemic.[5] For CH_4 and N_2O, the increase from 2019 to 2020 was higher than that observed from 2018 to 2019 and also higher than the average annual growth rate over the last decade.

Real-time data from specific locations, including Mauna Loa (Hawaii) and Cape Grim (Tasmania) indicate that levels of CO_2, CH_4 and N_2O continued to increase in 2021.

Atmospheric methane (CH_4) increase is an issue of concern because it is not only a powerful greenhouse gas, but it is also a precursor of tropospheric ozone, with implications for human health, agriculture and ecosystems.[6] The mean annual increase of CH_4 decreased from approximately 12 ppb per year during the late 1980s to nearly zero between 1999 and 2006. Since 2007, atmospheric CH_4 has been increasing, and in 2020 it increased by 11 ppb over 2019 levels. Studies using GAW CH_4 measurements indicate that increased CH_4 emissions from wetlands in the tropics and from anthropogenic sources at the mid-latitudes of the northern hemisphere are the likely causes of this recent increase.[7] These studies have also pointed to the short-term climate benefits and cost-effectiveness of mitigating CH_4 emissions. Such mitigation measures were presented in the United Nations Environment Programme (UNEP) methane assessment[8] and address major emitting sectors, namely oil and gas, agriculture and waste management.

Figure 1. Top row: Globally averaged mole fraction (measure of concentration), from 1984 to 2020, of CO_2 in parts per million (left), CH_4 in parts per billion (centre) and N_2O in parts per billion (right). The red line is the monthly mean mole fraction with the seasonal variations removed; the blue dots and line show the monthly averages. Bottom row: The growth rates representing increases in successive annual means of mole fractions are shown as grey columns for CO_2 in parts per million per year (left), CH_4 in parts per billion per year (centre) and N_2O in parts per billion per year (right). *Source:* WMO Global Atmosphere Watch.

[5] https://public.wmo.int/en/resources/united_in_science; https://library.wmo.int/index.php?lvl=notice_display&id=21946

[6] https://www.unep.org/resources/report/global-methane-assessment-benefits-and-costs-mitigating-methane-emissions

[7] Nisbet, E. G.; Manning, M. R.; Dlugokencky, E. J. et al. Very Strong Atmospheric Methane Growth in the 4 Years 2014–2017: Implications for the Paris Agreement. *Global Biogeochemical Cycles* **2019**, *33* (3), 318–342. https://doi.org/10.1029/2018GB006009.

[8] https://www.unep.org/resources/report/global-methane-assessment-benefits-and-costs-mitigating-methane-emissions

TEMPERATURE

The global mean temperature in 2021 was 1.11 ± 0.13 °C above the 1850–1900 average (Figure 2). The six data sets used in the analysis (see Global temperature data) place 2021 between the fifth and seventh warmest year on record globally, and all six show that the most recent seven years, 2015 to 2021, were the seven warmest years on record.

The year 2021 was less warm than some recent years due to the influence of moderate La Niña events at the start and end of the year, known as a "double-dip" La Niña (see Drivers of short-term variability). La Niña has a temporary cooling effect on the global mean temperature, which is strongest in the year following an event. Aside from the weak La Niña of 2018, the last significant La Niña event was in 2011. The year 2021 was around 0.22 °C to 0.29 °C warmer than 2011. The year 2016, which started during a strong El Niño, remains the warmest year on record in most of the data sets surveyed.

The method for calculating global temperature anomalies relative to the 1850–1900 baseline has been updated from previous state of the global climate reports. The new method uses the assessment of temperature change and its uncertainties from the IPCC Sixth Assessment Report as a foundation for estimating changes since 1850–1900. Details are given in the section on Global temperature data.

In the IPCC Sixth Assessment Report, Summary for Policymakers,[9] temperature crossing points – the point at which long-term warming exceeds a particular level – were assessed using a 20-year average centred on the crossing point. For the period 2001–2020, the average was estimated[10] to be 0.99 [0.84–1.10] °C. The provisional 20-year average for the period 2002–2021, based on

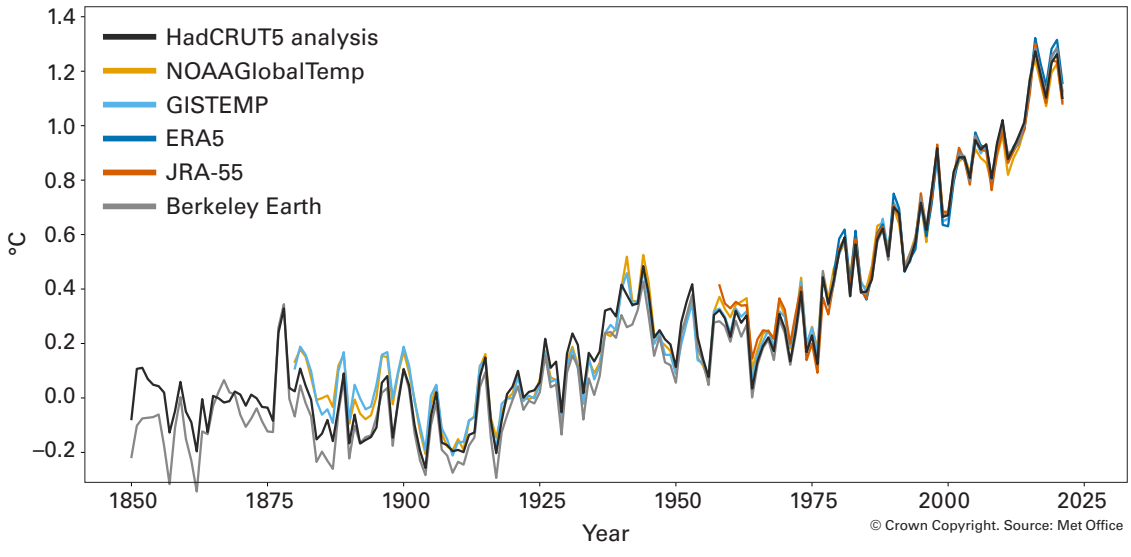

Figure 2. Global annual mean temperature difference from pre-industrial conditions (1850–1900) for six global temperature data sets (1850–2021). For details of the data sets and processing see Data sets and methods. *Source:* Met Office, United Kingdom of Great Britain and Northern Ireland.

[9] Intergovernmental Panel on Climate Change (IPCC), 2021: Summary for Policymakers. In: *AR6 Climate Change 2021: The Physical Science Basis*, https://www.ipcc.ch/report/ar6/wg1/downloads/report/IPCC_AR6_WGI_SPM_final.pdf.

[10] Intergovernmental Panel on Climate Change (IPCC), 2021: Summary for Policymakers, A.1.2. In: *AR6 Climate Change 2021: The Physical Science Basis*, https://www.ipcc.ch/report/ar6/wg1/downloads/report/IPCC_AR6_WGI_SPM_final.pdf. The IPCC average was based on four data sets: HadCRUT5, NOAAGlobalTemp—Interim, Berkeley Earth and Kadow, C.; Hall, D. M.; Ulbrich, U. Artificial Intelligence Reconstructs Missing Climate Information. *Nature Geoscience* **2020**, *13* (6), 408–413. https://doi.org/10.1038/s41561-020-0582-5. Bracketed values indicate the 5%–95% confidence range.

the average of the six data sets used in the present report, was 1.01 ± 0.12 °C above the 1850–1900 average.

Near-surface temperatures in 2021 were above the 1981–2010 average across a broad swath of North America and Greenland, Northern and Tropical Africa, the Middle East and Southern Asia (Figure 3). Areas with below-average temperatures included parts of Northern Asia, Australia, Southern Africa and North-west North America. The imprint of La Niña can clearly be seen in the Tropical Pacific. Cooler conditions in Southern Africa, India, and eastern Australia are characteristic of La Niña. The cooler-than-average area in Northern Asia stands in contrast to 2020, which saw exceptionally high temperatures in the region. This is partly associated with the different phases of the Arctic Oscillation in early 2020 (strongly positive) and early 2021 (strongly negative, see the section on Arctic Oscillation (AO)), which had an imprint on the average for the whole year.

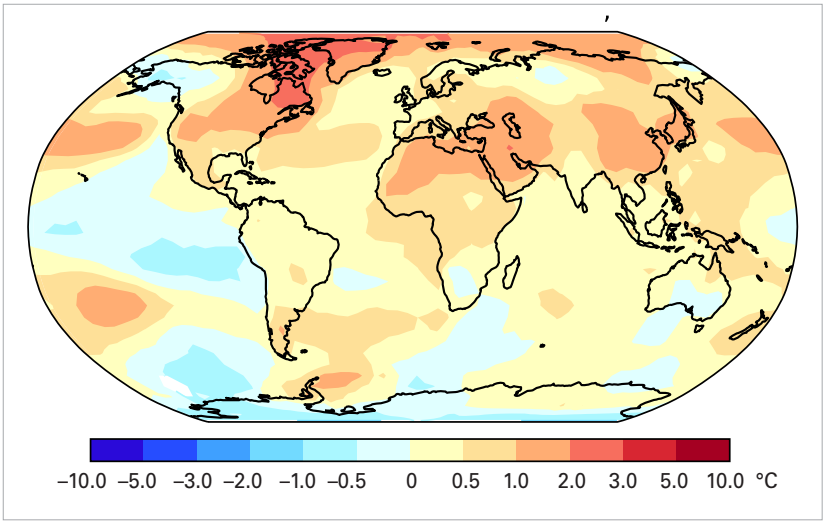

Figure 3. Near-surface temperature differences relative to the 1981–2010 average for 2021. The map shows the median anomaly calculated from five data sets: HadCRUT5, ERA5, GISTEMP, NOAAGlobalTemp and Berkeley Earth. *Source:* Met Office, United Kingdom.

OCEAN

Most of the excess energy that accumulates in the Earth system due to increasing concentrations of greenhouse gases is taken up by the ocean. The added energy warms the ocean, and the consequent thermal expansion of the water leads to sea-level rise, to which is added melting land ice. The surface layers of the ocean have warmed more rapidly than the interior, mirrored in the rise of global mean sea-surface temperature and in the increased incidence of marine heatwaves. As the concentration of CO_2 in the atmosphere increases, so too does the concentration of CO_2 in the ocean. This affects ocean chemistry, lowering the average pH of the water, a process known as ocean acidification. All these changes have a broad range of impacts and interactions[11] in the ocean and coastal areas.

OCEAN HEAT CONTENT

Increasing human emissions of CO_2 and other greenhouse gases cause a positive radiative imbalance at the top of the atmosphere – the Earth energy imbalance (EEI) – leading to an accumulation of energy in the form of heat in the Earth system which is driving global warming.[12,13,14] Around 90% of this accumulated heat in the Earth system is stored in the ocean, which is measured through ocean heat content (OHC). A positive EEI signals that the Earth's climate system is still responding to the current forcing[15] and that more warming will occur even if the forcing does not increase further.[16] This in turn is reflected in a continued increase of

[11] Gruber, N.; Boyd, P. W.; Frölicher, T. L. et al. Biogeochemical extremes and compound events in the ocean. *Nature* **2021**, *600*, 395–407. https://doi.org/10.1038/s41586-021-03981-7.

[12] Hansen, J.; Sato, M.; Kharecha, P. et al. Earth's energy imbalance and implications. *Atmospheric Chemistry and Physics* **2011**, *11* (24), 13421–13449. https://doi.org/10.5194/acp-11-13421-2011.

[13] Intergovernmental Panel on Climate Change (IPCC), 2013: *Climate change 2013: The physical science basis*, Chapter 3, https://www.ipcc.ch/report/ar5/wg1/.

[14] von Schuckmann, K.; Palmer, M. D.; Trenberth, K. E. et al. An imperative to monitor Earth's energy imbalance. *Nature Climate Change* **2016**, *6*, 138–144. https://doi.org/10.1038/nclimate2876.

[15] Hansen, J.; Nazarenko, L.; Ruedy, R. et al. Earth's Energy Imbalance: Confirmation and Implications. *Science* **2005**, *308* (5727), 1431–1435. https://doi.org/10.1126/science.1110252.

[16] Hansen, J.; Sato, M.; Kharecha, P. et al. Young people's burden: requirement of negative CO_2 emissions. *Earth System Dynamics* **2017**, *8* (3), 577–616. https://doi.org/10.5194/esd-8-577-2017.

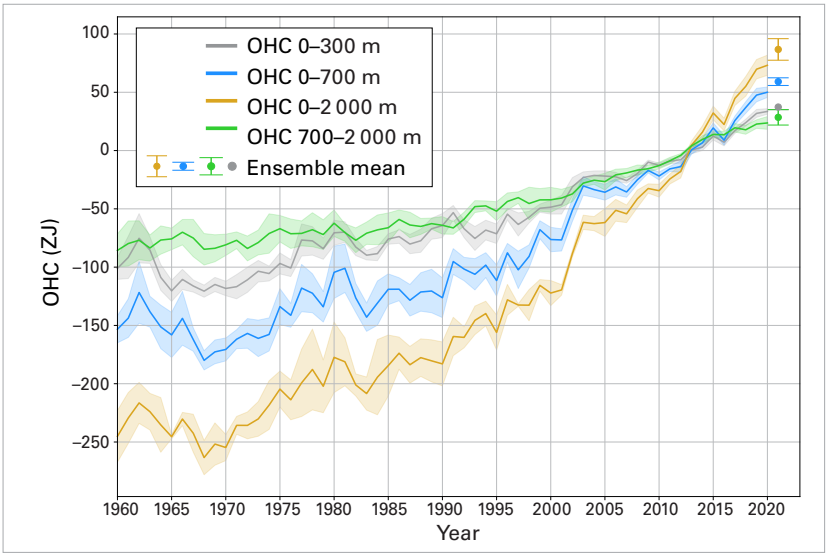

Figure 4. 1960–2021 ensemble mean time series and ensemble standard deviation (2 standard deviations, shaded) of global OHC anomalies relative to the 2005–2017 average for the 0–300 m (grey), 0–700 m (blue), 0–2 000 m (yellow) and 700–2 000 m (green) depth layers. The ensemble mean is an update of the outcome of a concerted international data and analysis effort (see footnote 24), and all products used are referenced in the section on Ocean heat content data. Note that values are given for the ocean surface area between 60°S and 60°N and limited to the 300 m bathymetry of each product. The ensemble-mean OHC (0–2 000 m) anomalies for 2021 have been added as separate points, together with the ensemble spread, and are based on the four products listed in Ocean heat content data. *Source:* Updated from von Schuckmann et al., 2016 (see footnote 22).

ocean heat content. The IPCC concluded that it is unequivocal that human influence has warmed the atmosphere, ocean and land, and that it is extremely likely that human influence was the main driver of the ocean heat increase observed since the 1970s.[17]

Historical measurements of subsurface temperature back to the 1940s mostly rely on shipboard measurement systems, which constrain the availability of subsurface temperature observations at a global scale and at depth.[18] With the deployment of the Argo network of autonomous profiling floats, which first achieved its target near-global coverage in 2006, it is now possible to routinely measure OHC changes down to a depth of 2 000 m.[19,20]

Various research groups have developed estimates of global OHC, and all results show continued ocean warming (Figure 4). Differences between the estimates at annual to decadal scale arise from the various statistical treatments of data gaps, the choice of climatology and the approach used to account for instrumental biases.[21,22,23] A concerted effort has been established to provide an international view on the global evolution of ocean warming up to the year 2021.[24]

The upper 2 000 m depth of the ocean continued to warm in 2021 and it is expected that it will continue to warm in the future – a change which is irreversible on centennial to millennial timescales.[25,26] The ocean heat content in 2021 was the highest on record, exceeding the 2020 value by 14 ± 9 ZJ (Figure 4). All data sets agree that ocean warming rates show a particularly strong increase in the past two decades. Ocean warming rates for the 0–2 000 m depth layer (relative to the ocean surface) reached 1.0 (0.6) ± 0.1 W m^{-2}

[17] Intergovernmental Panel on Climate Change (IPCC), 2021: Summary for Policymakers. In: *AR6 Climate Change 2021: The Physical Science Basis*, https://www.ipcc.ch/report/ar6/wg1/downloads/report/IPCC_AR6_WGI_SPM_final.pdf.

[18] Abraham, J. P.; Barlinger, M.; Bindoff, N. L. et al. A review of global ocean temperature observations: Implications for ocean heat content estimates and climate change. *Reviews of Geophysics* **2013**, *51* (3), 450–483. https://doi.org/10.1002/rog.20022.

[19] Riser, S. C.; Freeland, H. J.; Roemmich, D. et al. Fifteen years of ocean observations with the global Argo array. *Nature Climate Change* **2016**, *6* (2), 145–153. https://doi.org/10.1038/nclimate2872.

[20] Roemmich, D.; Alford, M. H.; Claustre, H. et al. On the Future of Argo: A Global, Full-Depth, Multi-Disciplinary Array. *Frontiers in Marine Science* **2019**, *6*, 439. https://www.frontiersin.org/article/10.3389/fmars.2019.00439.

[21] Boyer, T.; Domingues, C. M.; Good, S. A. et al. Sensitivity of Global Upper-Ocean Heat Content Estimates to Mapping Methods, XBT Bias Corrections, and Baseline Climatologies. *Journal of Climate* **2016**, *29* (13), 4817–4842. https://doi.org/10.1175/JCLI-D-15-0801.1.

[22] von Schuckmann, K.; Palmer, M. D.; Trenberth, K. E. et al. An imperative to monitor Earth's energy imbalance. *Nature Climate Change* **2016**, *6*, 138–144. https://doi.org/10.1038/nclimate2876.

[23] Cheng, L.; Abraham, J.; Goni, G. et al. XBT Science: Assessment of Instrumental Biases and Errors. *Bulletin of the American Meteorological Society* **2016**, *97* (6), 924–933. https://journals.ametsoc.org/view/journals/bams/97/6/bams-d-15-00031.1.xml.

[24] von Schuckmann, K.; Cheng, L.; Palmer, M. D. et al. Heat stored in the Earth system: where does the energy go? *Earth System Science Data* **2020**, *12* (3), 2013–2041. https://doi.org/10.5194/essd-12-2013-2020.

[25] Intergovernmental Panel on Climate Change (IPCC), 2021: Summary for Policymakers. In: *AR6 Climate Change 2021: The Physical Science Basis*, https://www.ipcc.ch/report/ar6/wg1/downloads/report/IPCC_AR6_WGI_SPM_final.pdf.

[26] Intergovernmental Panel on Climate Change (IPCC), 2019: Summary for Policymakers. In: *IPCC Special Report on the Ocean and Cryosphere in a Changing Climate*, https://www.ipcc.ch/site/assets/uploads/sites/3/2022/03/01_SROCC_SPM_FINAL.pdf.

over the period 2006–2021 (1971–2021). For comparison, the values for the upper 700 m depth amount to 0.7 (0.4) ± 0.1 W m^{-2} over the period 2006–2021 (1971–2021). Below the 2 000 m depth, the ocean also warmed, albeit at the lower rate[27] of 0.07 ± 0.04 W m^{-2}.

SEA LEVEL

Global mean sea level (GMSL) integrates changes occurring in many components of the climate system. On interannual to multidecadal time scales, changes to GMSL result from ocean warming via thermal expansion of sea water, melting of land ice and exchange of water with water bodies on land. Measured since the early 1990s by high-precision altimeter satellites, the GMSL rose by 2.1 mm per year between 1993 and 2002, and by 4.5 mm per year between 2013 and 2021, an increase by a factor of two between the periods, mostly due to the accelerated loss of ice mass from the ice sheets.[28] In 2021, GMSL reached a new record high. Compared to previous El Niño and La Niña years (for example, in 1997/1998, 2010/2011, 2015/2016), during which the GMSL displayed temporary positive or negative anomalies of several millimetres, 2021 was marked by an increase of the GMSL that was close to the long-term trend (Figure 5).

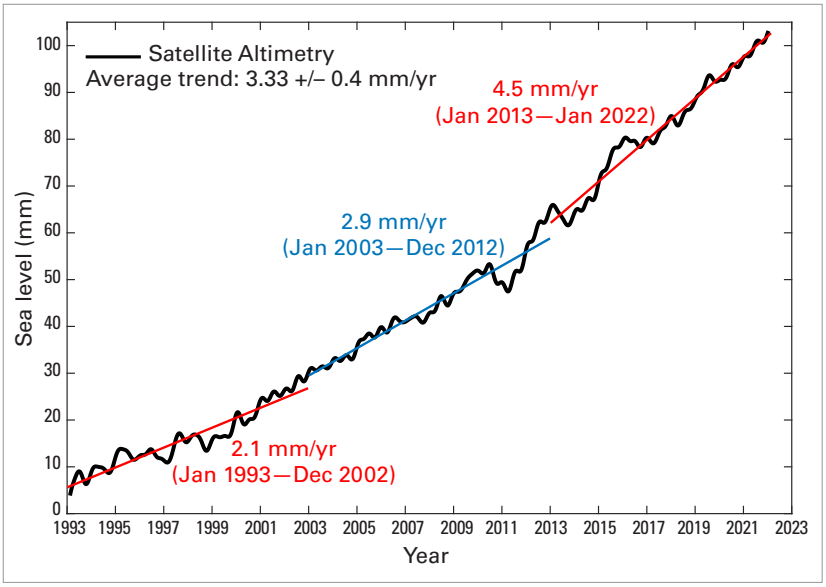

Although sea level has risen almost everywhere since 1993, it has not risen equally everywhere. Regional patterns of sea-level change are dominated by local changes in ocean heat content and salinity. Several regions continue to be affected by a rate of sea-level rise substantially faster than the global mean (see Figure 6, which shows the difference between local and global sea level). This is particularly the case in the western Tropical Pacific, the South-west Pacific, the North Pacific, the South-west Indian Ocean and the South Atlantic. In other regions, local

Figure 5. Global mean sea level evolution from January 1993 to January 2022 (black curve) based on high-precision satellite altimetry. The coloured straight lines represent the average linear trend over three successive time spans (January 1993 to December 2002; January 2003 to December 2012; January 2013 to January 2022). *Source:* AVISO altimetry (https://www.aviso.altimetry.fr).

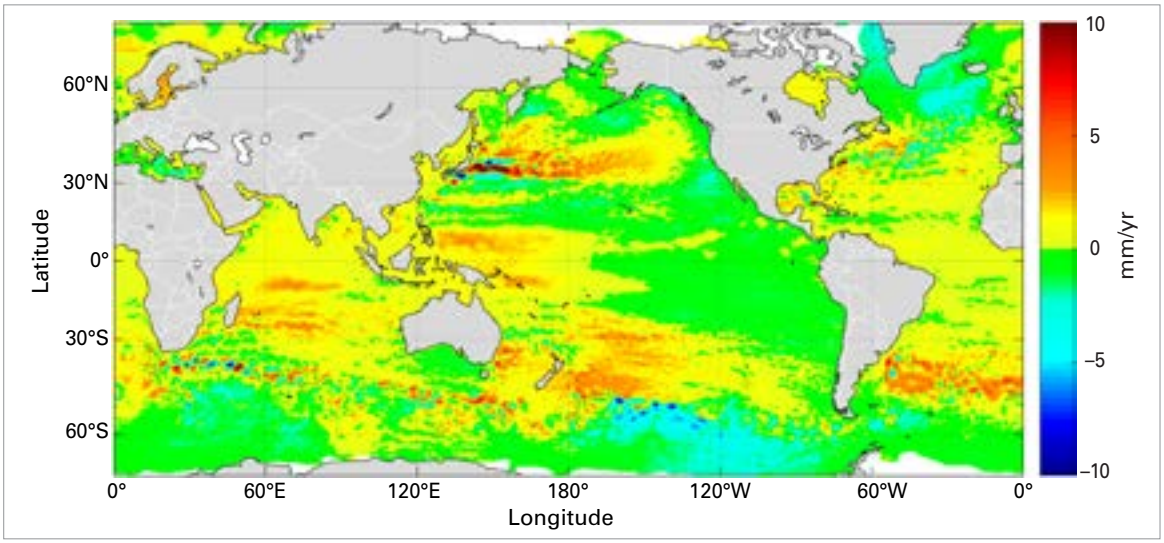

Figure 6. Regional trend patterns in sea level **after the global mean trend has been removed** (mm/yr), from 1993 to 2020, based on satellite altimetry. Note that the actual sea level has increased almost everywhere. *Source:* Copernicus Climate Change Service (https://climate.copernicus.eu).

[27] Update from Purkey, S. G.; Johnson, G. C. Warming of Global Abyssal and Deep Southern Ocean Waters between the 1990s and 2000s: Contributions to Global Heat and Sea Level Rise Budgets. *Journal of Climate* **2010**, *23*, 6336–6351. https://doi.org/10.1175/2010JCLI3682.1.

[28] WCRP Global Sea Level Budget Group. Global sea-level budget 1993–present. *Earth System Science Data* **2018**, *10* (3), 1551–1590, https://doi.org/10.5194/essd-10-1551-2018.

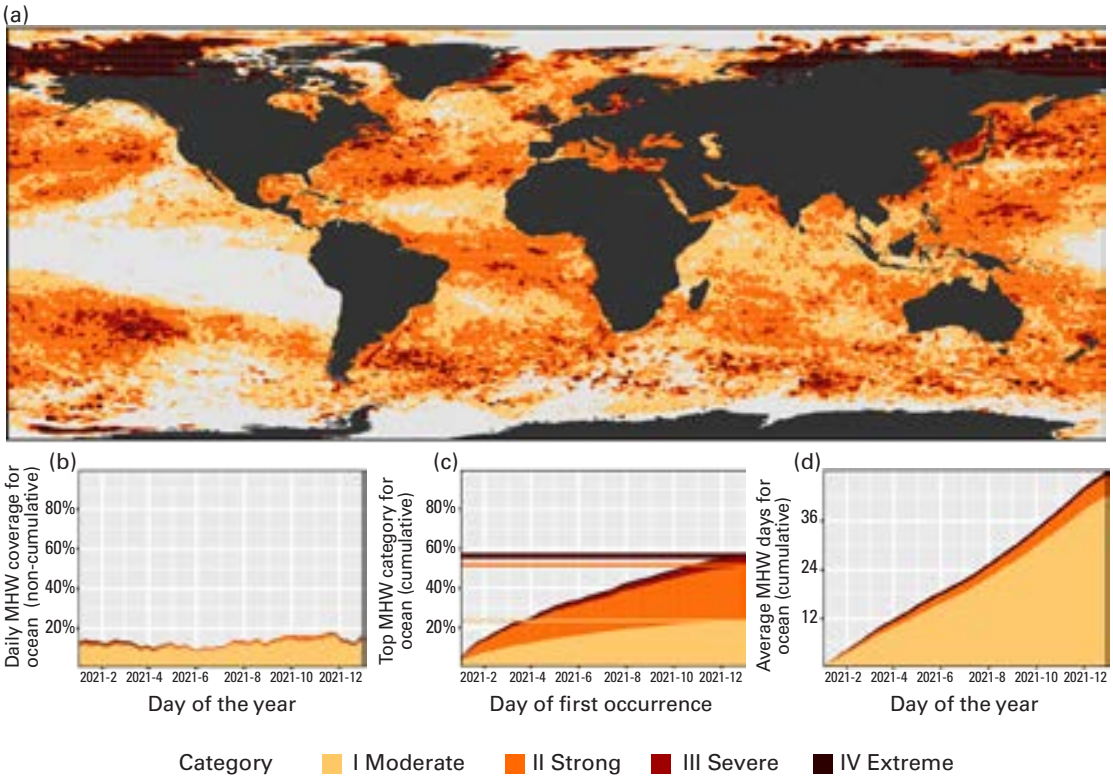

Figure 7. (a) Global map showing the highest MHW category (for definitions, see Marine heatwave and marine cold spell data) experienced at each pixel in 2021 (reference period 1982–2011). Light grey indicates that no MHW occurred in a pixel over the entire year. (b) Stacked bar plot showing the percentage of the surface of the ocean experiencing an MHW on any given day of the year. (c) Stacked bar plot showing the cumulative percentage of the surface of the ocean that experienced an MHW over the year. Note: These values are based on when in the year a pixel first experienced its highest MHW category, so no pixel is counted twice. Horizontal lines in this figure show the final percentages for each category of MHW. (d) Stacked bar plot showing the cumulative number of MHW days averaged over the surface of the ocean. Note: This average is calculated by dividing the cumulative sum of MHW days per pixel weighted by the surface area of those pixels. Data are from the National Oceanic and Atmospheric Administration Optimum Interpolation Sea Surface Temperature (NOAA OISST). *Source:* Robert Schlegel.

sea level has risen more slowly than the global mean, such as around Greenland and south of Iceland, and in the Southern Ocean around Antarctica. The patterns of trends in sea level have only varied a little over the last 30 years of the altimetry era, and changes from one year to another are small.

MARINE HEATWAVES AND COLD SPELLS

Analogous to heatwaves and cold spells on land, marine heatwaves (MHW) and marine cold spells (MCS) are prolonged periods of extreme heat or cold that affect the ocean. They can have a range of consequences for marine life and dependent communities,[29] and MHWs have become more frequent over the twentieth century. Satellite retrievals of sea-surface temperature are used to monitor MHWs and MCSs, categorized here as moderate, strong, severe or extreme (for definitions, see Marine heatwave and marine cold spell data).

Much of the ocean experienced at least one "strong" MHW at some point in 2021 (Figure 7). Due to the below-average sea-surface temperatures associated with the double-dip La Niña (see El Niño–Southern Oscillation (ENSO)), MHWs were conspicuously absent in the eastern Equatorial Pacific Ocean, which was also one of the only regions of the global ocean to see broad coverage of MCSs (Figure 8). The Laptev and Beaufort Seas experienced "severe" and "extreme" MHWs from January to April 2021. The ice-edge regions to the east of Greenland (August), north of Svalbard (October), and east of the Ross Sea (December) experienced notable "extreme" MHWs. In 2021, almost all MCSs were "moderate", except in areas of high variability such as the poleward extension of the Gulf Stream.

MHWs in 2021 showed an average daily coverage of 13%, which is less than the record of 17% in 2016 and 16% in 2020. For the eighth

[29] Smale, D. A.; Wernberg, T.; Oliver, E. C. J. et al. Marine heatwaves threaten global biodiversity and the provision of ecosystem services. *Nature Climate Change* **2019**, *9* (4), 306–312. https://www.nature.com/articles/s41558-019-0412-1.

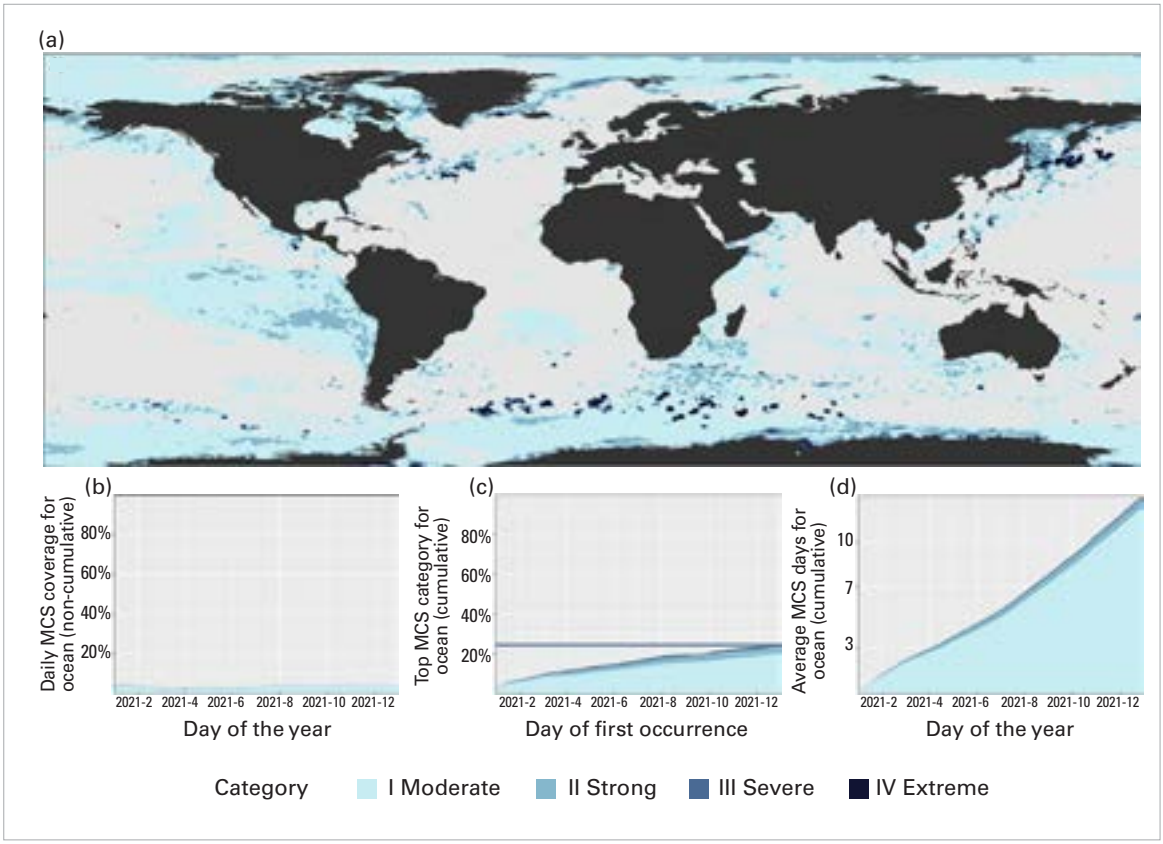

Figure 8. As for Figure 7, but showing MCSs rather than MHWs. Data are from the National Oceanic and Atmospheric Administration Optimum Interpolation Sea Surface Temperature (NOAA OISST). *Source:* Robert Schlegel.

consecutive year, the most common category of MHW in 2021 was "strong" (28%). Overall, 57% of the ocean surface experienced at least one MHW during 2021 (Figure 7c) – less than the record of 65% in 2016, and the lowest annual coverage since 2012 (57%).

The average daily coverage of the global ocean by MCSs in 2021 was 4% (Figure 8b) – a lower value than the record high in 1982 (7%) and comparable to 2020 (4%). In total, 25% of the ocean surface experienced at least one MCS during 2021 (Figure 8c), which is comparable to 2020 (25%), but much less than the 1985 record (63%).

OCEAN ACIDIFICATION

The ocean absorbs around 23% of the annual emissions of anthropogenic CO_2 into the atmosphere.[30,31] While this slows the rise of atmospheric concentration of CO_2,[32] CO_2 reacts with seawater and reduces the pH of the ocean,[33] a process known as ocean acidification (Figure 9). The current global rate of ocean acidification exceeds, by at least an order of magnitude, the rates inferred for the Paleocene–Eocene thermal maximum (PETM), which occurred around 56 million years ago and was associated with large perturbations of the global carbon cycle.[34] The IPCC Sixth

[30] Intergovernmental Panel on Climate Change (IPCC), 2019: Summary for Policymakers. In: *IPCC Special Report on the Ocean and Cryosphere in a Changing Climate*, https://www.ipcc.ch/site/assets/uploads/sites/3/2022/03/01_SROCC_SPM_FINAL.pdf.

[31] World Meteorological Organization (WMO). WMO Greenhouse Gas Bulletin (GHG Bulletin) - No.15: The State of Greenhouse Gases in the Atmosphere Based on Global Observations through 2018. Geneva, 2019.

[32] Le Quéré, C.; Andrew, R. M.; Friedlingstein, P. et al. Global carbon budget 2017. *Earth System Science Data* **2018**, *10*, 405–448. https://doi.org/10.5194/essd-10-405-2018.

[33] Intergovernmental Panel on Climate Change (IPCC), 2021: *Climate Change 2021: The Physical Science Basis*, https://www.ipcc.ch/report/ar6/wg1/#FullReport.

[34] Intergovernmental Panel on Climate Change (IPCC), 2021: *Climate Change 2021: The Physical Science Basis*, Chapter 2, section 2.3.3.5 Ocean pH, https://www.ipcc.ch/report/ar6/wg1/.

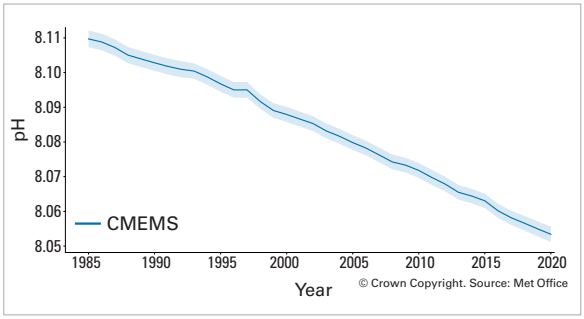

Figure 9. Global mean ocean surface pH (blue) covering the period 1985–2020. The shaded area indicates the estimated uncertainty in each estimate. Data from Copernicus Marine Environment Monitoring Service.
Source: Met Office, United Kingdom.

Assessment Report concluded that "[t]here is *very high confidence* that open ocean surface pH is now the lowest it has been for at least 26 kyr and current rates of pH change are unprecedented since at least that time". As the pH of the ocean decreases, its capacity to absorb CO_2 from the atmosphere also declines.[35]

Ocean acidification threatens organisms and ecosystem services, and hence food security, tourism and coastal protection. Local and regional acidification is of great relevance to marine organisms and biological processes. However, there is high variability in coastal areas due to a range of factors affecting CO_2 levels. National data sets of ocean acidification observations submitted towards the Sustainable Development Goal (SDG) 14.3 and the associated SDG Indicator 14.3.1 ("Average marine acidity (pH) measured at agreed suite of representative sampling stations") highlight the need for sustained, repeated observation and measurement of ocean acidification along the coastlines and in the open ocean. While there are currently still gaps in the global coverage, capacity building efforts increase the capability of many nations to measure, manage and report ocean acidification data, as confirmed by the growing number of countries participating in data collection towards the SDG Indicator 14.3.1.

CRYOSPHERE

The cryosphere comprises the frozen parts of the Earth. This includes sea ice, glaciers, ice sheets, snow and permafrost.

SEA ICE

Arctic sea ice

The 2020/2021 Arctic winter saw anomalously high sea-level pressure over the central Arctic Ocean (see Arctic Oscillation (AO)). The resulting anticyclonic wind pattern drove thicker multi-year ice into the Beaufort Sea.[36] The maximum Arctic sea-ice extent for the year was reached[37] on 21 March, at 14.8 million km². March 2021 was the ninth or tenth lowest extent on record (1979–2021), depending on the data source (Figure 10). For more details on the data sets used, see Sea-ice data.

Figure 10. Sea-ice extent difference from the 1981–2010 average in the Arctic (left) and Antarctic (right) for the months with maximum ice cover (Arctic: March; Antarctic: September) and minimum ice cover (Arctic: September; Antarctic: February) from 1979 to 2021.
Source: Data from EUMETSAT OSI SAF v2p1 and National Snow and Ice Data Centre (NSIDC) v3 (Fetterer et al., 2017) (see reference details in Sea-ice data).

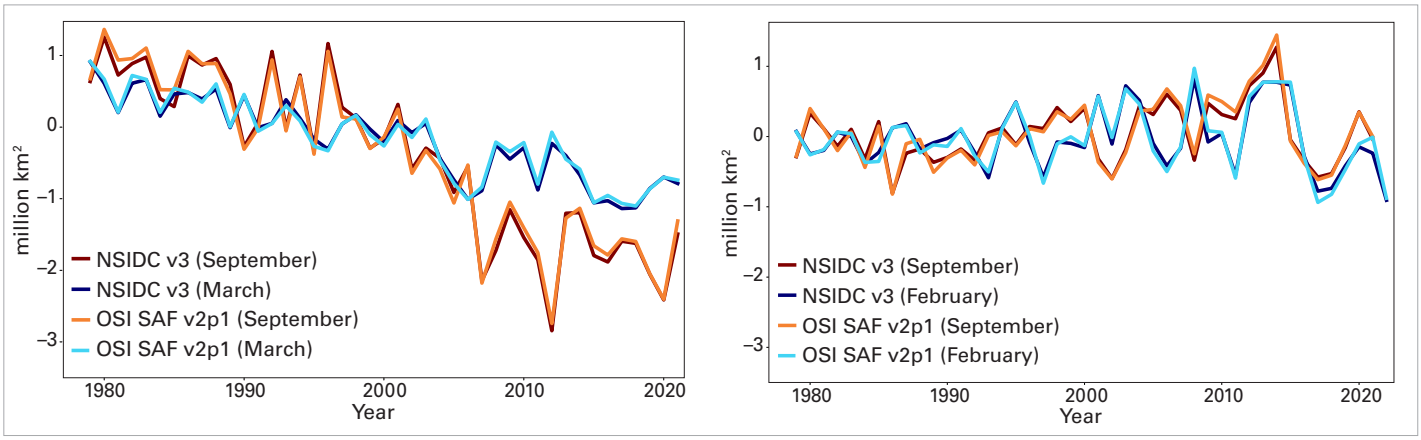

[35] Middelburg, J. J.; Soetaert, K.; Hagens, M. Ocean Alkalinity, Buffering and Biogeochemical Processes. *Reviews of Geophysics* **2020**, *58*, e2019RG000681. https://doi.org/10.1029/2019RG000681.

[36] Mallett, R. D. C.; Stroeve, J. C.; Cornish, S. B. et al. Record winter winds in 2020/21 drove exceptional Arctic sea ice transport. *Communications Earth & Environment* **2021**, *2*, 149. https://doi.org/10.1038/s43247-021-00221-8.

[37] https://nsidc.org/arcticseaicenews/2021/03/arctic-sea-ice-reaches-uneventful-maximum

Melt rates were close to the 1981–2010 average early in the melt season. However, sea-ice extent decreased very rapidly in June and early July in the Laptev Sea and east Greenland Sea regions. As a result, the Arctic-wide sea-ice extent reached a record low for the time of year in the first half of July. The monthly July average was the second to fourth lowest on record (tied with 2012 and 2019), with strong regional contrasts[38] (Figure 11). More ice than normal (1981–2010) was found in the Beaufort and Chukchi Seas, but the Siberian and European sectors (Laptev Sea and East Greenland Sea) had much less sea ice than normal. One exception was the eastern Kara Sea, where some sea ice persisted for the whole season. Conditions shifted rapidly after July, with a sustained period of colder weather across the Arctic Ocean. This slowed the sea-ice melt and August 2021 ended up with the tenth lowest extent on record.

With the slowdown in melt in August, the minimum September extent was greater than in recent years but still well below the 1981–2010 average, representing the twelfth lowest minimum ice extent in the 43-year satellite record (Figure 10). The 2021 minimum extent was observed[39] on 16 September at 4.72 million km^2, while the mean September ice extent was 4.92 million km^2, well below the 1981–2010 average.

Antarctic sea ice

Sea-ice extent across the Southern Ocean in 2021 was generally below the 1981–2010 mean, with below-average extents before the February minimum, slightly above-average extents during most of the winter, an exceptionally early maximum ice extent at the end of August, and the establishment of extents that were well below average by the end of the year.

The minimum in the 2021 annual cycle occurred on 19 February, when sea ice covered 2.60 million km^2, the fifteenth lowest extent in the record (1979–present). The extent of

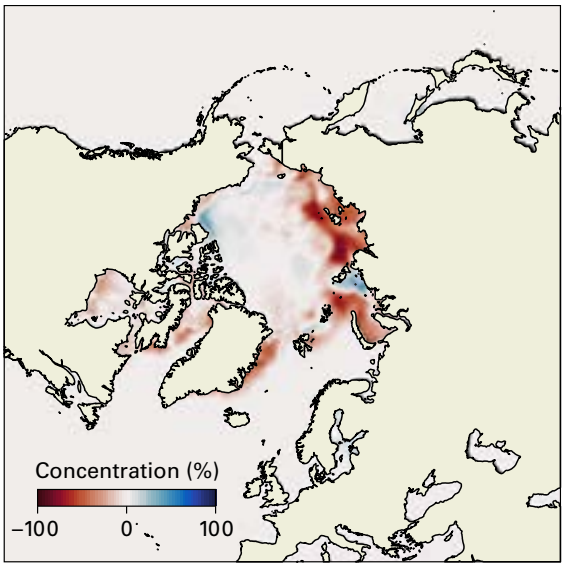

Figure 11. Arctic sea-ice concentration anomalies for July 2021 (difference from the 1981–2010 average). Red represents areas with less ice than normal, blue represents more ice.
Source: EUMETSAT OSI SAF data with research and development input from the European Space Agency Climate Change Initiative (ESA CCI).

ice at the annual minima began to increase in magnitude in the early 1990s, reaching a maximum of 3.68 million km^2 in 2013, before dropping sharply to 2.08 million km^2 in 2017, the lowest ice extent in the period 1979–2021. Since then, the extents at the annual minima have increased slowly. In February, most Antarctic sea ice was found in the Weddell Sea and therefore the sea-ice extents at the annual minima largely reflect regional changes in that area.

Antarctic sea ice reached its maximum annual extent of 18.80 million km^2 on 30 August 2021. This was close to the average magnitude in terms of extent, and the twenty-second largest in the 43 years of data. However, this was the second earliest maximum, with only one other maximum having occurred in August (that of 2016).

After the middle of September, the sea-ice extent for the whole Southern Ocean was persistently below average, with the ice extent decreasing to 6.77 million km^2 (–1.82 million km^2 below average) on 24 December, the third lowest for that day in the record. At that time, ice extents were below average in all sectors around the continent, but the lack of ice in the Weddell, Bellingshausen and Ross Seas had the greatest impact on the Antarctic-wide anomaly.

[38] Sea-ice cover for July 2021: https://climate.copernicus.eu/sea-ice-cover-july-2021

[39] https://nsidc.org/arcticseaicenews/2021/09/arctic-sea-ice-at-highest-minimum-since-2014

GLACIERS

Glaciers are formed from snow that has compacted to form ice, which can deform and flow downhill to lower and warmer altitudes, where it melts. If the glacier terminates in a lake or the ocean, ice loss also occurs through melting, where ice and water meet, or by calving of the glacier front to form icebergs. Glaciers are sensitive to changes in temperature, precipitation and sunlight, as well as other factors, such as changes in basal lubrication, warming ocean waters or the loss of buttressing ice shelves.

Over the period 2000–2019, global glaciers and ice caps (excluding the Greenland and Antarctic ice sheets) experienced[40] an average mass loss of 267 ± 16 Gt per year. Mass loss was higher, at 298 ± 24 Gt per year, in the later part of the period from 2015–2019. Glaciers in several mid-latitude regions thinned at more than double the global average (0.52 ± 0.03 m per year) from 2015 to 2019. Examples include thinning of 1.52 m per year in New Zealand, 1.24 m per year in Alaska, 1.11 m per year in Central Europe, and 1.05 m per year in Western North America (not including Alaska).

The World Glacier Monitoring Service collates and analyses global glacier mass balance data, including a set of 42 reference glaciers with long-term observations. For the glaciological year 2020/2021, preliminary data available from 32 of these reference glaciers indicate an average global mass balance of –0.77 m water equivalent (m w.e.[41] Figure 12). This is a smaller mass loss than the average for the last decade (–0.94 m w.e. from 2011 to 2020), but is larger than the average mass loss for the period 1991–2020, –0.66 m w.e.

Although the glaciological year 2020/2021 was characterized by a less negative glacier mass balance than in recent years, there is a clear trend towards an acceleration of mass loss on multidecadal timescales (Figure 12). On average, the reference glaciers have thinned by 33.5 m (ice equivalent) since 1950, with 76% of this thinning (25.5 m) occurring since 1980.

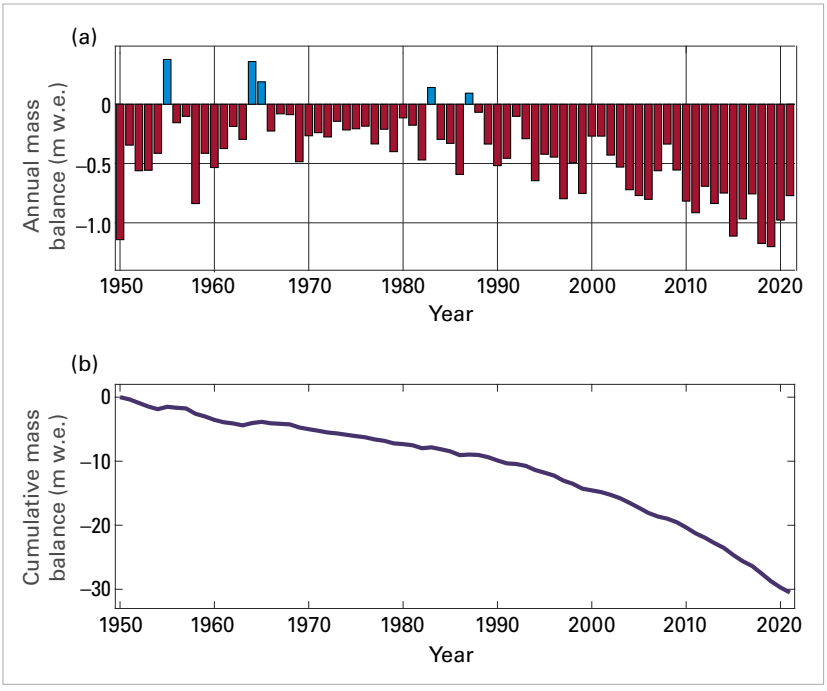

Figure 12. Global glacier mass balance 1950–2021, from a set of approximately 40 global reference glaciers.
(a) Average annual mass balance for the set of reference glaciers.
(b) Cumulative mass balance since 1950.
Units are m w.e.
Source: Data are provided by the World Glacier Monitoring Service, http://www.wgms.ch.

Exceptional glacier mass loss in western Canada

Mass loss from North American glaciers accelerated over the last two decades. Glacier mass loss in Western North America increased from 53 ± 13 Gt per year for the period 2000–2004 to 100 ± 17 Gt per year for 2015–2019.[42]

An exceptionally warm, dry northern hemisphere summer in 2021 (see Heatwaves and wildfires) exacerbated mass loss for most glaciers in Alberta and southern British Columbia in Canada, and the Pacific Northwest of the United States of America. In the Coast Mountains of British Columbia, Place and Helm Glaciers lost more mass during the period 2020–2021 than in any year since

[40] Hugonnet, R.; McNabb, R.; Berthier, E. et al. Accelerated global glacier mass loss in the early twenty-first century. *Nature* **2021**, *592* (7856), 726–731. https://www.nature.com/articles/s41586-021-03436-z.

[41] Metres water equivalent is the depth of water that would result if the lost ice were melted and spread across the surface area of the glacier.

[42] Hugonnet, R.; McNabb, R.; Berthier, E. et al. Accelerated global glacier mass loss in the early twenty-first century. *Nature* **2021**, *592* (7856), 726–731. https://www.nature.com/articles/s41586-021-03436-z.

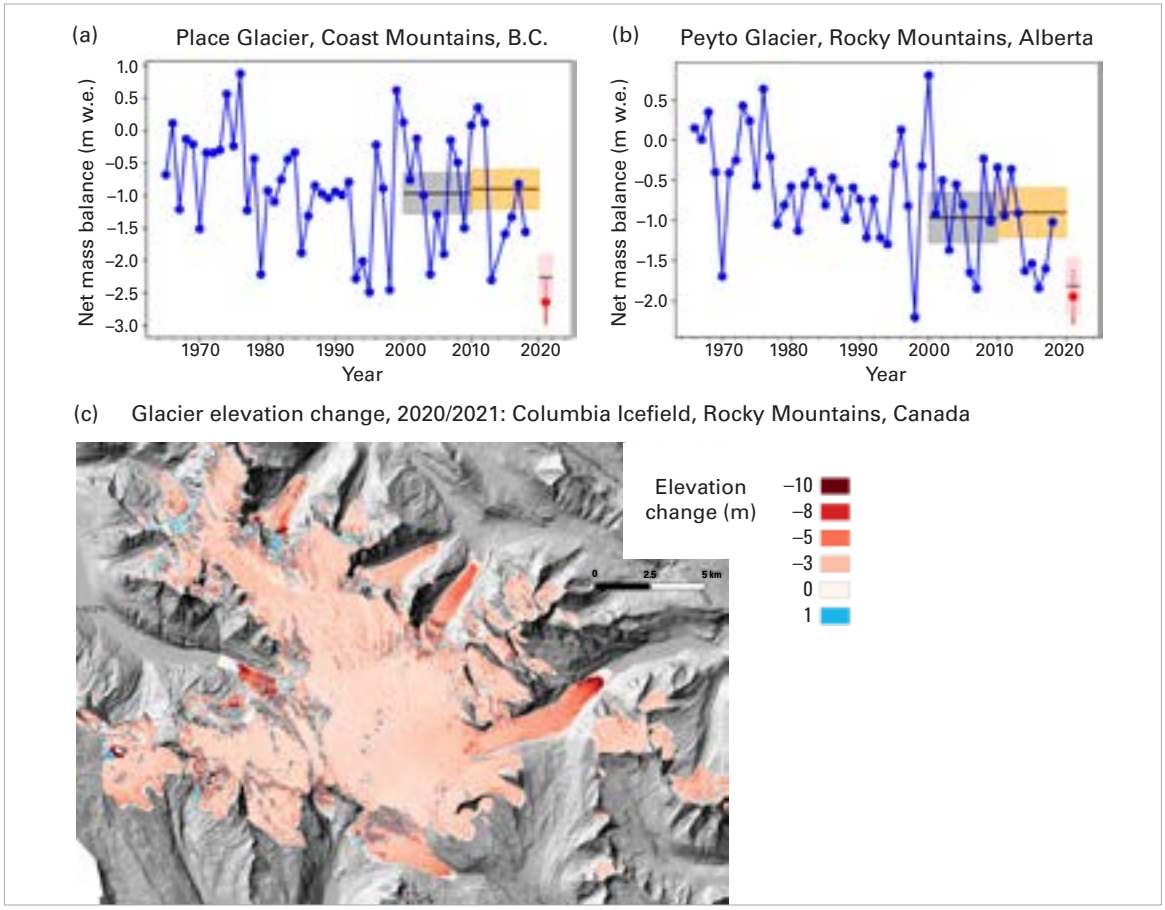

Figure 13. Glacier mass balance records from (a) Place Glacier, British Columbia, and (b) Peyto Glacier, Alberta from 1965 to 2021. Data for 1965–2019 are from the World Glacier Monitoring Service. Mass balance estimates for 2021 are from LiDAR surveys, with firn-density corrections based on Pelto et al. (2019) (see Glacier mass balance data). The blue and yellow horizontal bars indicate decadal mean values for the region from Hugonnet et al. (2021) (see Glacier mass balance data). Data from 2021 indicate the uncertainty (pink bar), the mass balance calculation using the contemporaneous LiDAR-derived glacier area (red circles), and the specific mass balance calculated from the Randolph Glacier Inventory glacier areas/outlines as used by Hugonnet et al. (2021) (black crosshairs). (c) LiDAR-derived elevation change on the Columbia Icefield, Canadian Rocky Mountains, for the 2020/2021 mass balance year.

measurements began in 1965 (Figure 13a). In the Canadian Rocky Mountains, mass loss from Peyto Glacier was the second greatest since 1965, after the strong El Niño year of 1998 (Figure 13b). Repeat LiDAR surveys[43] indicate mass balances of –2.66, –3.30, and –1.95 m w.e. on Place, Helm and Peyto Glaciers, respectively. This represents roughly twice the mean regional rate of thinning from 2015 to 2019.

Little snow remained on most of the mountain glaciers in this region by mid-August 2021, and many of these glaciers have lost their firn zone, where multi-year snow undergoes the transformation from snow to glacial ice. Particulate deposition – including soot and ash – from extensive regional wildfire activity in summer 2021 meant that the surfaces of the glaciers were unusually dark in July and August and absorbed more sunlight than usual, contributing to the extreme mass loss. Kokanee Glacier, British Columbia, lost 5%–6% of its total volume in 2021, while Columbia Icefield, the largest icefield in the Rocky Mountains (210 km^2), lost about 0.34 Gt of ice (Figure 13c).

ICE SHEETS

Ice sheets are expanses of glacial ice that cover an area larger than 50 000 km^2. In the current climate, there are two ice sheets, found on Greenland and Antarctica.

Greenland ice sheet

Changes in the total mass balance of the Greenland ice sheet reflect the combined effects of: surface mass balance, defined as the difference between snowfall and meltwater

[43] Pelto, B. M.; Menounos, B.; Marshall, S. J. Multi-year evaluation of airborne geodetic surveys to estimate seasonal mass balance, Columbia and Rocky Mountains, Canada. *The Cryosphere* **2019**, *13*, 1709–1727. https://doi.org/10.5194/tc-13-1709-2019.

run-off from the ice sheet; the marine mass balance, which is the sum of mass losses at the periphery from the calving of icebergs and the melting of glacier tongues on contact with the ocean; and the basal mass balance, which consists of basal melting due to geothermal heat and frictional heat generated by sliding at the base of the glacier and by deformation of the ice.

For Greenland, an ensemble of regional climate models[44] gives an estimated total mass balance[45] of –166 Gt for the 2021 mass balance year (1 September 2020 to 31 August 2021). Estimates based on satellite observations and the PROMICE surface weather station network give a total mass balance of –85 Gt over the same period.[46] GRACE satellite gravity data processed by NASA[47] give a total mass balance of –126 Gt for this same period.[48] The estimated magnitude of mass loss differs due to different methods and assumptions, but there is agreement that the Greenland ice sheet had a negative mass balance for the twenty-fifth year in a row.

Over the period September 1986 to August 2021, climate modelling indicates that the Greenland ice sheet lost a total of 5 511 Gt of ice,[49] an average mass loss of 157 Gt per year (Figure 14). Mass loss has accelerated over the past two decades. Based on the GRACE and GRACE-FO satellite gravity data,[50] Greenland lost 5 151 Gt of ice from April 2002

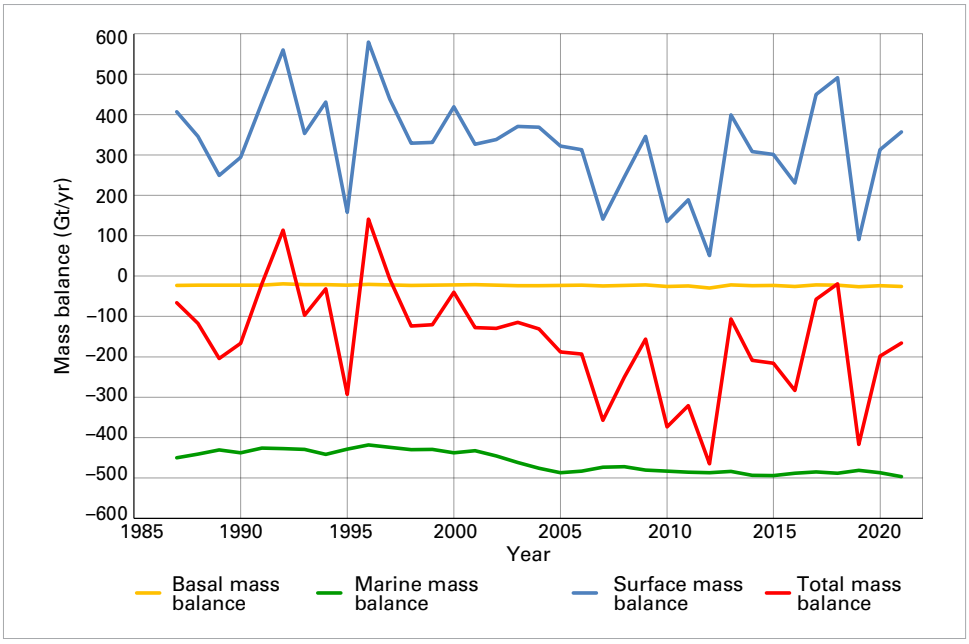

Figure 14. Components of the total mass balance of the Greenland ice sheet 1987–2021. Blue: surface mass balance (SMB); green: marine mass balance (MMB, also referred to as discharge); orange/yellow: basal mass balance (BMB), red: total mass balance (TMB), the sum of SMB, MMB and BMB (see footnote 44). *Source:* Mankoff, K. D.; Solgaard, A.; Colgan. W. et al. Greenland Ice Sheet solid ice discharge from 1986 through March 2020. *Earth System Science Data* **2020**, *12*(2), 1367–1383. https://doi.org/10.5194/essd-12-1367-2020.

[44] Based on the average of three regional climate and mass balance models. See Mankoff, K. D.; Fettweis, X.; Langen, P. L. et al. Greenland ice sheet mass balance from 1840 through next week. *Earth System Science Data* **2021**, *13*, 5001–5025. https://doi.org/10.5194/essd-13-5001-2021.

[45] A negative mass balance indicates a loss of ice mass; a positive mass balance indicates a gain.

[46] Moon, T. A.; Tedesco, M.; Box, J. E. et al. Greenland Ice Sheet. In *Arctic Report Card 2021*; Moon, T. A.; Druckenmiller, M. L.; Thoman, R. L., Eds.; National Oceanic and Atmospheric Administration, 2021. https://doi.org/10.25923/546g-ms61.

[47] https://climate.nasa.gov/vital-signs/ice-sheets/.

[48] Wiese, D.N.; Yuan, D.-N.; Boening, C. et al. 2019. JPL GRACE and GRACE-FO Mascon Ocean, Ice, and Hydrology Equivalent Water Height RL06M CRI Filtered Version 2.0, Ver. 2.0, PO.DAAC, CA, USA. http://dx.doi.org/10.5067/TEMSC-3MJ62.

[49] Based on the average of three regional climate and mass balance models. See Mankoff, K. D.; Fettweis, X.; Langen, P. L. et al. Greenland ice sheet mass balance from 1840 through next week. *Earth System Science Data* **2021**, *13*, 5001–5025. https://doi.org/10.5194/essd-13-5001-2021.

[50] Wiese, D.N.; Yuan, D.-N.; Boening, C. et al. 2019. JPL GRACE and GRACE-FO Mascon Ocean, Ice, and Hydrology Equivalent Water Height RL06M CRI Filtered Version 2.0, Ver. 2.0, PO.DAAC, CA, USA. http://dx.doi.org/10.5067/TEMSC-3MJ62.

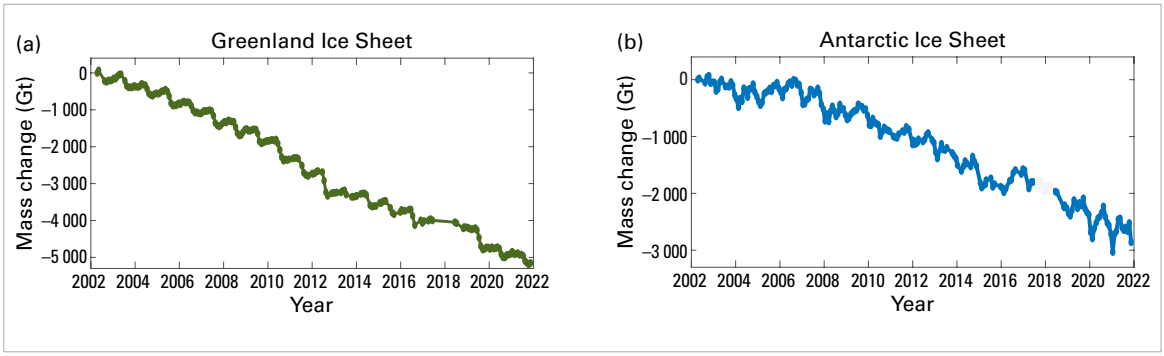

Figure 15. GRACE and GRACE-FO satellite gravity data of Greenland and Antarctic ice sheet mass change from April 2002 to November 2021 (see footnote 48). The Greenland ice sheet lost mass at an average rate of 276 Gt per year over this period, while the average rate of mass loss in Antarctica was 152 Gt per year. Combined, this is equivalent to about 1.2 mm per year of global sea-level rise.

to November 2021, an average rate of mass loss of 276 Gt per year (Figure 15). Greenland's mass balance in 2021 was close to the 35-year normal, but mass loss was below the average for the period 2002–2020 for which satellite gravity data are available.

For the summer 2021 melt season in Greenland, melt extent was close to the long-term average through the early summer, but temperatures and meltwater run-off were well above normal in late July and August 2021 (Figure 16).[51] The August event was associated with a warm, humid air mass that moved in from Baffin Bay and covered much of south-western and central Greenland. On 14 August, rain was observed for several hours at Summit Station, the highest point on the Greenland ice sheet (3 216 m), and air temperatures remained above freezing for about nine hours.[52,53] There is no previous report of rainfall at Summit, and this is the

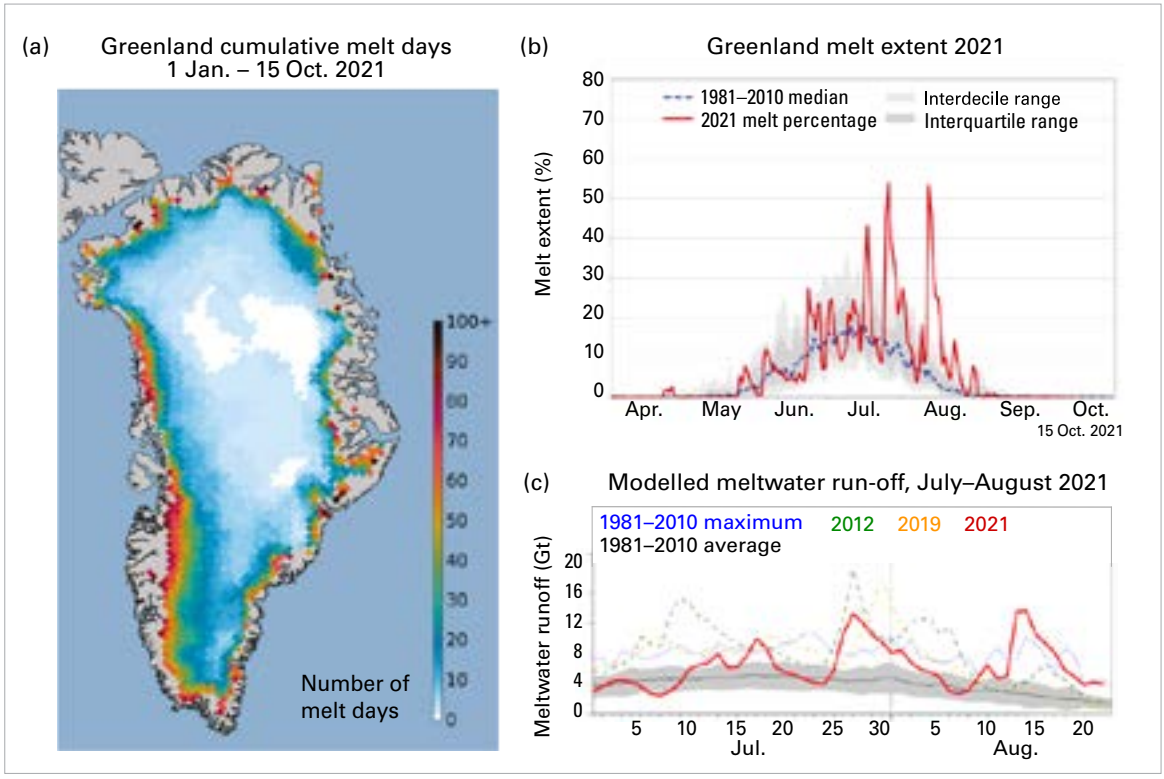

Figure 16. (a) Cumulative melt days on the Greenland ice sheet, 2021, indicating melt impacts over most of the ice sheet in summer 2021. (b) Melt extent (%) over the ice sheet through the 2021 melt season on Greenland, relative to the median melt extent from 1981 to 2010. (c) Greenland meltwater run-off through July–August 2021 relative to the recent extensive melt seasons of 2012 and 2019, indicating the record amount of late-season ice sheet melting associated with the mid-August rainfall event at Summit. *Source:* All images are courtesy of the USA National Snow and Ice Data Center http://nsidc.org/greenland-today/, with thanks to Ted Scambos and the Greenland Ice Sheet Today team. Analysis in (a) and (b) is from Thomas Mote, University of Georgia, USA, and meltwater run-off in (c) is estimated from the regional climate model MARv3.12, courtesy of Xavier Fettweis, University of Liège, Belgium.

[51] http://nsidc.org/greenland-today/2021/08/rain-at-the-summit-of-greenland/

[52] Moon, T. A.; Tedesco, M.; Box, J. E. et al. Greenland Ice Sheet. In *Arctic Report Card 2021*; Moon, T. A.; Druckenmiller, M. L.; Thoman, R. L., Eds.; National Oceanic and Atmospheric Administration, 2021. https://doi.org/10.25923/546g-ms61.

[53] http://nsidc.org/greenland-today/2021/08/rain-at-the-summit-of-greenland/

latest date in the year that above-freezing temperatures have been recorded at this location. Melt events at Summit were also observed in 1995, 2012 and 2019. Ice core records indicate that prior to 1995, the last time melting occurred at Summit was in the late nineteenth century.[54]

Antarctic ice sheet

The Antarctic ice sheet experiences negligible surface melt compared to Greenland, but some melt typically occurs on the Antarctic Peninsula between November and February, as well as on some of the low-lying ice shelves and in coastal zones. The summer 2020/2021 melt season in Antarctica was moderate and was below the 1990–2020 average.[55] The northern Filchner Ice Shelf in the Weddell Sea experienced a strong but brief melt event in mid-December 2020. The summer melt season in Antarctica concluded in mid-February 2021. The strongest positive melt anomalies of the year were over the remnant Larsen B and C ice shelves on the Antarctic Peninsula; most other locations experienced near-normal melt extent relative to the mean 1990–2020 conditions.

Despite near-normal surface melting in Antarctica in summer 2020/2021, GRACE-FO satellite gravity data indicate that the Antarctic ice sheet continued to lose mass in early 2021 (Figure 15), associated with calving and marine ice sheet melting in the Amundsen Sea sector of West Antarctica. Antarctic ice sheet mass loss since 2010 is largely driven by thinning and grounding-line retreat of Thwaites Glacier, triggered by ocean warming in this sector of the ice sheet.[56] GRACE-FO data[57] indicate that Antarctica lost a mass of 296 Gt from November 2020 to November 2021, which is roughly double the average rate of ice loss in Antarctica from 2002 to 2021 (Figure 15).

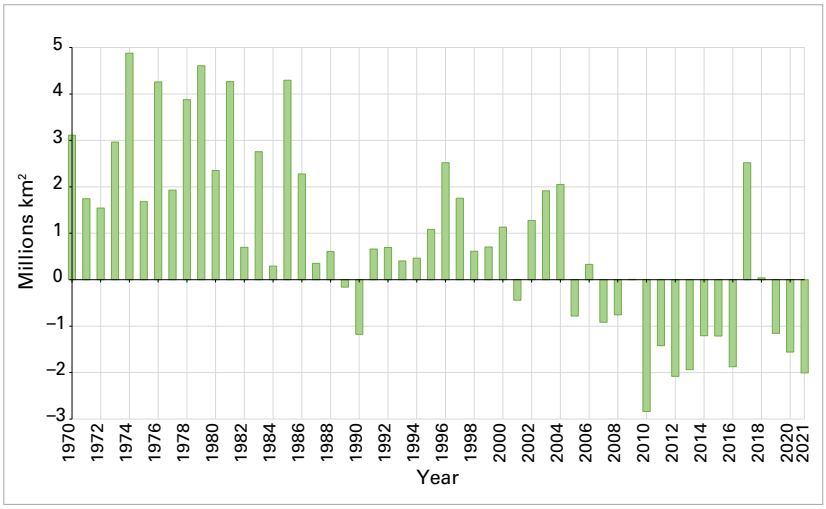

Figure 17. May snow-cover extent (SCE) anomaly in the northern hemisphere (NH) for the period 1970–2021, relative to the 1991–2020 average.
Source: Rutgers Northern Hemisphere Snow Cover Extent product: https://snowcover.org.

SNOW

Seasonal snow cover in the northern hemisphere (NH) has been experiencing a long-term decline in the late spring and summer, along with evidence of relative stability or increases in snow extent in the autumn.[58] Snow-cover extent (SCE) in 2021 was consistent with these long-term trends, with a May NH snow cover anomaly of –2 million km², the third lowest in the SCE record from 1970–2021 (Figure 17), based on analyses of the Rutgers Northern Hemisphere (NH) Snow Cover Extent (SCE) product.[59] Reductions in northern hemisphere spring snow extent are consistent across data sets, and in 2021 this was driven by below-normal snow cover in

[54] Meese, D. A.; Gow, A. J.; Grootes, P. et al. The Accumulation Record from the GISP2 Core as an Indicator of Climate Change Throughout the Holocene. *Science* **1994**, *266* (5191), 1680–1682. https://doi.org/10.1126/science.266.5191.1680.

[55] http://nsidc.org/greenland-today/2021/04/the-antarctic-2020-to-2021-melt-season-in-review/

[56] Velicogna, I.; Mohajerani, Y.; Landerer, G. A. F. et al. Continuity of Ice Sheet Mass Loss in Greenland and Antarctica from the GRACE and GRACE Follow-On Missions. *Geophysical Research Letters* **2020**, *47* (8), e2020GL087291. https://doi.org/10.1029/2020GL087291. See also Rignot, E.; Mouginot, J.; Scheuchl, B. et al. Four decades of Antarctic Ice Sheet mass balance from 1979–2017. *Proceedings of the National Academy of Sciences* **2019**, *116* (4) 1095–1103. https://doi.org/10.1073/pnas.1812883116.

[57] Wiese, D.N.; Yuan, D.-N.; Boening, C. et al. 2019. JPL GRACE and GRACE-FO Mascon Ocean, Ice, and Hydrology Equivalent Water Height RL06M CRI Filtered Version 2.0, Ver. 2.0, PO.DAAC, CA, USA. http://dx.doi.org/10.5067/TEMSC-3MJ62.

[58] Intergovernmental Panel on Climate Change (IPCC), 2021: Summary for Policymakers. In: *AR6 Climate Change 2021: The Physical Science Basis*, https://www.ipcc.ch/report/ar6/wg1/downloads/report/IPCC_AR6_WGI_SPM_final.pdf.

[59] https://snowcover.org

Figure 18. Recent slope instability associated with permafrost thaw, including active layer detachment slides and retrogressive thaw slumps. In the foreground, large amounts of material have pushed into the river to form a debris tongue. Foothills of the Mackenzie Mountains south of Norman Wells, north-western Canada. *Credit:* Government of Northwest Territories, Canada.

Eurasian high latitudes. Eurasian Arctic snow extent in May and June 2021 were the fifth and third lowest on record for the period 1967–2021.[60]

PERMAFROST

Permafrost occurs beneath about one eighth of Earth's exposed land area. It is ground that remains at or below 0 °C for at least two consecutive years. Permafrost thaw can lead to landscape instability and other impacts, including the emission of greenhouse gases from previously frozen organic material. As permafrost temperature approaches 0 °C, changes in temperature in the ice-rich ground are stalled due to the phase change between ice and water. While temperature increase may level off near 0 °C for several years or decades due to the phase change, the impacts of permafrost warming and thaw on ground stability (including subsidence and mass movements), hydrology, ecosystems and infrastructure are often clearly visible (Figure 18).

Since the 1990s, the Global Terrestrial Network for Permafrost (GTN-P) has compiled data sets of permafrost temperatures (temperature measured in boreholes) and active layer thickness (the maximum thickness of the seasonally thawed layer above the permafrost). GTN-P products rely mostly on research projects to sustain activities. Long-term data series from national and regional networks operating in mountain and polar areas show a continuation of past warming trends up to 2020, which is the most recent data available.

STRATOSPHERIC OZONE

Following the success of the Montreal Protocol, the use of halons and chlorofluorocarbons (CFCs) has been reported as discontinued, although their levels in the atmosphere continue to be monitored. Because of their long lifetime, these compounds will remain in the atmosphere for many decades. Even if there were no new emissions, there is still more than enough chlorine and bromine present to cause the complete destruction of ozone over Antarctica from August to December. As a result, the formation of the Antarctic ozone hole – an area of low ozone concentration – continues to be an annual

[60] Mudryk, L.; Chereque, A. E.; Derksen, C. et al. Terrestrial Snow Cover. In *Arctic Report Card 2021*; Moon, T. A.; Druckenmiller, M. L.; Thoman, R. L., Eds.; National Oceanic and Atmospheric Administration, 2021. https://doi.org/10.25923/16xy-9h55.

spring event, with the year-to-year variation in its size and depth governed to a large degree by meteorological conditions.

The 2021 Antarctic ozone hole developed relatively early and continued growing, resulting in a large and deep ozone hole. It expanded to 24 million km^2 on 24 September and remained close to this value until mid-October 2021. The development of the hole, and its extent and severity, were close to that for the 2020 and 2018 seasons. The ozone hole reached its maximum area of 24.8 million km^2 on 7 October 2021, similar to the areas in 2020 and 2018, and close to the highest values observed in earlier years, such as 28.2 million km^2 in 2015 and 29.6 million km^2 in 2006, according to an analysis from the National Aeronautics and Space Administration (NASA) (Figure 19, left).

In terms of the total ozone column, NASA reported a minimum ozone of 92 DU (Dobson Units) on 7 October 2021, which was the lowest value for the 2021 season and for the past 17 years (Figure 19, right). After September 2021, the concentration of stratospheric ozone was persistently reduced to near-zero values between 15 and 20 km altitude over Antarctica. Together with the 2020 season, these are some of the lowest ozone values ever measured via sondes at the Antarctic stations, as reported by the National Oceanic and Atmospheric Administration (NOAA).

The 2021 hole was larger and deeper than 70% of the ozone holes since 1979, and remained as such until the closing of the hole in the second half of December. It ranked as the thirteenth largest ozone hole by area and the sixth deepest ozone hole in terms of minimum ozone. The unusually deep and large ozone hole in 2021 was driven by a strong and stable polar vortex and colder-than-average conditions in 2021 in the stratosphere.

DRIVERS OF SHORT-TERM VARIABILITY

There are many different natural phenomena, often referred to as climate patterns or climate modes, that affect weather at timescales ranging from days to several months. Surface temperatures change relatively slowly over the ocean, so recurring patterns in sea-surface temperature can be used to understand and, in some cases, predict the more rapidly changing patterns of weather over land on seasonal timescales. Similarly, albeit at a faster rate, known pressure changes in the atmosphere can help explain certain regional weather patterns.

In 2021, the El Niño–Southern Oscillation (ENSO), the Indian Ocean Dipole (IOD), the Arctic Oscillation (AO) and the Southern Annular Mode (SAM) each contributed to

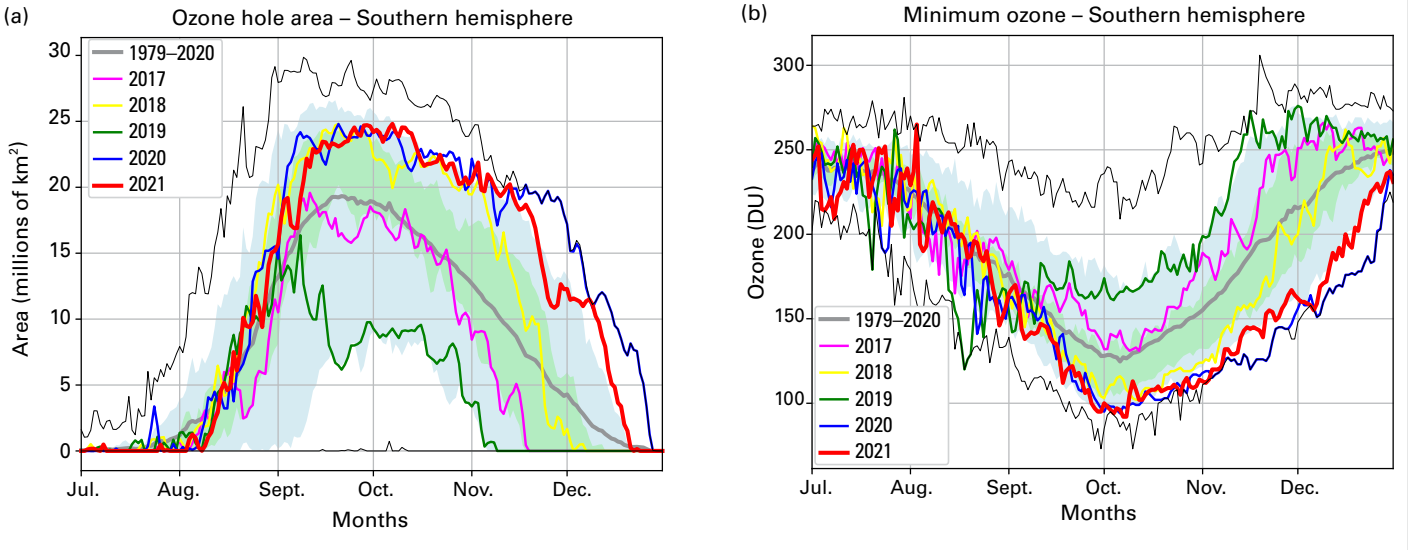

Figure 19. Left: Ozone hole area (millions of km^2). Right: Minimum ozone, where the total ozone column is less than 220 Dobson Units. The year 2021 is shown in red. The most recent years are shown for comparison as indicated by the legend. The smooth, thick grey line is the 1979–2020 average. The blue shaded area represents the 10th to 90th percentiles, and the green shaded area represents the 30th to 70th percentiles for the period 1979–2020. The thin black lines show the maximum and minimum values for each day in the 1979–2020 period. *Source:* The plot was generated at WMO on the basis of data downloaded from the NASA Ozone Watch (https://ozonewatch.gsfc.nasa.gov/). The NASA data are based on satellite observations from the OMI and TOMS instruments.

major weather and climate events in different parts of the world, and are described in further detail below.

EL NIÑO–SOUTHERN OSCILLATION

ENSO is one of the most important drivers of year-to-year variability in weather patterns worldwide. It is linked to hazards such as heavy rains, floods and drought. El Niño, characterized by higher-than-average sea-surface temperatures in the eastern Tropical Pacific and a weakening of the trade winds, typically has a warming influence on global temperatures. La Niña, which is characterized by below-average sea-surface temperatures in the central and eastern Tropical Pacific and a strengthening of the trade winds, has the opposite effect.

La Niña conditions emerged in mid-2020 and peaked in the October–December period at moderate strength, with average sea-surface temperatures 1.3 °C below the 1991–2020 normal in the Niño 3.4 region (5°N–5°S, 120°W–170°W). La Niña weakened through the first half of 2021, reaching an ENSO-neutral state (temperatures within 0.5 °C of normal) in May, according to both oceanic and atmospheric indicators. However, sea-surface temperatures cooled after mid-year, reaching La Niña thresholds once again by the July–September period. By the October–December period, average sea-surface temperatures once again reached moderate strength, at 1.0 °C below normal.

In addition to having a temporary cooling influence on Earth's global temperature, La Niña is associated with drier-than-normal conditions in East Africa. Kenya, Ethiopia and Somalia experienced consecutive below-average rainfall seasons in late 2020, early 2021 and late 2021, which led to drought in the region. In early 2021, precipitation was higher than normal over the Maritime Continent[61] (the climatologically important region of islands and seas between mainland South-east Asia and Australia and between the Indian and Pacific Oceans) and lower than normal in Patagonia at the beginning of the year, which are typical patterns associated with La Niña. Additionally, La Niña conditions can contribute to above-average hurricane activity in the North Atlantic, which experienced 21 named tropical cyclones during its 2021 hurricane season (the 1981–2010 average for the entire season is 14). La Niña is also associated with warmer and drier areas across the southern tier of the United States of America. In December, most states in this region reported record or near-record high temperatures, and several states were also drier than average.

INDIAN OCEAN DIPOLE

The positive phase of the IOD is characterized by below-average sea-surface temperatures in the Eastern Indian Ocean and above-average sea-surface temperatures in the west. The negative phase has the opposite pattern. The resulting change in the gradient of sea-surface temperature across the ocean basin affects the weather of the surrounding continents, primarily in the southern hemisphere. Positive IOD events are often associated with El Niño and negative events with La Niña.[62]

A negative IOD developed during July 2021 and returned to neutral, although on the negative side, by the end of the year. This marked the first negative IOD since 2016. In combination with La Niña, this phase contributed to wet conditions in much of Australia in the late austral winter and spring. South-west Western Australia reported its highest July rainfall totals since 1996, as did many locations in South Australia. Australia as a whole observed its tenth wettest spring in its 122-year record, with the state of New South Wales observing its fourth wettest. November was the wettest November since records began for both New South Wales and Australia as a whole.[63] Conversely, the negative IOD, again in combination with La Niña, likely contributed to the extreme dry conditions in Eastern Africa.

---

[61] Ramage, C. S. Role of a Tropical "Maritime Continent" in the Atmospheric Circulation. *Monthly Weather Review* **1968**, *96* (6), 365–370. https://journals.ametsoc.org/view/journals/mwre/96/6/1520-0493_1968_096_0365_roatmc_2_0_co_2.xml.

[62] http://www.bom.gov.au/climate/enso/history/ln-2010-12/IOD-what.shtml

[63] http://www.bom.gov.au/climate/current/statements/scs75.pdf

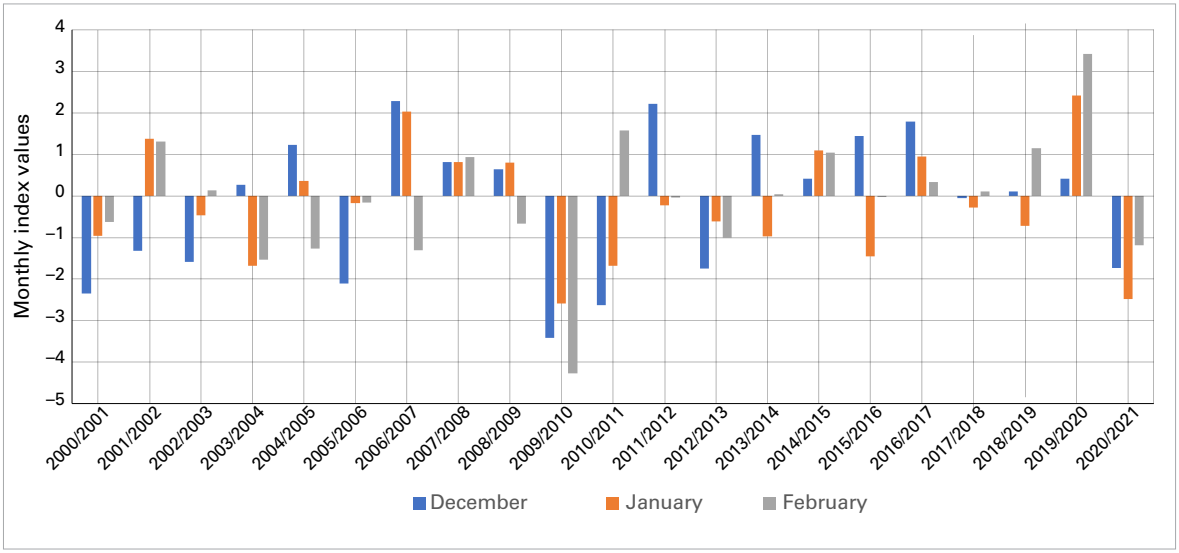

Figure 20. Arctic Oscillation monthly index values for northern hemisphere winter months 2000/2021. December is in blue, January in orange and February in grey. *Source:* National Oceanic and Atmospheric Administration (NOAA) Climate Prediction Center.

ARCTIC OSCILLATION

The AO is a large-scale atmospheric pattern that influences weather throughout the northern hemisphere.[64] The positive phase is characterized by lower-than-average air pressure over the Arctic and higher-than-average pressure over the Northern Pacific and Atlantic Oceans. The jet stream runs parallel to the lines of latitude and farther north than average, locking up cold Arctic air, and storms can be shifted northward of their usual paths. The mid-latitudes of North America, Europe, Siberia and East Asia generally see fewer cold air outbreaks than usual during the positive phase of the AO. A negative AO has the opposite effect, associated with a more meandering jet stream and cold air spilling south into the mid-latitudes where the jet stream dips southward.

The AO was negative during the northern hemisphere 2020/2021 winter and, seasonally, was the most negative on record since winter 2009/2010 (Figure 20). The jet stream swept down over North America, contributing to the coldest February for the continent since 1994. However, the same wavy jet stream also contributed to extreme warmth in parts of Northern and Eastern Asia in February 2021 as it surged northward over the area, with regions in Mongolia, China, Japan and the Republic of Korea reporting record high temperatures for this time of year. The contrast between the positive AO (winter 2019/2020) and the negative AO (winter 2020/2021) could explain some of the differences between temperature patterns in the first quarters of 2020 and 2021. The negative winter phase of the Arctic Oscillation has also been linked to more moderate Arctic sea-ice loss the following summer[65] (see Arctic sea ice).

SOUTHERN ANNULAR MODE

On the opposite side of the world, the SAM (also referred to as the Antarctic Oscillation, AAO) is a large-scale atmospheric pattern that influences weather in the southern hemisphere. It is measured by the north–south movement of the westerly wind belt that circles Antarctica, dominating the middle to higher latitudes of the southern hemisphere. The positive phase is characterized by the belt of strong westerly winds contracting towards Antarctica and is linked to the La Niña phase of ENSO. During a positive SAM, warm and moist westerly flow over the northern Peninsula leads to foehn warming on the eastern side and anomalous warmth. The negative phase, in contrast, is characterized

[64] Thompson, D. W. J.; Wallace, J. M. The Arctic Oscillation signature in the wintertime geopotential height and temperature fields. *Geophysical Research Letters* **1998**, *25* (9), 1297–1300.

[65] Rigor, I. G.; Wallace, J. M.; Colony, R. L. Response of Sea Ice to the Arctic Oscillation. *Journal of Climate* **2002**, *15* (18), 2648–2663. https://doi.org/10.1175/1520-0442(2002)015<2648:ROSITT>2.0.CO;2.

by an expansion of the belt of strong westerly winds towards the equator.[66] Notably, the SAM can have large impacts on Antarctic surface temperatures, ocean circulation and rainfall patterns in parts of Australia.

The SAM was primarily positive or neutral throughout 2021, and was strongly positive both at the beginning of the year and near the end of the year.[67] This positive pattern likely contributed to the record cold austral winter and April–September cold season at the South Pole, as it created anomalous low wind speed and wind directions predominantly from the northeast at the pole and prevented warm air masses from reaching the area. Conversely, Esperanza Station, on the north-east Antarctic Peninsula, experienced its warmest year on record, with an average temperature of –2.6 °C. On 18 December, the temperature reached 14.6 °C, an all-time December high for the station.

[66] http://www.bom.gov.au/climate/sam/

[67] http://www.nerc-bas.ac.uk/icd/gjma/sam.html

High-impact events in 2021

Although understanding broad-scale changes in the climate is important, the acute impacts of weather and climate are most often felt during extreme meteorological events such as heavy rain and snow, droughts, heatwaves, cold waves and storms, including tropical storms and cyclones. These can lead to or exacerbate other high-impact events such as flooding, landslides, wildfires and avalanches. This section is based largely on input from WMO Members. The wider socioeconomic risks and impacts associated with these events are described in Risks and impacts.

HEATWAVES AND WILDFIRES

Exceptional heatwaves affected Western North America on several occasions during June and July. By some measures, the most extreme was in late June in the north-western United States and western Canada. Lytton, in south-central British Columbia, reached 49.6 °C on 29 June, breaking the previous Canadian national record by 4.6 °C, with temperatures reaching the mid-40s as far west as the eastern suburbs of Vancouver and the interior of Vancouver Island. It was also more than 5 °C higher than the previous highest known temperature north of 50°N. Large numbers of heat-related deaths occurred, with 569 reported in British Columbia alone between 20 June and 29 July,[68] and 185 in Alberta,[69] while in the United States over a similar period, 154 heat-related deaths were reported in Washington[70] and at least 83 in Oregon.[71] Many long-term stations broke records by 4 °C to 6 °C, including Portland, Oregon (46.7 °C). There were also multiple heatwaves in the south-western United States. Death Valley, California reached 54.4 °C on 9 July, equalling a similar 2020 value as the highest recorded in the world since at least the 1930s. It went on to be the hottest summer on record averaged over the continental United States.

There were numerous major wildfires during and after the heatwaves (including one which largely destroyed the town of Lytton the day after its record temperature). The Dixie fire in northern California, which started on 13 July, burned about 390 000 hectares before being fully contained in October, making it the largest single fire on record in California. A rare winter wildfire caused major property losses east of Boulder, Colorado on 30 December, with more than 1 000 homes and other buildings destroyed or damaged. The overall area burned during the season in the United States was slightly below average,[72] but in Canada it was well above average, with Ontario having its largest seasonal area burned on record and British Columbia its third largest. Prolonged smoke pollution affected many parts of North America during the summer, with Calgary reporting a record 512 hours of smoke or haze, compared with the long-term average of 12.

Extreme heat affected the broader Mediterranean region on several occasions during the second half of the northern hemisphere summer. The most exceptional heat was in the second week of August. On 11 August, an agrometeorological station near Syracuse in Sicily, Italy, reached 48.8 °C, a provisional European record, while Kairouan (Tunisia) reached a record 50.3 °C. Montoro (47.4 °C) set a national record for Spain on 14 August, while on the same day Madrid (Barajas Airport) had its hottest day on record with 42.7 °C. Earlier, on 20 July, Cizre (49.1 °C) set a Turkish national record and Tbilisi (Georgia) had its hottest day on record (40.6 °C). Major wildfires occurred across many parts of the region, with Algeria, southern Turkey and Greece especially badly affected. Over 40 deaths[73] occurred in the Algerian fires. France, Italy, North Macedonia, Lebanon, Israel, Libya, Tunisia and Morocco also experienced significant wildfires during the period.

---

[68] https://www2.gov.bc.ca/gov/content/life-events/death/coroners-service/news-and-updates/heat-related

[69] https://www.canada.ca/en/environment-climate-change/services/top-ten-weather-stories/2021.html

[70] https://www.doh.wa.gov/Emergencies/BePreparedBeSafe/SevereWeatherandNaturalDisasters/HotWeatherSafety/HeatWave2021#heading88455

[71] Oregon Medical Examiner's Office, quoted in media reports, https://flashalert.net/id/OSPOre/146352

[72] https://www.nifc.gov/

[73] https://www.emdat.be/

June was exceptionally warm in many parts of Eastern and Central Europe. National June records were set for Estonia (34.6 °C) and Belarus (37.1 °C), while locations which had their hottest June day on record included St. Petersburg (35.9 °C) and Moscow (34.8 °C), both on 23 June, Yerevan (Armenia, 41.1 °C) on the 24th, and Baku (Azerbaijan, 40.5 °C) on the 26th. Tampere in Finland reported its highest temperature on record (33.2 °C) on 22 June. Latvia had its hottest June and summer on record. Further afield, Libya also saw a prolonged heatwave in late June. Later in the summer, abnormal warmth also reached North-west Europe; 31.3 °C at Castlederg on 21 July was a record for Northern Ireland. Two tropical nights were observed in Ireland in July, with daily minimum temperatures exceeding 20 °C in County Kerry.

For the third successive year, there were major wildfires during the summer in Siberia, particularly in the Sakha Republic around Yakutsk. According to a report by the Federal Forestry Agency of Russia, the number of fires in Yakutia by the end of the summer was 2 295, with an area of about 8.9 million hectares burned since the beginning of the forest fire season.

Fire activity in the Amazon region during the August–September peak season was less than in 2019 or 2020,[74] but there was extensive fire activity in other parts of Brazil, including the Pantanal.

COLD SPELLS AND SNOW

Abnormally cold conditions affected many parts of the central United States and northern Mexico in mid-February. The most severe impacts were in Texas, which generally experienced its lowest temperatures since at least 1989, with temperatures in some areas staying below freezing continuously for 6 to 9 days. On 16 February, Oklahoma City reached –25.6 °C and Dallas –18.9 °C, their lowest temperatures since 1899 and 1949 respectively. Electricity transmission was severely disrupted, with power outages affecting nearly 10 million people at the event's peak. Frozen pipes were another major cause of damage. A total of 226 deaths were reported in the United States along with an estimated US$ 24 billion in economic losses, making it the costliest winter storm on record for the United States.[75]

The winter of 2020/2021 was a cold winter in many parts of Northern Asia. The Russian Federation had its coldest winter since 2009/2010. Below-average temperatures affected much of Japan in late December and early January, with heavy snowfalls on a number of occasions. A number of locations on the Sea of Japan coast of Honshu had their heaviest 72-hour snowfall on record in early January. Much of China was also unusually cold during this period, with Beijing reaching –19.6 °C on 7 January, its lowest temperature since 1966.

A severe snowstorm hit many parts of Spain from 7 to 10 January, followed by a week of freezing air temperatures. A total of 53 cm of snow fell at the central city location of Retiro (Madrid), and heavy falls were also reported in many other parts of Spain.[76] Some locations, including Toledo (–13.4 °C) and Teruel (–21.0 °C), had their lowest temperatures on record on 12 January in the wake of the storm. There were major disruptions to land and air transport. Later in the winter, in the second week of February, the Netherlands experienced its most significant snowstorm since 2010, with heavy snow also falling in Germany, Poland and the United Kingdom; in the wake of the storm, Braemar recorded –23.0 °C on 12 February, the lowest temperature in the United Kingdom since 1995. In South-eastern Europe, Athens had its heaviest snow since 2009 on 15 February. Libya experienced unusual snowfalls between 15 and 21 February and again, on high ground, in late December.

An abnormal spring cold outbreak affected many parts of Europe in early April. Record

[74] https://queimadas.dgi.inpe.br/queimadas/portal-static/estatisticas_estados/

[75] https://www.ncdc.noaa.gov/billions/events/US/2021

[76] http://www.aemet.es/en/conocermas/borrascas/2020-2021/estudios_e_impactos/filomena

low April temperatures in France included –7.4 °C at Saint-Etienne on the 8th and –6.9 °C at Beauvais on the 6th, while Belgrade (Serbia) had its heaviest April snowfall on record on the 7th. It was the coldest April in Poland in the twenty-first century. At high elevations, national records for April were set for Switzerland (–26.3 °C at Jungfraujoch) and Slovenia (–20.6 °C at Nova vas na Blokah). This followed a very warm end to March with France having its warmest March day on record on the 31st. Frost damage to agriculture was widespread and severe, with losses to vineyards and other crops in France alone exceeding US$ 4.6 billion. The United Kingdom went on to have its lowest monthly mean temperature for April since 1922.

PRECIPITATION

Compared to temperature, precipitation is characterized by higher spatial and temporal variability. In 2021, large regions with above-normal precipitation totals, relative to the chosen climatology period (1951–2000), were Eastern Europe, South-east Asia, the Maritime Continent, areas of Northern South America and parts of South-eastern North America (Figure 21). Large regions with a rainfall deficit included South-west Asia and the Middle East, parts of Southern Africa, parts of Southern South America and areas in Central North America.

The onset of the West African Monsoon was delayed. Later in the season, rainfall totals were higher than normal, especially in the western monsoon region. In total, the seasonal rainfall was close to normal. In Southern Africa, in an area centred on Zambia, rainfall amounts during the wet season until May were below the long-term mean. It was at least the second year in a row with below-normal rainfall for Madagascar; rainfall totals have been below average in most years since 2011. In addition, both the wet seasons (April to May and October to November) were drier than usual in the Greater Horn of Africa region.

Above average rainfall totals were observed in Alaska and the north of Canada, and in the south-eastern United States and parts of the Caribbean. Between these two wetter-than-average bands was a swath of unusually dry conditions extending across the width of the continent.

Unusually high precipitation amounts, relative to the reference period, were recorded in south-western and south-eastern Australia. On the other hand, abnormally low precipitation amounts were received on the North Island of New Zealand.

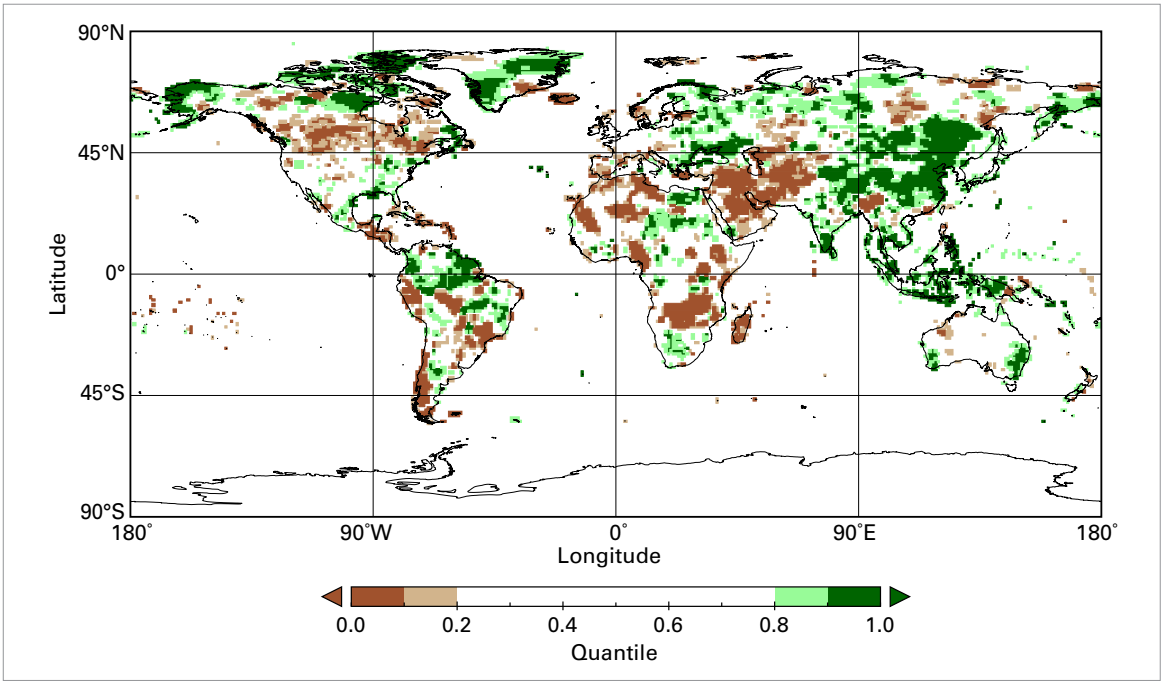

Figure 21. Total precipitation in 2021, expressed as a percentile of the 1951–2010 reference period, for areas in the driest 20% (brown) and wettest 20% (green) of years during the reference period, with darker shades of brown and green indicating the driest and wettest 10%, respectively. *Source:* Global Precipitation Climatology Centre (GPCC), Deutscher Wetterdienst, Germany.

Unusually low precipitation amounts fell around the Mediterranean Sea, while unusually high totals were detected around the Black Sea and in parts of Eastern Europe.

FLOOD

Extreme rainfall, which was enhanced by the moisture influx ahead of Typhoon *In-fa*, hit Henan province in central China from 17 to 21 July. The most severely affected area was around the city of Zhengzhou (the capital of Henan Province), which on 20 July received 201.9 mm of rainfall in one hour (a Chinese national record) and 382 mm in 6 hours. For the event as a whole, the area received 720 mm, more than its annual average. The city experienced extreme flash flooding, with many buildings, roads and subways inundated. The flooding was associated with 380 deaths or missing persons, and economic losses of US$ 17.7 billion were reported.[77] Further late-season flooding occurred in early October, focused on Shanxi and Hebei provinces.

Western Europe experienced some of its most severe flooding on record in mid-July. The worst-affected area was western Germany and eastern Belgium, where 100 to 150 mm of rain fell over a wide area on 14–15 July onto ground which was already unusually wet after high recent rainfall. Hagen (Germany) reported 241 mm of rainfall in 22 hours. Numerous rivers experienced extreme flooding, with several towns inundated, and there were also several landslides. France, the Netherlands, Luxembourg and Switzerland also experienced significant flooding. The number of deaths reported in Germany was 183, and in Belgium it was 36, with economic losses in Germany exceeding US$ 20 billion.[78]

Persistent heavy rainfall in mid-March resulted in major flooding in eastern New South Wales in Australia.[79] The week from 18 to 24 March was the wettest on record averaged over coastal New South Wales. The most severe flooding was along the Hastings, Karuah and Manning Rivers north of Sydney, but there was also significant flooding in other areas, including parts of western Sydney. There was also flooding on many inland rivers, which led to substantial recovery in water storages severely depleted by the 2017–2019 drought. At least US$ 2.1 billion in economic losses were reported.

Two flash flood events associated with localized heavy rainfall occurred in Afghanistan during 2021, in early May around Herat in the west, and on 28–29 July centred on Nuristan in the east. There was significant loss of life in both events, with 61 deaths reported in the May event and 113 in the July event.[80]

Flash flooding occurred on several occasions around the Mediterranean and Black Sea coasts. The most impactful event was on the Black Sea coast of Turkey on 10 August, where several towns experienced severe damage and 77 deaths were reported. Rainfall of 399.9 mm was recorded at Bozkurt in 24 hours. This event was associated with a "Medicane" – a storm forming outside the tropics that nevertheless has characteristics of a tropical storm – in the Black Sea. Extreme rainfall and flooding were also reported on the Black Sea coast of the Russian Federation from 12 to 14 August.

On 4 October, exceptional rainfall fell in coastal regions of Liguria (north-west Italy), including 496.0 mm in 6 hours at Montenotte Inferiore and 740.6 mm in 12 hours at Rossiglione.

Persistent above-average rainfall in the first half of the year in parts of Northern South America, particularly the northern Amazon basin, led to significant and long-lived flooding in the region. The Rio Negro at Manaus (Brazil) reached its highest level on record, peaking at 30.02 m on 20 June.[81] The most

[77] RM 114.3 billion, from China's national contribution

[78] National contribution, Germany

[79] http://www.bom.gov.au/climate/current/statements/scs74.pdf?20210621

[80] https://reliefweb.int/disaster/fl-2021-000050-afg

[81] http://www.cprm.gov.br/sace/boletins/Amazonas/20211022_11-20211025%20-%20114229.pdf

widespread flooding was reported in northern Brazil, but Guyana, Bolivarian Republic of Venezuela and Colombia were also affected.

The progress and withdrawal of the Indian Monsoon was delayed, but overall Indian monsoon rainfall was close to average, with above-average rainfalls in the west offset by below-average values in the north-east. During the course of the season, 529 deaths in India and 198 in Pakistan (as of 30 September) were attributed to flooding, with further deaths in Bangladesh and Nepal.[82] There was further flooding in eastern India and Nepal during the north-east monsoon season in October and November. In Eastern Asia, eastern China (except for Henan) was generally less wet during the monsoon season than in 2020, but August was extremely wet in Japan. Western Japan had its wettest August on record,[83] with some locations receiving more than 1400 mm of rain between 11 and 26 August. A tropical depression made landfall in Malaysia on 16 December, leading to severe flooding in Selangor and Kuala Lumpur, with at least 52 deaths reported. At Kuala Lumpur International Airport, 230 mm of rain was reported in 12 hours on 17–18 December.[84]

The rainy season in the African Sahel was generally close to the average (1951–2000), and less wet than in some recent years, although there was still some significant flooding reported, especially in Niger, Sudan and South Sudan as well as Mali. Elsewhere in Africa, Lake Tanganyika rose to more than 3 m above its normal level in May,[85] displacing lakeshore residents in Burundi, while Lake Victoria rose to its highest level since satellite data began in 1992, surpassing its peak from the previous year. High flows in the Nile downstream of Lake Victoria, along with substantial standing water still remaining from floods in 2020, contributed to continued flooding in parts of South Sudan and Sudan despite near-normal rainfall in 2021. In Southern Africa, much of which had been experiencing long-term drought, rainfall during the 2020/2021 rainy season was above average in some regions, including northern South Africa and Zimbabwe, with some flooding reported, but was near or below average further north.

Western Canada was affected by severe flooding in November. At numerous locations in southern British Columbia 200 to 300 mm of rain fell in 60 hours, causing floods and landslides (in some cases exacerbated by runoff from fire-affected areas). Transport was severely disrupted, with most major routes connecting Vancouver with the rest of Canada closed for several weeks, and several communities were partly or wholly inundated. Six deaths were reported, and economic losses exceeded Can$ 2 billion. Flooding also affected adjacent areas of the north-western United States. Seattle and Vancouver both had their wettest autumns on record.

DROUGHT

Significant drought affected much of subtropical South America for the second successive year. Rainfall was well below average over much of central and southern Brazil,[86] Paraguay, Uruguay and northern Argentina. The drought led to significant agricultural losses, exacerbated by a cold outbreak at the end of July, in which maximum temperatures were below 10 °C for five consecutive days over higher parts of southern Brazil and which contributed to damage in many of Brazil's coffee-growing regions. Low river levels also reduced hydroelectricity production[87] and disrupted river transport. The Brazilian government declared a situation of critical scarcity of water resources in the Paraná

[82] National contributions of India and Pakistan; EM-DAT has 120 deaths in Nepal over two incidents and 21 in Bangladesh from one

[83] https://ds.data.jma.go.jp/tcc/tcc/news/press_20210924.pdf

[84] https://reliefweb.int/disaster/fl-2021-000209-mys

[85] https://reliefweb.int/disaster/fl-2021-000039-bdi

[86] https://clima.inmet.gov.br/prec

[87] http://www.ons.org.br/Paginas/Noticias/20210707-escassez-hidrica-2021.aspx

hydrographic region, with numerous water stores at or near their lowest levels in the last 20 years.[88] The 24-month Standardized Precipitation Index (SPI) over the region reached its lowest level since the 1960s. The Paraguay River at Asuncion fell to a record low 0.75 m below the reference level on 6 October, 0.21 m below the previous record set in 2020. In Chile, where long-term drought has persisted for the last decade, 2021 was another dry year, with most locations having rainfall at least 30% below average. A number of locations south of Santiago had their driest year on record in 2021 with totals 40% to 50% below normal, including Concepción (559.2 mm), Valdivia (949.0 mm) and Puerto Montt (921.7 mm).

Widespread drought in Western North America, which had become established during 2020, spread and intensified in 2021. By September, extreme to exceptional drought covered most of the United States over and west of the Rocky Mountains, despite some slight easing from July onwards in parts of the inland south-west, due to an active summer monsoon. Extreme to exceptional drought also extended eastwards on both sides of the United States–Canada border, affecting northern border states as far east as Minnesota and the Prairie Provinces of Canada. The 20 months from January 2020 to August 2021 were the driest on record for the south-western United States,[89] with precipitation more than 10% below the previous record. Forecast wheat and canola crop production for Canada in 2021 was 35% to 40% below 2020 levels,[90] while in the United States, the level of Lake Mead on the Colorado River fell in July to 47 m below full supply level, the lowest level on record since the reservoir was fully commissioned. The drought situation in California was eased by heavy rain in late October and December – Sacramento had its wettest day on record with 138 mm on 24 October, only days after ending a record 211-day period with no measurable precipitation – but drought continued away from the west coast and extended farther east through the south-central United States as the year ended.

Significant drought affected large areas of South-west Asia during 2021. Well-below-average precipitation fell during the 2020/2021 cool season in regions including most of the Islamic Republic of Iran, Afghanistan, Pakistan, south-east Turkey, and Turkmenistan. Pakistan had its third-driest February and fifth-driest January–March on record. Mountain snowpack was also well below average, with snow cover extent in Islamic Republic of Iran about half the long-term average for most of January and February, leading to reduced streamflow in rivers depending on snowmelt, and reduced water availability for irrigation.

Drought developed during the course of the year in the Greater Horn of Africa region, particularly affecting Somalia, Kenya and parts of Ethiopia, after three successive below-average rainy seasons. The October–December rainy season was especially poor, despite some rains in Kenya late in the season.

A severe drought, which has persisted for at least two years, continues to affect southern Madagascar.[91] Rainfall for the 12 months from July 2020 to June 2021 was around 50% below normal over the region. There were significant food security issues in the area, with 1.14 million people classified by the World Food Programme as needing urgent assistance as of August 2021.[92]

TROPICAL CYCLONES

Tropical cyclone activity around the globe in 2021 was close to average (1981–2010). For the second successive year, the North Atlantic

[88] https://www.gov.br/ana/pt-br/assuntos/noticias-e-eventos/noticias/ana-declara-situacao-de-escassez-quantitativa-dos-recursos-hidricos-da-regiao-hidrografica-do-parana

[89] https://www.drought.gov/news/new-noaa-report-exceptional-southwest-drought-exacerbated-human-caused-warming

[90] https://www150.statcan.gc.ca/n1/daily-quotidien/210914/dq210914b-eng.htm

[91] https://reliefweb.int/sites/reliefweb.int/files/resources/cb7310en.pdf

[92] https://reliefweb.int/sites/reliefweb.int/files/resources/WFP%20Madagascar%20Country%20Brief%20-%20August%202021.pdf

had a very active season, with 21 named storms, well above the 1981–2010 average of 14. It was also an active season in the North Indian Ocean, but activity in the western North Pacific and eastern North Pacific was near to or below average. The 2020/2021 southern hemisphere season was also slightly below average in both the Pacific and Indian Oceans.

The most significant hurricane of the North Atlantic season was *Ida*. *Ida* made landfall as a category 4 system in Louisiana (United States) on 29 August with sustained one-minute winds of 240 km per hour, equalling the strongest landfall on record for the state, with major wind damage and storm surge inundation. The system then continued on a north-east track over land with significant flooding, especially in the New York City area. New York, which had already experienced flooding from Hurricane *Henri* two weeks earlier, had a record hourly rainfall of 80 mm, with 24-hour totals exceeding 200 mm in parts of the city. Before it developed into a tropical cyclone, *Ida's* precursor system also caused significant flooding in Venezuela. In total, 72 deaths were directly attributed to *Ida* and 43 deaths were indirectly attributed to it in the United States and Venezuela, with economic losses in the United States estimated at US$ 75 billion.[93] Another significant landfall during the season was *Grace*, which hit Veracruz (Mexico) as a category 3 hurricane, having earlier resulted in impacts, mostly from flooding, in Haiti (where it hindered post-earthquake recovery), the Dominican Republic, Jamaica, and Trinidad and Tobago.

In the southern hemisphere, 2021's most significant cyclone[94] was *Seroja* in April. *Seroja* formed south of Indonesia and tracked south-east towards Western Australia. It made landfall near Kalbarri on 11 April as an (Australian) category 3 cyclone, the strongest landfall so far south in Western Australia since 1956. *Seroja's* most severe impacts were from flooding and associated landslides from its precursor system in Timor-Leste, and the Indonesian region of East Nusa Tenggara. Kupang (Timor) received 700.4 mm of rainfall in the four days from 2 to 5 April. A total of 226 deaths were associated with *Seroja*, 181 in Indonesia, 44 in Timor-Leste and one in Australia.[95] In January, *Eloise* contributed to flooding in Southern Africa, with damage and casualties reported in Mozambique, South Africa, Zimbabwe, Eswatini and Madagascar, while in the South Pacific, *Ana* and *Niran* caused flooding and power outages in Fiji and New Caledonia, respectively.

The most severe cyclone of the North Indian Ocean season was *Tauktae*, which tracked north off the west coast of India, with a peak three-minute sustained wind speed[96] of 50–53 m per second, before making landfall in Gujarat on 17 May at slightly below peak intensity, equalling the strongest known landfall in Gujarat. At least 144 deaths were reported in India and 4 in Pakistan.[97] Later in the season, Cyclone *Gulab* crossed the eastern coast of India from the Bay of Bengal in late September; the remnant system crossed India before emerging and re-intensifying in the Arabian Sea, where it was renamed *Shaheen*. *Shaheen* made landfall on 3 October on the northern coast of Oman north-west of Muscat, the first cyclone since 1890 to make landfall in this area. Al Suwaiq recorded 294 mm rain in 24 hours, about three times the region's annual average. A total of 39 deaths were reported across India, Pakistan, Oman and the Islamic Republic of Iran, mostly from flooding.

The most significant tropical cyclone of the season in the western North Pacific was Typhoon *Rai* (*Odette*), which crossed the central Philippines on 16 December, making landfall at near peak intensity, with a minimum central pressure of 915 hPa, after rapidly intensifying prior to landfall. It reintensified on 18 December after entering the South

---

[93] https://www.ncdc.noaa.gov/billions/events/US/2021

[94] Tropical Cyclone *Yasa* (December 2020) forms part of 2020/2021 seasonal statistics but was reported on in the 2020 State of the Climate.

[95] https://reliefweb.int/disaster/tc-2021-000033-idn

[96] https://rsmcnewdelhi.imd.gov.in/uploads/report/26/26_e0cc1a_Preliminary%20Report%20on%20ESCS%20TAUKTAE-19july.pdf

[97] From national contributions

China Sea, before weakening and dissipating without making further landfall. Severe damage occurred across the Philippines, with at least 406 deaths reported, while flooding also occurred in Viet Nam. There were several other significant landfalls, most notably from Typhoon *Chanthu* on the Batanes Islands (the Philippines). *Chanthu* and Typhoon *In-fa*, in July, also both contributed to flooding and disruptions to shipping around Shanghai, while *Dianmu* contributed to flooding in Thailand in September after making landfall in Viet Nam.

SEVERE STORMS

There were multiple severe thunderstorm outbreaks in Western and Central Europe in the second half of June and in July. An F4 tornado[98] struck several villages in southern Moravia on 24 June, with major damage and six deaths reported. This was the strongest tornado on record in the Czech Republic. Tornadoes were also reported during the month in Belgium, France and Poland. Large hail (6–8 cm in diameter) was reported in multiple countries, including the Czech Republic, Slovakia, Switzerland and Germany. In the Czech Republic alone, losses were around US$ 700 million.

In the United States, 1 376 tornadoes were provisionally reported during 2021, above the 1991–2010 average. A significant outbreak hit the south-east on 25 March, with the most severe impacts in Alabama and western Georgia. Six deaths and US$ 1.8 billion in economic losses were reported. During December 2021, there were 193 confirmed tornado reports, around eight times the 1991–2010 December average of 24. This was double the previous record of 97 from 2002. On 10 December there was an historic outbreak across several south-eastern and central states in which 93 people died and economic losses of US$ 3.9 billion were reported. This was the deadliest December tornado outbreak in the United States, surpassing the Vicksburg, Mississippi tornado of 5 December 1953, which led to 38 deaths. Hailstorms in Texas and Oklahoma on 27–28 April resulted in US$ 3.3 billion in losses.

ATTRIBUTION

Attribution of individual extreme events can often take several months because of the need to complete peer review. But it is becoming increasingly possible to carry out near-real-time attribution assessments that use peer-reviewed methods to reach conclusions within just a few days of a weather record being broken. Such "rapid attribution" studies have been carried out for the heatwave in Western North America in June and July,[99,100,101] the floods in Western Europe in July[102] and the British Columbia floods in November.[103] Studies of the Western North America heatwave found that while such a heatwave is rare in today's climate, it would have been virtually impossible without climate change.

---

[98] On both the Fujita scale and the Enhanced Fujita scale, a tornado that causes devastating damage is classified as category 4 tornado (F4 and EF4 respectively). The scales differ in the wind speeds thought to be associated with "devastating damage", with lower wind speeds assumed in the enhanced system for the same level of damage.

[99] https://www.worldweatherattribution.org/western-north-american-extreme-heat-virtually-impossible-without-human-caused-climate-change/

[100] Philip, S. Y.; Kew, S. F.; van Oldenborgh, G. J. et al. Rapid Attribution Analysis of the Extraordinary Heatwave on the Pacific Coast of the US and Canada June 2021. *Earth System Dynamics Discussions*, In review, 1–34. Preprint: https://doi.org/10.5194/esd-2021-90.

[101] Christidis N., 2021. *Using CMIP6 Multi-model Ensembles for Near Real-time Attribution of Extreme Events*; Hadley Centre Technical Notes 107. United Kingdom Met Office Hadley Centre: Exeter, 2021. https://digital.nmla.metoffice.gov.uk/IO_e2e76d02-d72e-49d6-8419-728fb313d075/; https://blog.metoffice.gov.uk/2021/06/29/heatwave-record-for-pacific-north-west/

[102] https://www.worldweatherattribution.org/heavy-rainfall-which-led-to-severe-flooding-in-western-europe-made-more-likely-by-climate-change/

[103] Gillett, N.; Cannon, A.; Malinina, E. et al. *Human Influence on the 2021 British Columbia Floods*; SSRN Scholarly Paper ID 4025205; Social Science Research Network: Rochester, 2022. https://doi.org/10.2139/ssrn.4025205.

For the Western Europe flooding, the rapid attribution study found that the detection of trends in extreme precipitation at the scale of the event in question was challenging, and that saturated soils and the local hydrology were also factors in the event. However, significant trends in extreme precipitation were found across a wider area of Western Europe, and the study concluded that over this broader region, human-induced climate change had increased the likelihood of an extreme precipitation event comparable to that which occurred.

More generally, events such as these fit into a broader pattern of change. The IPCC assessed[104] that hot extremes in the regions of Western North America and North-western North America have increased, and that there is at least medium confidence in a human contribution to this increase. Similarly, the IPCC assessed that heavy precipitation has increased in the region of Western and Central Europe affected by flooding, but that there is currently low confidence in the attribution of this change to human influence.

[104] Intergovernmental Panel on Climate Change (IPCC), 2021: Summary for Policymakers. In: *AR6 Climate Change 2021: The Physical Science Basis*, https://www.ipcc.ch/report/ar6/wg1/downloads/report/IPCC_AR6_WGI_SPM_final.pdf.

Risks and impacts

The risk of climate-related impacts depends on complex interactions between climate-related hazards and the vulnerability, exposure and adaptive capacity of human and natural systems. Climate-related events pose humanitarian risks to society through impacts on health, food and water security as well as human security, human mobility, livelihoods, economies, infrastructure and biodiversity. Climate and extreme weather events also affect the use and distribution of natural resources across regions and within countries, and have large negative impacts on the environment. These negative environmental effects include impacts on the land such as droughts, wildfires in forest and peatland areas, land degradation, sand and dust storms, desertification, flooding and coastal erosion. At current levels of global greenhouse gas emissions, the world remains on course to exceed the agreed temperature thresholds of either 1.5 °C or 2 °C above pre-industrial levels, which would increase the risks of pervasive climate change impacts beyond what is already being seen.

FOOD SECURITY

GLOBAL FOOD SECURITY OUTLOOK IN 2021

The compounded effects of conflict, extreme weather events and economic shocks, further exacerbated by the COVID-19 pandemic, have led to a rise in hunger, undermining decades of progress towards improving food security (Figure 22). Worsening humanitarian crises in 2021 have also caused the number of countries at risk of famine to grow. Of the total number of undernourished people in 2020, more than half live in Asia (418 million) and a third in Africa (282 million). Following a peak in undernourishment in 2020 (768 million people), projections indicated a decline in global hunger to around 710 million in 2021 (9% of the world population).[105] However, as of October 2021, the numbers in many countries were already higher than in 2020. This striking increase was mostly felt among groups already suffering from food crises

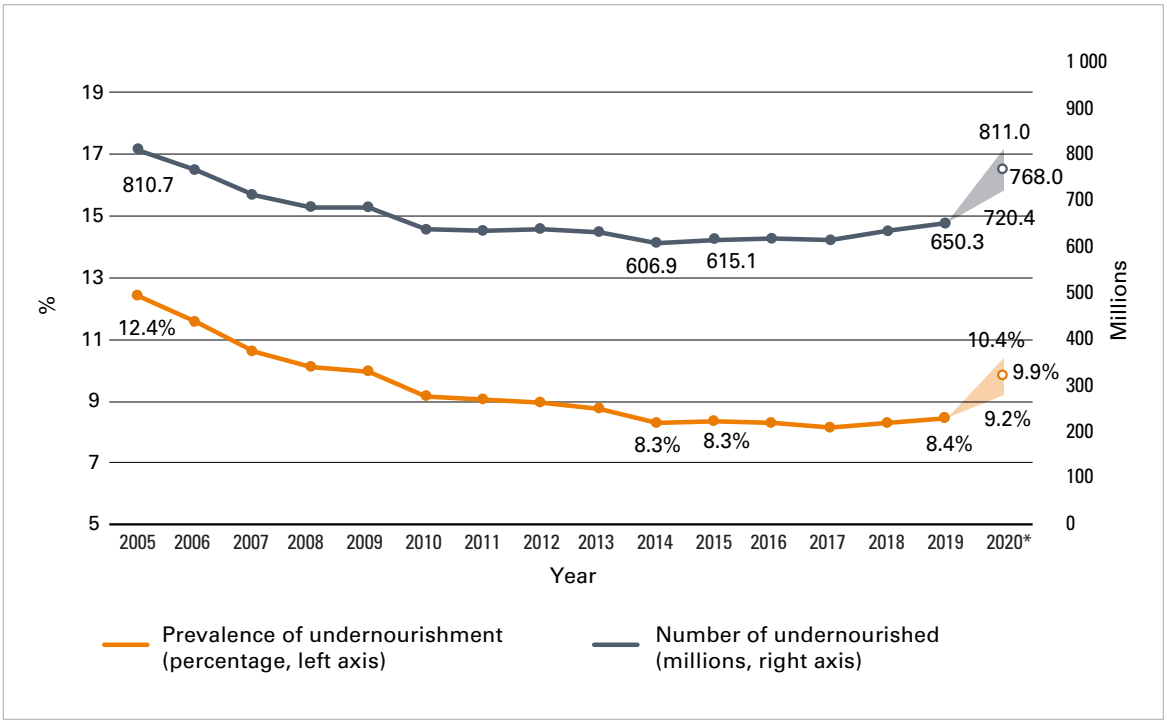

Figure 22. The number of undernourished people in the world significantly increased during the COVID-19 pandemic, from 650 million people in 2019 to 768 million people in 2020. Dotted lines and empty circles illustrate projected values in the figure. *Source:* Food and Agriculture Organization of the United Nations (FAO).

[105] Food and Agriculture Organization of the United Nations (FAO), 2021: *The State of Food Security and Nutrition in the World 2021: Transforming Food Systems for Food Security, Improved Nutrition and Affordable Healthy Diets for All*, https://docs.wfp.org/api/documents/WFP-0000130141/download/?_ga=2.47516911.931354890.1634299853-763856357.1633873374.

or worse (IPC/CH Phase 3 or above[106]); the number of people in these groups rose from 135 million in 2020 to 161 million by September 2021, a 19% increase.[107] Another consequence of these shocks was growth in the number of people facing starvation and a total collapse of livelihoods (IPC/CH Phase 5); a total of 584 000 people were in this group, mostly in Ethiopia, South Sudan, Yemen and Madagascar. The first quarter of 2021 also saw the highest global consumer food prices in the last six years, concentrated in Latin America and the Caribbean.[108] In West Africa, prices of coarse grains increased, driving food prices to record and near-record highs in several countries. The price increases were exacerbated by civil insecurity and torrential rains. In North Africa, food inflation rates remained at modest levels in 2021, buffered by subsidies on many basic commodities that prevented price increases.

IMPACTS OF HYDRO-METEOROLOGICAL HAZARDS ON FOOD PRODUCTION

The 2020/2021 La Niña altered rainfall seasons, disrupting livelihoods and agricultural campaigns across the world. Associated extreme weather, water and climate events during the 2021 rainfall season compounded shocks from the previous year or years, making it increasingly difficult to quantify impacts resulting from a single event. Consecutive droughts across large parts of Africa, Asia and Latin America associated in places with the double-dip La Niña, as well as regional impacts from severe storms, cyclones and hurricanes, have significantly affected livelihoods and the ability to recover from recurrent weather shocks.

Dry conditions across wide areas of South America could further threaten crop yields within this region. However, larger plantings have largely compensated for crop productivity losses throughout the continent (–3.6% in 2021 compared to 2020).[109] In the Caribbean, Haiti has been triply hit – by earthquakes, irregular rains and political instability – contributing to agricultural damage and significantly worsening food insecurity.

In West Africa, floods and dry spells have led to crop damage and losses in localized areas resulting in small production downturns in 2021, but the forecasted aggregate outputs for the whole continent of Africa remained above average (+2.9% in 2021 over 2020).[110] The 2021 first season harvest in central and southern areas of East Africa was negatively affected by prolonged droughts, mostly in Kenya where maize outputs were officially estimated to be 42%–70% below average.[111] In northern parts of East Africa, the scale of seasonal flooding and its impact on crops was lower than in 2020. In Southern Africa, the second consecutive below-average rainfall season in Madagascar has led to a severe reduction in staple food production and a decline in livestock herd size. In addition, weather-related hazards, pests and diseases were expected to result in sharp harvest declines, with yield estimates

---

[106] The Integrated Food Security Phase Classification (IPC) is a common global scale for classifying the severity and magnitude of food insecurity and malnutrition. https://www.ipcinfo.org/ipcinfo-website/resources/ipc-manual/en/. The Cadre Harmonisé (CH) is a unifying tool for classifying the nature and severity of current and projected acute food and nutrition insecurity.

[107] Global Network Against Food Crises, 2021: *Global Report on Food Crises: Joint Analysis for Better Decisions. September 2021 Update*, http://www.fightfoodcrises.net/fileadmin/user_upload/fightfoodcrises/doc/resources/FINAl_GRFC2021_Sept_Update.pdf.

[108] Food and Agriculture Organization of the United Nations (FAO), 2021: *The State of Food Security and Nutrition in the World 2021: Transforming Food Systems for Food Security, Improved Nutrition and Affordable Healthy Diets for All*, https://docs.wfp.org/api/documents/WFP-0000130141/download/?_ga=2.47516911.931354890.1634299853-763856357.1633873374.

[109] Food and Agriculture Organization of the United Nations (FAO), 2021: *Crop Prospects and Food Situation: Quarterly Global Report*, https://www.fao.org/3/cb6901en/cb6901en.pdf.

[110] Food and Agriculture Organization of the United Nations (FAO), 2021: *Crop Prospects and Food Situation: Quarterly Global Report*, https://www.fao.org/3/cb6901en/cb6901en.pdf.

[111] Food and Agriculture Organization of the United Nations (FAO), 2021: *Crop Prospects and Food Situation: Quarterly Global Report*, https://www.fao.org/3/cb6901en/cb6901en.pdf.

50%–70% below the five-year average.[112] In Mozambique, Cyclone *Eloise* made landfall in late January during the region's lean season, when vulnerabilities are at their highest, affecting communities still recovering from Cyclone *Idai* barely two years ago. According to the Government of Mozambique, more than 441 000 people were affected by the cyclone, which displaced nearly 44 000 and destroyed more than 45 000 hectares of cropland.[113]

Drought conditions in South-west Asia and the Middle East reduced cereal production to below-average levels, exacerbating the impacts on agriculture and food security in fragile contexts, mostly in Afghanistan and the Syrian Arab Republic. While cereal production decreased in the Middle East, wheat production in Eastern Asia reached a record high in 2021, with paddy rice outputs at high levels due to suitable weather conditions. In contrast, central China was hit by torrential rains in mid-July 2021, leading to significant loss of life and damage to property. This sparked concerns over the nation's food supplies, as 1 million hectares of cropland – mostly corn, soybeans and peanuts – were affected, a third of which was wiped out by heavy rains.

HUMANITARIAN IMPACTS AND POPULATION DISPLACEMENT

Refugees, internally displaced people and stateless people are often among those most vulnerable to climate and weather-related hazards. Many vulnerable individuals who are displaced end up settling in high-risk areas, where they are exposed to climate and weather hazards at a range of scales. Hydrometeorological hazards and human mobility may also intersect with social and political tensions and conflict in complex settings and, therefore, require the integrated consideration of multi-hazard disaster risk reduction measures, including early warning systems and preparedness, and longer-term sustainable development concerns, such as land use and urban planning.

CLIMATE-RELATED HAZARDS WERE A MAJOR DRIVER OF NEW DISPLACEMENT

Extreme weather, water and climate events and conditions had major and diverse impacts on population displacement and on the vulnerability of people already displaced throughout the year. From Afghanistan to Central America, droughts, flooding and other extreme events hit those least equipped to recover and adapt.[114] As in previous years, many of the largest-scale displacements in 2021 occurred in populous Asian countries. Most disaster displacements in 2021 resulted from tropical storms and floods in East Asia and the Pacific, South Asia, the Americas and Sub-Saharan Africa.

Over the course of 2021, hazardous hydrometeorological events and environmental degradation further contributed to the displacement of millions more people in exposed and vulnerable situations. This includes the impact of rapid-onset events such as floods, storms and wildfires, as well as slow-onset processes such as drought and desertification. This affects people's safety and ability to meet their basic needs for survival such as food, water, resilient housing and productive land. Over the first half of the year in Afghanistan, for example, disasters resulted in some 22 500 new displacements, primarily linked to floods.[115] In June, the Government declared a national drought, with 80% of the country classified as being in either severe or serious drought status, on top of escalating conflict, food insecurity, and health and socioeconomic impacts of COVID-19, with humanitarian, development and government actors foreseeing that

[112] Famine Early Warning Systems Network (FEWSNET), 2021: *Madagascar Food Security Alert*, https://reliefweb.int/sites/reliefweb.int/files/resources/Madagascar%20Food%20Security%20Alert%20-%20June%2010%2C%202021.pdf.

[113] https://www.fao.org/mozambique/news/detail-events/en/c/1393190/

[114] https://www.unhcr.org/news/stories/2021/4/60806d124/data-reveals-impacts-climate-emergency-displacement.html

[115] https://story.internal-displacement.org/2021-midyear-review/index.html

agricultural families would very likely become displaced.[116] People forced to leave their homes had to sell their assets and engage in dangerous work to survive, while some children were sent to work in other areas or in neighbouring countries or were married off as a way to reduce financial burdens.[117] Displaced people in the Syrian Arab Republic, a country decimated by over a decade of conflict, also faced flooding due to heavy rainfall, with close to 142 000 internally displaced people affected in mid-January 2021.[118] In India, more than 100 000 people were displaced between November and December 2021.[119]

In line with established trends, 2021 saw the overwhelming majority of new displacements related to hazardous weather events take place within national borders. Most of these internal displacements were triggered by tropical cyclones, floods, earthquakes and volcanic eruptions, especially in the East Asia and Pacific region. The countries with the largest numbers of displacements recorded as of October 2021 were China (more than 1.4 million displacements recorded in July), Viet Nam (more than 664 000 recorded in September), and the Philippines (more than 214 000 in July and more than 386 000 in October).[120]

In East Africa, floods and droughts resulted in large-scale displacement, especially in Somalia and Ethiopia. Many of the people affected were already living in overcrowded and insecure camps for internally displaced people to which many newly flood-displaced people also moved. Farmers whose crops were devastated by desert locusts were also forced to move in search of survival assistance.[121] In Sudan, Alganaa refugee camp was submerged by flood waters in November 2021, leaving 35 000 South Sudanese refugees in need of urgent assistance.[122]

High-income countries were also affected. In the western parts of the United States and Canada exceptional heatwaves, drought and wildfires displaced thousands from their homes. Wildfires also compounded risks related to other hazards, further increasing the risk of displacement. For instance, 15 000 people were displaced in California in January 2021, following mandatory pre-emptive evacuation orders following heavy rains.[123]

PROTRACTED, PROLONGED AND REPEATED DISPLACEMENT FUELLED BY HYDROMETEOROLOGICAL HAZARDS

Many displacement situations triggered by hydrometeorological events have become prolonged or protracted for people unable to return to their former homes or without options for integrating locally or settling elsewhere. At the beginning of 2021, at least 7 million people were living in internal displacement following disasters[124] related to natural hazard events in previous years, according to the Internal Displacement Monitoring Centre (IDMC). The largest numbers of people in this situation were in Afghanistan, India and Pakistan, followed by Ethiopia, Sudan, Bangladesh, Niger and Yemen.[125]

Due to continuing or growing risk in their areas of origin (and return) or settlement, people who have been displaced by hydrometeorological events may also be subject to repeated and frequent displacement, leaving

[116] https://prod.drc.ngo/about-us/for-the-media/press-releases/2021/7/drought-crisis-in-afghanistan-intensifies-risk-of-displacement

[117] https://prod.drc.ngo/about-us/for-the-media/press-releases/2021/7/drought-crisis-in-afghanistan-intensifies-risk-of-displacement

[118] https://reliefweb.int/disaster/fl-2021-000007-syr

[119] https://www.internal-displacement.org/global-displacement-map

[120] https://www.internal-displacement.org/global-displacement-map

[121] https://www.unhcr.org/news/stories/2021/8/611a2bca4/displaced-somalis-refugees-struggle-recover-climate-change-brings-new-threats.html

[122] https://www.unhcr.org/news/stories/2021/11/619c9aea4/refugees-count-losses-floods-destroy-camp-sudan.html

[123] https://story.internal-displacement.org/2021-midyear-review/index.html

[124] https://www.internal-displacement.org/sites/default/files/publications/documents/grid2021_idmc.pdf

[125] https://www.internal-displacement.org/global-displacement-map

little time for recovery between one shock and the next. In Indonesia, for example, 557 000 new disaster displacements were recorded in the first half of the year, mostly triggered by major rainy season floods. Human activities, including deforestation, urbanization and land degradation have reduced the capacity of some regions of Indonesia to absorb heavy rainfall. Between October and November 2021, well before the peak of the rainy season, heavy rainfall and flooding further displaced more than 50 000, double the figure for 2020.[126] Such situations highlight the importance of disaster preparedness and risk management, but also the importance of supporting solutions to displacement that are sustainable and supporting the resilience of people who might otherwise see their living conditions progressively eroded through repeated disasters and displacement.

HAZARDOUS EVENTS AND CHANGING CLIMATIC CONDITIONS ALSO ADDED TO THE MULTIPLE RISKS FACED IN CONFLICT-AFFECTED COUNTRIES BY INTERNALLY DISPLACED PEOPLE AND REFUGEES

In Yemen, people's vulnerabilities were further exacerbated by hazard events, such as floods and droughts, that have led to the destruction of shelters and infrastructure, restricted access to markets and basic services, wrecked livelihoods, facilitated the spread of deadly diseases and contributed to fatalities. In mid-April, heavy rain and flooding hit several parts of the country, affecting 7 000 people, 75% of whom were internally displaced people living in precarious conditions.[127] This contributed to population displacement in what was already the world's fourth biggest internal displacement crisis, with over 4 million internally displaced people. The annual rainy season brings heavy rainfall, high winds and flooding, particularly to coastal areas, with thousands of families affected by flash floods in 2021. Flooding also blocks roads, impeding the delivery of life-saving assistance.[128]

In Mozambique, multiple tropical storms and floods, on top of recurrent disease outbreaks and conflict, significantly increased the vulnerability of affected people,[129] including thousands of families still displaced since Cyclones *Idai* and *Kenneth* in 2019. In January, strong winds and floods from Tropical Storm *Chalane* and then Cyclone *Eloise* damaged or destroyed the shelters of over 8 700 of these internally displaced families as well as schools and hospitals.[130] These events also resulted in new displacement, with Cyclone *Eloise* displacing more than 43 300 people.[131] Tens of thousands of people remain displaced and held back from recovery.[132] The impacts of compounding disasters, recurrent disease outbreaks and conflicts have significantly increased the vulnerability of people in the region. This situation, and similar ones in other regions, could be ameliorated through greater effort to reduce climate-related vulnerability and risks in fragile and conflict-affected contexts and to strengthen community-based preparedness.[133]

Nigeria also experienced drought and floods, which affected agricultural activities, resulting in loss of shelter and increased vulnerability of people already displaced by conflict in the north-east. The situation further deteriorated in the first half of 2021, with around 294 000 new displacements reported between January and June 2021.[134]

---

[126] https://story.internal-displacement.org/10-internal-displacement-situations-to-watch-in-2022/index.html

[127] https://reliefweb.int/sites/reliefweb.int/files/resources/Humanitarian%20Update_May%202021%20v4.pdf

[128] https://reliefweb.int/report/yemen/climate-crisis-exacerbates-humanitarian-situation-yemen-enar

[129] https://www.unhcr.org/news/briefing/2021/4/606c17bf4/unhcr-scales-response-thousands-flee-attacks-northern-mozambique.html

[130] https://displacement.iom.int/reports/mozambique-%E2%80%93-flash-report-16-tropical-cyclone-eloise-january-2021?close=true

[131] https://reliefweb.int/report/afghanistan/internal-displacement-mid-year-10-situations-review

[132] https://www.unhcr.org/news/stories/2020/3/5e6a6e50b/year-people-displaced-cyclone-idai-struggle-rebuild.html

[133] https://www.unhcr.org/news/stories/2020/3/5e6a6e50b/year-people-displaced-cyclone-idai-struggle-rebuild.html

[134] https://www.unhcr.org/news/stories/2020/3/5e6a6e50b/year-people-displaced-cyclone-idai-struggle-rebuild.html

In Bangladesh, monsoon rains led to massive flooding and the displacement of millions of people following Cyclone *Yaas* in May and June 2021. Flooding in July 2021 in the Rohingya refugee sites in Cox's Bazar damaged over 6 000 shelters and more than 25 000 refugees were forced to seek shelter in communal facilities or with other families.[135] Floods also heavily affected people living in China, Nepal and the Philippines, where thousands of people were displaced by Typhoon *In-fa* in July 2021. Without preparedness measures undertaken in the camp areas, including the strengthening of shelters, the building of retaining structures on hillsides and improved drainage, roads and bridges, these impacts would have been far worse.

CLIMATE IMPACTS ON ECOSYSTEMS

Ecosystems – including terrestrial, freshwater, coastal and marine ecosystems – and the services they provide, are affected by the changing climate, and some are more vulnerable than others.[136] In addition, some ecosystems are degrading at an unprecedented rate, limiting their ability to support human well-being and harming their adaptive capacity to build resilience.[137]

For example, mountain ecosystems – the water towers of the world – are vulnerable and can be profoundly affected by climate change due to their low capacity to adapt. This may affect the 1.9 billion people living in mountain areas or directly downstream from them.[138] Climate change may exacerbate water stress, especially in areas of decreased precipitation and where groundwater is already depleted, affecting agricultural production, arable land, and the more than 2 billion people who already experience water stress.[139]

Climate change is also affecting climate-sensitive species. There is evidence that temperature-sensitive plants are flowering and starting to produce leaves earlier in spring and dropping their leaves later in autumn.[140] Also, there has been a clear shift in the timing of marine and freshwater fish spawning events and animal migrations worldwide. Substantial changes in species' abundance and distribution may in turn affect the interactions between species.[141,142] Risks to ecosystems and individual species from pests, pathogens and diseases are changing. Climate change also exacerbates other threats to biodiversity. The number of species projected to become extinct increases dramatically as global temperature rises – and is 30% higher at 2 °C warming than at 1.5 °C warming.[143]

Meanwhile, large-scale changes have been observed in marine ecosystems, including declining ocean productivity, migration of species to higher latitudes and altitudes, and damage to coral reefs and mangroves. Warming towards 1.5 °C will increase water temperatures and change the ocean's

---

[135] https://www.unhcr.org/news/stories/2021/7/6103c43c4/floods-bring-new-misery-rohingya-refugees-bangladesh-camps.html

[136] United Nations Environment Programme (UNEP), 2021: *Adaptation Gap Report 2020*, https://www.unep.org/resources/adaptation-gap-report-2020.

[137] United Nations Environment Programme (UNEP), 2021: *Making Peace with Nature: A Scientific Blueprint to Tackle the Climate, Biodiversity and Pollution Emergencies*, https://www.unep.org/resources/making-peace-nature.

[138] Immerzeel, W. W.; Lutz, A. F.; Andrade, M. et al. Importance and Vulnerability of the World's Water Towers. *Nature* **2020**, *577* (7790), 364–369. https://doi.org/10.1038/s41586-019-1822-y.

[139] United Nations Environment Programme (UNEP), 2021: *Making Peace with Nature: A Scientific Blueprint to Tackle the Climate, Biodiversity and Pollution Emergencies*, https://www.unep.org/resources/making-peace-nature.

[140] Hemming, D.L.; Garforth, J.; Park, T. et al. Phenology of Primary Producers. In *State of the Climate in 2020*, supplement. *Bulletin of the American Meteorological Society* **2021**, *102* (8), S57–S60. https://doi.org/10.1175/BAMS-D-21-0098.1.

[141] Scheffers, B. R.; De Meester, L.; Bridge, T.C. et al. The Broad Footprint of Climate Change from Genes to Biomes to People. *Science* **2016**, *354* (6313), aaf7671. https://doi.org/10.1126/science.aaf7671 .

[142] Thackeray, S. J.; Henrys, P. A.; Hemming, D. et al. Phenological Sensitivity to Climate across Taxa and Trophic Levels. *Nature* **2016**, *535* (7611), 241–245. https://doi.org/10.1038/nature18608.

[143] United Nations Environment Programme (UNEP), 2021: *Making Peace with Nature: A Scientific Blueprint to Tackle the Climate, Biodiversity and Pollution Emergencies*, https://www.unep.org/resources/making-peace-nature.

chemistry (for example, acidification), resulting in new ecosystems. Species that are less able to relocate are projected to experience high rates of mortality and decline.[144] Climate change is also affecting the Greenland and Antarctic ice sheets and increasing the chances of the Arctic Ocean being ice-free in the summer, further disrupting ocean circulation and Arctic ecosystems.[145]

Rising temperatures heighten the risk of irreversible loss of marine and coastal ecosystems, including seagrass meadows and kelp forest. Coral reefs are especially vulnerable to climate change. They are projected to lose between 70% and 90% of their former coverage area at 1.5 °C of warming and over 99% at 2 °C. Between 20% and 90% of current coastal wetlands are at risk of being lost by the end of this century, depending on how fast sea levels rise. This will further compromise food provision, tourism and coastal protection, among other ecosystem services.[146]

[144] Intergovernmental Panel on Climate Change (IPCC), 2019: Summary for policymakers. In: *Global Warming of 1.5°C: An IPCC Special Report on the Impacts of Global Warming of 1.5°C above Pre-industrial Levels and Related Global Greenhouse Gas Emission Pathways, in the Context of Strengthening the Global Response to the Threat of Climate Change, Sustainable Development, and Efforts to Eradicate Poverty*, https://www.ipcc.ch/sr15/chapter/spm/.

[145] United Nations Environment Programme (UNEP), 2021: *Making Peace with Nature: A Scientific Blueprint to Tackle the Climate, Biodiversity and Pollution Emergencies*, https://www.unep.org/resources/making-peace-nature.

[146] United Nations Environment Programme (UNEP), 2021: *Making Peace with Nature: A Scientific Blueprint to Tackle the Climate, Biodiversity and Pollution Emergencies*, https://www.unep.org/resources/making-peace-nature.

Northern hemisphere summer extremes: the role of the quasi-stationary planetary waves and the Arctic warming amplification

José Álvaro Silva (WMO)

2021 NORTHERN HEMISPHERE EXTREMES: BRIEF DESCRIPTION

In 2021, during the boreal summer, several extreme weather and climate events occurred in the mid-latitude regions of the northern hemisphere (NH). Record hot days and heatwaves, severe droughts, powerful and destructive wildfires, and heavy rain events led to vast damage and high death tolls, as is described in depth in the section on High-impact events in 2021.

Hot summer conditions started early, and several NH regions experienced extreme heat in June, including North Africa, Eastern Europe and the Middle East. The high temperatures were particularly exceptional in the north-western United States and western Canada in late June (Figure 23). Lytton, in British Columbia, recorded 49.6 °C on 29 June, which was a new record for Canada. On 9 July, during one of the multiple heatwaves that affected the south-western United States during the summer, the Furnace Creek weather station (Death Valley, California), reached 54.4 °C for the second year in a row (the world's highest recorded temperature in at least the last 90 years).

On 14 and 15 July, exceptional severe floods occurred in some countries in the Western part of Europe. Parts of western Germany and eastern Belgium were the most affected by the long-lasting heavy precipitation. Just a few days later, in the Chinese province of Henan, more rain fell on Zhengzhou between 17 and 21 July than falls there in an average year, and a one-hour rainfall total of 201.9 mm, on 20 July, was a new record for China.

In August, the extreme heat was associated with powerful and destructive wildfires that affected some Mediterranean countries. On 11 August, a station near Syracuse, in Sicily, Italy, reached 48.8 °C, a provisional European record.

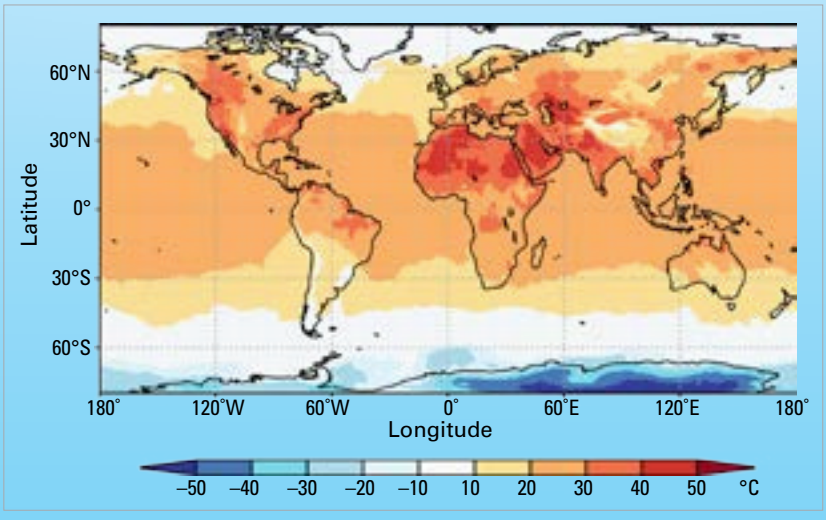

Figure 23. ERA5 reanalysis of maximum air temperature (°C) on 29 June 2021. *Source:* Copernicus Climate Change Service and KNMI Climate Explorer.

POTENTIAL CAUSES AND MECHANISMS OF NORTHERN HEMISPHERE SUMMER EXTREMES

Following the trend that has emerged in recent decades, NH summer 2021 saw numerous weather and climate extremes. But what might be the causes for the increase in number and the intensification of the NH summer extremes?

The frequency of certain types of weather and climate extremes is increasing due to climate change,[1] and some attribution studies[2,3,4,5,6,7,8] have shown that it has made many single recent events more intense. Some of these studies suggest that a wide diversity of spatio-temporal scales and atmospheric processes are involved in the evolution of extreme events, but it is usually the anomalous large-scale circulation patterns that set the background for their occurrence, and quasi-resonant circulation regimes play an important role here.

THE QUASI-RESONANT AMPLIFICATION

There is growing evidence that physical mechanisms involving atmospheric dynamics, in particular planetary wave dynamics, can explain the characteristics associated with persistent disturbances in the polar jet stream and NH summer extremes.[9,10,11] The Rossby waves[12] (Figure 24), particularly the quasi-resonant amplification (QRA)[13] of these mid-latitude high-amplitude waves (zonal wavenumber 6–8), is an important mechanism driving the conditions associated with extremes.[14,15,16] The jet stream plays a major role in shaping weather patterns, and when it becomes weaker and wavier, in association with these slow-moving waves, the air motion from west to east is slowed, leading to blocking situations in which weather systems remain near-stationary over a prolonged period which can last several weeks.[17,18]

ARCTIC WARMING AMPLIFICATION

Over the past 50 years, temperatures in the Arctic have increased at more than twice the global rate,[19] a prominent feature of climate change known as Arctic amplification (AA).[20] The AA influences mid-latitude summer circulation by weakening the storm tracks, shifting the position of the jet stream and amplifying the quasi-stationary waves. While some uncertainties related to how these dynamical changes affect regional weather conditions remain,[21] it is generally accepted that in recent decades the occurrence of conditions favourable for QRA[22,23] promoted the occurrence of persistent extreme weather events that might be linked to the amplified Arctic warming, and thus that climate change influence is carried through amplified arctic warming.[24] Nevertheless, it is argued that the observations and climate-model simulations do not support a clear cause–effect relation, making it difficult to establish a definite link.

The causes of AA are not yet fully understood, but as highlighted in Chapter 4 of the Working Group I contribution to the IPCC Sixth Assessment Report, the understanding of the physical mechanisms driving AA has improved in the last decade, and the results of several studies mentioned in the report identify a variety of processes and positive feedbacks contributing to these phenomena.[25] The first is related to sea-ice loss (Figure 25), which causes a change of surface albedo (reflective ice is replaced by the darker ocean), leading to more heat absorption from solar radiation. This is known as the sea-ice albedo feedback. Other important atmospheric processes inducing AA are the temperature (both Planck and lapse rate) and the cloud and water vapour feedbacks.[26] Increases in the atmospheric and oceanic equator-to-pole transport of heat and moisture have also been identified as drivers of AA.

In summary, research focusing on summer circulation and climate change needs to be further developed to fill important knowledge gaps, but there is evidence to support the idea that changes in mid-latitude summer circulation – amplified and more stationary planetary waves, a weaker and wavier jet stream – associated with Arctic warming, may be linked to increased blocking situations thus favouring the occurrence of extreme events in the NH.

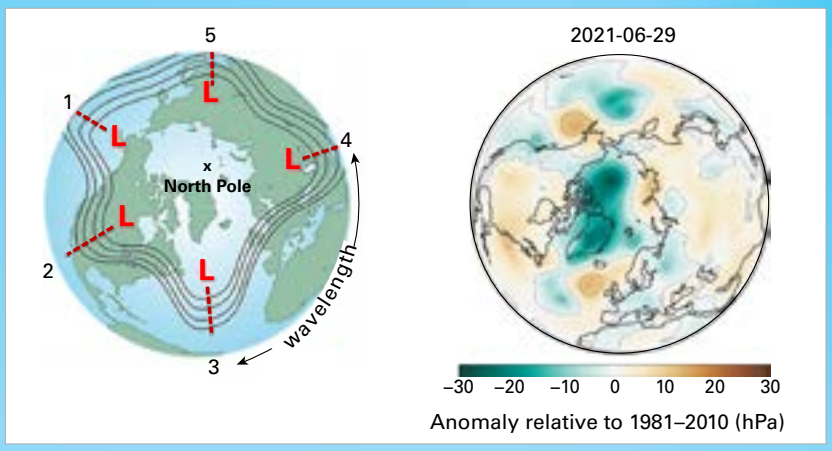

Figure 24. Left: Schematic example of a five planetary-wave pattern. *Source:* NOAA/NWS. Right: Sea level pressure anomaly for 29 June 2021 (difference from 1981–2010), associated with a slow and meandering jet stream. Data from the ERA5 reanalysis product. *Source:* Copernicus Climate Change Service.

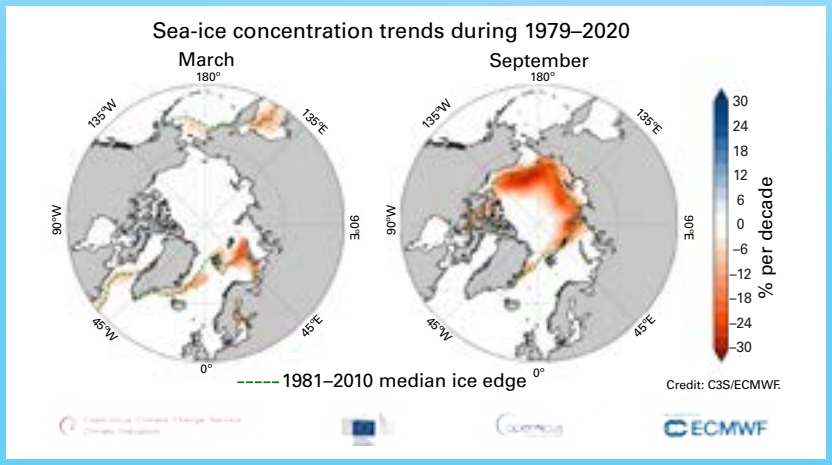

Figure 25. Sea-ice concentration trends in March and September, 1979–2020. *Source:* C3S, https://climate.copernicus.eu/climate-indicators/sea-ice.

REFERENCES

1. Intergovernmental Panel on Climate Change (IPCC), 2021: *AR6 Climate Change 2021: The Physical Science Basis*, https://www.ipcc.ch/report/ar6/wg1/.
2. Philip, S. Y.; Kew, S. F.; van Oldenborgh, G. J. et al. Rapid Attribution Analysis of the Extraordinary Heatwave on the Pacific Coast of the US and Canada June 2021. *Earth System Dynamics Discussions*, In review, 1–34. Preprint: https://doi.org/10.5194/esd-2021-90.
3. Kreienkamp, F.; Philip, S. Y.; Tradowsky, J. S. et al. *Rapid Attribution of Heavy Rainfall Events Leading to the Severe Flooding in Western Europe During July 2021*. World Weather Attribution, 2021. https://www.worldweatherattribution.org/wp-content/uploads/Scientific-report-Western-Europe-floods-2021-attribution.pdf.
4. van Oldenborgh, G. J.; van der Wiel, K.; Kew, S. et al. Pathways and Pitfalls in Extreme Event Attribution. *Climatic Change* **2021**, *166* (1), 13. https://doi.org/10.1007/s10584-021-03071-7.
5. Herring, S. C.; Christidis, N.; Hoell, A. et al., Eds.; Explaining Extreme Events of 2017 from a Climate Perspective. *Bulletin of the American Meteorological Society* **2019**, *100* (1), S1–S117. https://doi.org/10.1175/BAMS-ExplainingExtremeEvents2017.1.
6. Lu, C.; Lott, F.; Sun Y. et al. Detectable Anthropogenic Influence on Changes in Summer Precipitation in China. *Journal of Climate* **2020**, *33* (13), 5357–5369. https://doi.org/10.1175/JCLI-D-19-0285.1.
7. Kahraman, A.; Kendon, E. J.; Chan, S. C. et al. Quasi-stationary Intense Rainstorms Spread across Europe under Climate Change. *Geophysical Research Letters* **2021**, *48* (13), e2020GL092361. https://doi.org/10.1029/2020GL092361.
8. Sun, Y.; Dong, S.; Zhang X. et al. Anthropogenic Influence on the Heaviest June Precipitation in Southeastern China since 1961. In: *Explaining Extremes of 2017 from a Climate Perspective*, supplement. *Bulletin of the American Meteorological Society* **2019**, *100* (1), S79–S84. https://doi.org/10.1175/BAMS-ExplainingExtremeEvents2017.1.
9. Mann, M. E.; Rahmstorf, S.; Kornhuber, K. et al. Projected Changes in Persistent Extreme Summer Weather Events: The Role of Quasi-resonant Amplification. *Sci. Advance* **2018**, *4* (10), eaat3272. https://doi.org/10.1126/sciadv.aat3272.
10. Coumou, D.; Petoukhov, V.; Rahmstorf, S. et al. Quasi-resonant Circulation Regimes and Hemispheric Synchronization of Extreme Weather in Boreal Summer. *Proceedings of the National Academy of Sciences* **2014**, *111* (34), 12331–12336. https://doi.org/10.1073/pnas.1412797111.
11. Petoukhov, V.; Petri, S.; Rahmstorf, S. et al. Role of Quasiresonant Planetary Wave Dynamics in Recent Boreal Spring-to-autumn Extreme Events. *Proceedings of the National Academy of Sciences* **2016**, *113* (25), 6862–6867. https://doi.org/10.1073/pnas.1606300113.
12. A Rossby wave is a large horizontal atmospheric undulation associated with the polar jet stream and separates cold polar air from warm tropical air. These planetary waves play an important role in the poleward transports of energy and moisture.
13. The amplified Rossby waves associated with a meandering jet stream become slow and cause wave resonance known as quasi-resonant amplification (QRA).
14. Petoukhov, V.; Rahmstorf, S.; Petri, S. et al. Quasiresonant Amplification of Planetary Waves and Recent Northern Hemisphere Weather Extremes. *Proceedings of the National Academy of Sciences* **2013**, *110* (14), 5336–5341. https://doi.org/10.1073/pnas.1222000110.
15. Kornhuber, K.; Petoukhov, V.; Petri, S. et al. Evidence for Wave Resonance as a Key Mechanism for Generating High-amplitude Quasi-stationary Waves in Boreal Summer. *Climate Dynamics* **2016**, *49* (5), 1961–1979. https://doi.org/10.1007/s00382-016-3399-6.
16. Kornhuber, K.; Coumou, D.; Vogel, E. et al. Amplified Rossby Waves Enhance Risk of Concurrent Heatwaves in Major Breadbasket Regions. *Nature Climate Change* **2020**, *10* (1), 48–53. https://doi.org/10.1038/s41558-019-0637-z.
17. Teng, H.; Branstator, G.; Wang, H. et al. Probability of US Heat Waves Affected by a Subseasonal Planetary Wave Pattern. *Nature Geoscience* **2013**, *6* (12), 1056–1061. https://doi.org/10.1038/ngeo1988.
18. Grams, C. M.; Binder, H.; Pfahl, S. et al. Atmospheric Processes Triggering the Central European Floods in June 2013, *Natural Hazards and Earth System Sciences* **2014**, *14* (7), 1691–1702. https://doi.org/10.5194/nhess-14-1691-2014.

19. Intergovernmental Panel on Climate Change (IPCC), 2021: *AR6 Climate Change 2021: The Physical Science Basis*, https://www.ipcc.ch/report/ar6/wg1/.
20. Francis, J. A.; Vavrus, S. J. Evidence Linking Arctic Amplification to Extreme Weather in Mid-latitudes. *Geophysical Research Letters* **2012**, *39* (6), L06801. https://doi.org/10.1029/2012GL051000.
21. Coumou, D.; Di Capua, G.; Vavrus, S. et al. The Influence of Arctic Amplification on Mid-latitude Summer Circulation. *Nature Communications* **2018**, *9* (1), 2959. https://doi.org/10.1038/s41467-018-05256-8.
22. Petoukhov, V.; Rahmstorf, S.; Petri, S. et al. Quasiresonant Amplification of Planetary Waves and Recent Northern Hemisphere Weather Extremes. *Proceedings of the National Academy of Sciences* **2013**, *110* (14), 5336–5341. https://doi.org/10.1073/pnas.1222000110.
23. Kornhuber, K.; Petoukhov, V.; Petri, S. et al. Evidence for Wave Resonance as a Key Mechanism for Generating High-amplitude Quasi-stationary Waves in Boreal Summer. *Climate Dynamics* **2016**, *49* (5), 1961–1979. https://doi.org/10.1007/s00382-016-3399-6.
24. Mann, M.; Rahmstorf, S.; Kornhuber, K. et al. Influence of Anthropogenic Climate Change on Planetary Wave Resonance and Extreme Weather Events. *Scientific Reports* **2017**, *7* (1), 45242. https://doi.org/10.1038/srep45242.
25. Intergovernmental Panel on Climate Change (IPCC), 2021: *AR6 Climate Change 2021: The Physical Science Basis*, https://www.ipcc.ch/report/ar6/wg1/.
26. Previdi, M.; Smith, K. L.; Polvani, L. M. Arctic Amplification of Climate Change: A Review of Underlying Mechanisms. *Environmental Research Letters* **2021**, *16* (9), 093003. https://doi.org/10.1088/1748-9326/ac1c29.

Observational basis for climate monitoring

Climate monitoring is performed by a system of observing systems covering the atmosphere, the ocean, hydrology, the cryosphere and the biosphere. Each of these areas is monitored in different ways by a range of organizations. Cutting across all these areas, satellite observations provide major contributions to global climate monitoring.

In 1992, the Global Climate Observing System (GCOS) was established by WMO, the Intergovernmental Oceanographic Commission (IOC) of the United Nations Educational, Scientific and Cultural Organization (UNESCO), the United Nations Environment Programme (UNEP) and the International Science Council (ISC) to coordinate and facilitate the development and improvement of global climate observations. GCOS has identified a set of Essential Climate Variables (ECVs) that together provide the information necessary to understand, model and predict the trajectory of the climate as well as plan mitigation and adaptation strategies (Figure 26). The status of the observational basis for these ECVs is published in regular status reports. GCOS also identifies what is needed to improve the system in implementation reports.

In addition to observations provided by the GCOS-coordinated Global Surface Network (GSN) and Global Upper-Air Network (GUAN), National Meteorological and Hydrological Services (NMHSs) of WMO Members provide a more comprehensive and widespread network of observation, acquired primarily for operational weather prediction. WMO's Global Basic Observing Network (GBON), a globally designed network with prescribed capabilities and observing schedules and for which international data exchange is mandatory, will provide critically needed observations for numerical weather prediction and will help substantially strengthen climate monitoring.

In order to provide the necessary financial and technical assistance for the implementation and operation of GBON in the poorest and most poorly observed areas of the globe, WMO and the members of the Alliance for

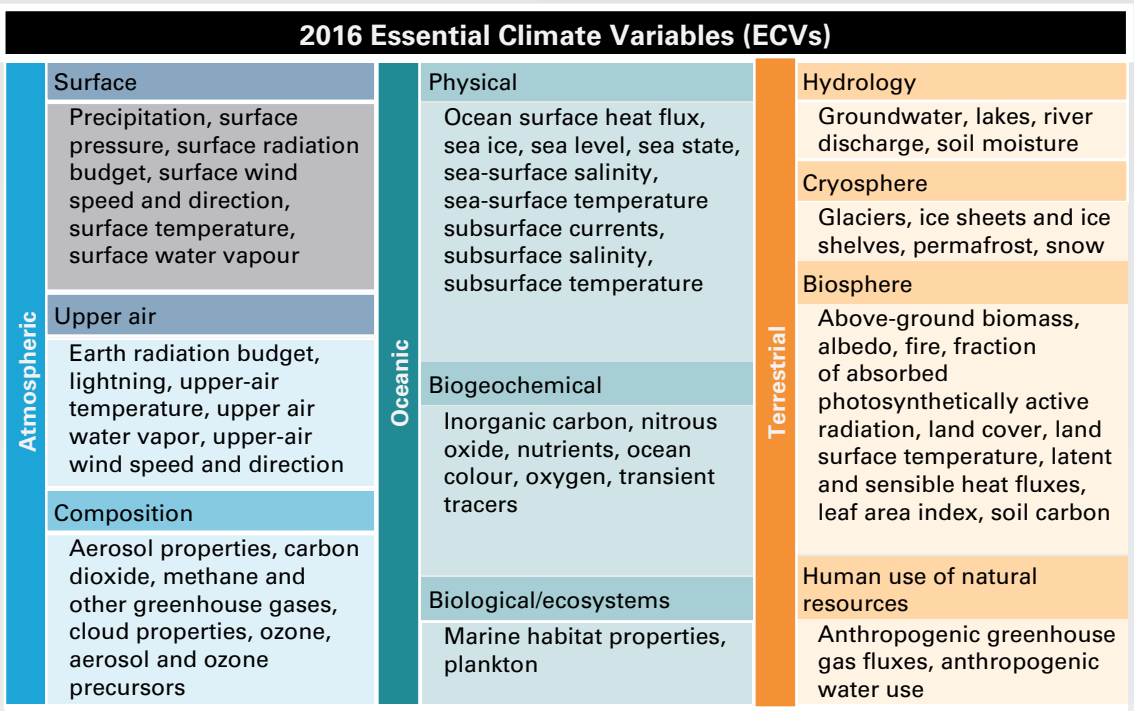

Figure 26. Essential Climate Variables (ECVs) identified by GCOS

Hydromet Development[a] are establishing a Systematic Observations Financing Facility (SOFF).

Complementing the observations of the physical and dynamic properties of the atmosphere, WMO's Global Atmospheric Watch (GAW) coordinates atmospheric composition measurements, ensuring that reliable and accurate data are obtained from measurements made by WMO Members, research institutions and/or agencies and other contributing networks.

Ocean observations of ocean physics, biogeochemistry, biology and ecosystems are coordinated through the Global Ocean Observing System (GOOS). The GOOS Observations Coordination Group (OCG) monitors the performance of these observations[b] and produces an annual Ocean Observing System Report Card. Ocean observations are generally made widely available to international users.

In the terrestrial domain, there is a wider group of observing networks. Hydrological observations are generally operated by NMHSs and coordinated through WMO. A number of specialized Global Terrestrial Networks (GTNs), for example, on hydrology, permafrost, glaciers, land use, and biomass, also report to GCOS. Data exchange agreements are generally less developed for the terrestrial networks, and many important observations are not made available to international users.

The Committee on Earth Observation Satellites/Coordination Group for Meteorological Satellites (CEOS/CGMS) Joint Working Group on Climate (WGClimate) bases the development of satellite observations for climate on the ECV requirements established by GCOS. It has produced an ECV Inventory that includes records for 766 climate data records for 33 ECVs covering 72 separate ECV products, with more planned. Satellite observations have some advantages – they have near-global coverage – but optical observations can be interrupted by clouds. Used with ground-based observations, either as complementary data sets, or for validation and calibration, they form an invaluable part of the global observing system.

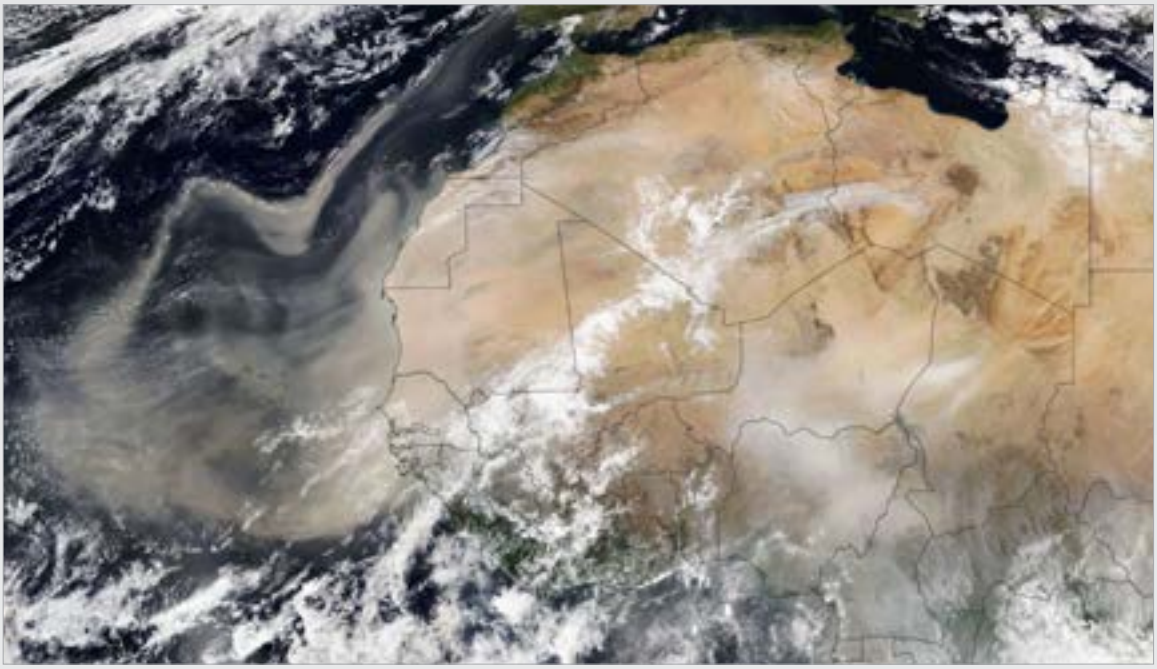

Figure 27. Dust storm in the Sahara Desert on 18 February 2021. This event led to widespread poor air quality for several days and followed another one, earlier in the month, that coated the snow in the Pyrenees and Alps and turned skies orange in some parts of Europe, including France, Germany and Switzerland.

[a] https://public.wmo.int/en/our-mandate/how-we-do-it/partnerships/wmo-office-of-development-partnerships

[b] https://www.ocean-ops.org/

Can sub-seasonal-to-seasonal predictions improve disaster risk preparedness for the South-east Asia region?

A review of the 20–26 September 2021 case study

Estelle De Coning[1], **Thea Turkington**[2], **Frederic Vitart**[3], **Andrew Robertson**[4], **Ryan Kang**[2], **Wee Leng Tan**[2]

[1] WMO

[2] National Environment Agency, Singapore

[3] S2S Co-chair, European Centre for Medium Range Weather Forecasts

[4] S2S Co-chair, International Research Institute for Climate and Society

South-east Asia (SEA) is in a prime location to benefit from sub-seasonal-to-seasonal (S2S) climate services, as a region with some of the highest skill at the S2S timescale. The Association of Southeast Asian Nations (ASEAN) Specialised Meteorological Centre (ASMC) and partners (UN ESCAP,[a] RIMES,[b] the AHA Centre[c]) are working to develop S2S products in SEA for disaster risk reduction under the S2S SEA Pilot Project, which is part of the S2S Prediction Project real-time pilot initiative undertaken by WMO, the World Weather Research Programme (WWRP) and the World Climate Research Programme (WCRP). The project aims to explore the usefulness of S2S predictions for disaster risk reduction.

Between 20 and 26 September 2021, more than 50 000 people[d] were affected by floods in the Philippines, and Sulawesi and eastern Borneo in Indonesia. During the same week, Tropical Cyclone *Dianmu* contributed to severe floods in parts of Viet Nam, Cambodia and Thailand, affecting more than 180 000 people.[e] Based on the S2S SEA Pilot Project's predictions, a small increased chance of extreme rainfall was forecasted for south-eastern Indonesia three weeks before the case study week. This evolved by the week before to a moderate increase in chance for Sulawesi, Maluku Islands and West Papua and expanded to small increase in chance over parts of Thailand, Lao People's Democratic Republic, Viet Nam, and southern Philippines, southern Sumatra, eastern Borneo and Java. This outlook was reported in the AHA Centre's weekly report[f] to national disaster management organizations and others, supporting the preparations for *Dianmu*[g] and other hazards along with subsequent weather forecasts, an example in the region of steps towards a seamless prediction approach.

These results are typical of the findings of the pilot project so far, where increased chance of extreme rainfall for the Maritime Continent is a good indicator three weeks beforehand that one or more hazardous events may occur in the general area. The indicator works less well for mainland South-east Asia though, where the outlooks often only predict an increased chance one week before. Increased probabilities of hazardous events signal an increased probability of disaster as well. While there may not always be an indication of impending hazardous events at the sub-seasonal timescale, the relatively small number of false alarms means that action can be taken at the sub-seasonal timescale, such as targeted monitoring of the development of the events and activating institutional processes earlier so that preparedness and response are more efficient.

---

[a] United Nations Economic and Social Commission for Asia and the Pacific: https://www.unescap.org/

[b] Regional Integrated Multi-Hazard Early Warning System for Africa and Asia: https://www.rimes.int/

[c] ASEAN Coordinating Centre for Humanitarian Assistance on Disaster Management: https://ahacentre.org/

[d] https://adinet.ahacentre.org

[e] https://adinet.ahacentre.org

[f] https://ahacentre.org/wp-content/uploads/2021/09/DWeek_37_13-19Sep2021.pdf

[g] https://ahacentre.org/flash-update/flash-update-no-01-tropical-depression-21w-twentyone-viet-nam-23-september-2021/

Data sets and methods

GREENHOUSE GAS DATA

Estimated concentrations from 1750 are used to represent pre-industrial conditions. Calculations assume a pre-industrial mole fraction of 278 ppm for CO_2, 722 ppb for CH_4 and 270 ppb for N_2O.

World Data Centre for Greenhouse Gases operated by Japan Meteorological Agency https://gaw.kishou.go.jp/.

World Meteorological Organization (WMO). *WMO Greenhouse Gas Bulletin – No. 17: The State of Greenhouse Gases in the Atmosphere Based on Global Observations through 2020.* Geneva, 2021.

World Ozone and Ultraviolet Radiation Data Centre operated by Environment and Climate Change Canada https://woudc.org/home.php.

GLOBAL TEMPERATURE DATA

GLOBAL MEAN TEMPERATURE TIME SERIES

The method for calculating global mean temperature anomalies relative to an 1850–1900 baseline has been updated since the *State of the Global Climate 2020* report. The method was updated to take advantage of the assessment made by Working Group I, in its contribution to the IPCC Sixth Assessment Report, of long-term change and its uncertainty. The new method also makes use of a wider range of shorter data sets that are routinely updated to provide an authoritative assessment of recent temperature changes.

In the 2020 report (and earlier reports), changes relative to the 1850–1900 baseline were based on the HadCRUT4 data set which was the only data set that extended back to 1850. Other data sets were offset to match the average of HadCRUT4 over the period 1880–1900 (NASA GISTEMP and NOAA GlobalTemp) or 1981–2010 (ERA5, JRA-55).

In 2021, the IPCC Sixth Assessment Report Working Group I assessed change from 1850–1900 to other periods based on an average of four data sets – HadCRUT5, Berkeley Earth, NOAA–Interim and Kadow et al. (2020) – which all extend back to 1850. They assessed uncertainty by considering the range from the four estimates, taken from the lower bound of the uncertainty range of the coolest data set to the upper bound of the uncertainty range of the warmest. By making use of four data sets that extend back to 1850, Working Group I was able to make a more comprehensive estimate of uncertainty.

As two of the four IPCC data sets are not regularly updated, in the present report the estimate made by the IPCC for the temperature change between 1850–1900 and 1981–2010 is combined with estimated changes between 1981–2010 and the current year from six data sets to calculate anomalies for 2021 relative to 1850–1900.

There is good, though not perfect, agreement between the six data sets on changes from 1981–2010 to the present, as this is a period with good observational coverage. The additional modest uncertainty from the spread of the six data sets is combined with that of the IPCC's estimate of the uncertainty in the change from 1850–1900 to 1981–2010.

More precisely, six data sets (cited below) were used in the calculation of global temperature. Global mean temperature anomalies were calculated relative to an 1850–1900 baseline using the following steps:

1. The starting point was a time series of global annual mean temperatures for each data set, as provided by the data providers. The anomalies were presented on different baselines.

2. For each data set, anomalies were calculated relative to the 1981–2010 average by subtracting the average for the period 1981–2010.

3. The amount 0.69 °C was added to each series, based on the estimated difference between 1850–1900 and 1981–2010, calculated using the method from the IPCC Sixth Assessment Report Working Group I (the number is provided in the caption for Figure 1.12 in that report).

4. The mean and standard deviation of the six estimates were calculated.

5. The uncertainty in the IPCC estimate was combined with the standard deviation, assuming the two are independent and assuming the IPCC uncertainty range (0.54 °C to 0.79 °C) is representative of a 90% confidence range (1.645 standard deviations).

The number quoted in this report for 2021 (1.11 ± 0.13 °C) was calculated in this way with 1.11 °C being the mean of the six estimates.

Annual temperature maps

The method for calculating the map of annual temperature anomalies has also been updated. In the 2020 report, a map showing anomalies relative to 1981–2010 from a single data set (ERA5) was used. While the map was based on a single data set, the accompanying assessment was based on all available data sets.

For the map of temperature anomalies for 2021, a median value of five of the data sets was used – HadCRUT5, ERA5, NOAAGlobalTemp, Berkeley Earth and GISTEMP – regridded to the spatial grid of the lowest resolution data sets (NOAAGlobalTemp and HadCRUT5 data sets), which are presented on a 5° latitude by 5° longitude grid. The median is used in preference to the mean to minimize the effect of potential outliers. The half-range of the data sets provides an indication of the uncertainty. The spread between the data sets is largest at high latitudes and in Central Africa, both regions with sparse data coverage.

The following six data sets were used:

Berkeley Earth – Rohde, R. A.; Hausfather, Z. The Berkeley Earth Land/Ocean Temperature Record. *Earth System Science Data* **2020**, *12*, 3469–3479. https://doi.org/10.5194/essd-12-3469-2020.

ERA5 — Hersbach, H.; Bell, B.; Berrisford, P. et al. The ERA5 global reanalysis. *Quarterly Journal of the Royal Meteorological Society* **2020**, *146* (730), 1999–2049. https://doi.org/10.1002/qj.3803.

GISTEMP v4 — GISTEMP Team, 2022: *GISS Surface Temperature Analysis (GISTEMP), version 4.* NASA Goddard Institute for Space Studies, https://data.giss.nasa.gov/gistemp/.
Lenssen, N.;Schmidt, G.; Hansen, J. et al. Improvements in the GISTEMP Uncertainty Model. *Journal of Geophysical Research: Atmospheres* **2019**, *124* (12): 6307–6326. https://doi.org/10.1029/2018JD029522.

HadCRUT.5.0.1.0 — Morice, C. P.; Kennedy, J. J.; Rayner, N. A. et al. An Updated Assessment of Near-Surface Temperature Change From 1850: The HadCRUT5 Data Set. *Journal of Geophysical Research: Atmospheres* **2021**, *126* (3), e2019JD032361. https://doi.org/10.1029/2019JD032361. HadCRUT.5.0.1.0 data were obtained from http://www.metoffice.gov.uk/hadobs/hadcrut5 on 24 October 2021 and are © British Crown Copyright, Met Office 2021, provided under an Open Government License, http://www.nationalarchives.gov.uk/doc/open-government-licence/version/3/.

JRA-55 — Kobayashi, S.; Ota, Y.; Harada, Y. et al. The JRA-55 Reanalysis: General Specifications and Basic Characteristics. *Journal of the Meteorological Society of Japan.* Ser. II **2015**, *93* (1), 5–48. https://doi.org/10.2151/jmsj.2015-001, https://www.jstage.jst.go.jp/article/jmsj/93/1/93_2015-001/_article.

NOAAGlobalTemp v5 — Zhang, H.-M., et al., NOAA Global Surface Temperature Dataset (NOAAGlobalTemp), Version 5.0. NOAA National Centers for Environmental Information. doi:10.7289/V5FN144H. Huang, B.; Menne, M. J.; Boyer, T. et al. Uncertainty Estimates for Sea Surface Temperature and Land Surface Air Temperature in NOAAGlobalTemp Version 5. *Journal of Climate* **2020**, *33* (4), 1351–1379. https://journals.ametsoc.org/view/journals/clim/33/4/jcli-d-19-0395.1.xml.

Figure 28.
(a) Near-surface air temperature anomalies for 2021 relative to the 1981–2010 average for the median of five data sets on a 5° grid. (b) Range of the five estimates; near surface temperature anomalies on the native resolution grid of the dataset for (c) HadCRUT5 (5° resolution), (d) ERA5 (0.25°), (e) Berkeley Earth (1°), (f) GISTEMP (2°) and (g) NOAAGlobalTemp (5°).

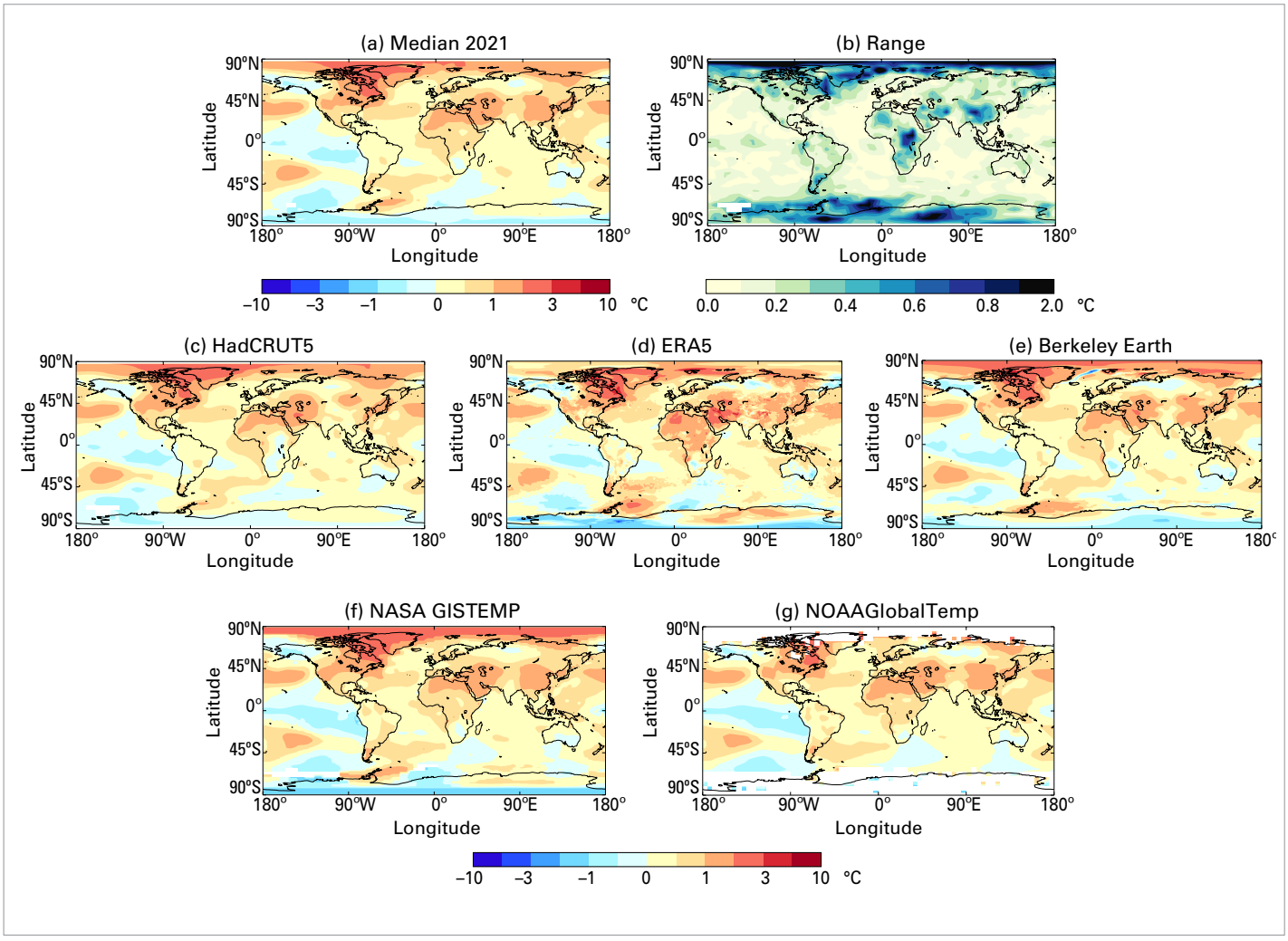

OCEAN HEAT CONTENT DATA

Data used for estimates up to 2021:

Cheng, L.; Trenberth, K. E.; Fasullo, J. et al. Improved estimates of ocean heat content from 1960 to 2015, *Science Advances* **2017**, *3* (3), e1601545. https://doi.org/10.1126/sciadv.1601545.

Ishii, M.; Fukuda, Y.; Hirahara, S. et al. Accuracy of Global Upper Ocean Heat Content Estimation Expected from Present Observational Data Sets. *SOLA* **2017**, *13*, 163–167. https://doi.org/10.2151/sola.2017-030.

Lyman, J. M.; Johnson, G. C. Estimating Global Ocean Heat Content Changes in the Upper 1800 m since 1950 and the Influence of Climatology Choice. *Journal of Climate* **2014**, *27* (5), 1945–1957. https://doi.org/10.1175/JCLI-D-12-00752.1.

von Schuckmann, K.; Le Traon, P.-Y. How well can we derive Global Ocean Indicators from Argo data? *Ocean Science* **2011**, *7* (6), 783–791. https://doi.org/10.5194/os-7-783-2011.

In addition, data used up to 2020:

Desbruyères, D. G.; Purkey, S. G.; McDonagh, E. L. et al. Deep and abyssal ocean warming from 35 years of repeat hydrography, *Geophysical Research Letters* **2016**, *43* (19), 310–356. https://doi.org/10.1002/2016GL070413.

Gaillard, F.; Reynaud, T.; Thierry, V. et al. In Situ–Based Reanalysis of the Global Ocean Temperature and Salinity with ISAS: Variability of the Heat Content and Steric Height, *Journal of Climate* **2016**, *29* (4), 1305–1323. https://doi.org/10.1175/JCLI-D-15-0028.1.

Hosoda, S.; Ohira, T.; Nakamura, T. A monthly mean dataset of global oceanic temperature and salinity derived from Argo float observations. *JAMSTEC Report of Research and Development* **2008**, *8*, 47–59. https://www.jstage.jst.go.jp/article/jamstecr/8/0/8_0_47/_article.

Kuusela M.; Stein, M. L. Locally stationary spatio-temporal interpolation of Argo profiling float data. *Proceedings of the Royal Society A* **2018**, *474*, 20180400. http://dx.doi.org/10.1098/rspa.2018.0400.

Levitus, S.; Antonov, J. I.; Boyer, T. P. et al. World Ocean heat content and thermosteric sea level change (0-2 000 m) 1955–2010. *Geophysical Research Letters* **2012**, *39* (10), L10603. https://doi.org/10.1029/2012GL051106.

Li, H.; Xu, F.; Zhou, W. et al. Development of a global gridded Argo data set with Barnes successive corrections, *Journal of Geophysical Research: Oceans* **2017**, *122* (2), 866–889, https://doi.org/10.1002/2016JC012285.

Roemmich, D.; Gilson, J. The 2004–2008 mean and annual cycle of temperature, salinity, and steric height in the global ocean from the Argo Program, *Progress in Oceanography* **2009**, *82* (2), 81–100. https://doi.org/10.1016/j.pocean.2009.03.004.

von Schuckmann, K.; Le Traon, P. -Y.; Smith, N. et al., Eds. Copernicus Marine Service Ocean State Report, *Journal of Operational Oceanography* **2018**, *11*, S1–S142. https://doi.org/10.1080/1755876X.2018.1489208.

SEA LEVEL DATA

GMSL from CNES/Aviso+ https://www.aviso.altimetry.fr/en/data/products/ocean-indicators-products/mean-sea-level/data-acces.html#c12195

MARINE HEATWAVE AND MARINE COLD SPELL DATA

Marine heatwaves (MHWs) are categorized as moderate when the sea-surface temperature (SST) is above the 90th percentile of the climatological distribution for five days or longer; the subsequent categories are defined with respect to the difference between the SST and the climatological distribution average: strong, severe or extreme, if that difference is,

respectively, more than two, three or four times the difference between the 90th percentile and the climatological distribution average (Hobday et al., 2018). Marine cold spell (MCS) categories are analogous, but are categorized with reference to sea-surface temperatures below the 10th percentile.

The baseline used for MHWs and MCSs is 1982–2011, which is shifted by one year from the standard normal period of 1981–2010 because the first full year of the satellite SST series on which it is based is 1982.

Hobday, A.J.; Oliver, E. C. J.; Sen Gupta, A. et al. Categorizing and naming marine heatwaves. *Oceanography* **2018**, *31* (2), 1–13. https://doi.org/10.5670/oceanog.2018.205.

NOAA OISST v2: Optimum Interpolation Sea Surface Temperature (OISST): Banzon, V.; Smith, T. M.; Chin, T. M. et al. A long-term record of blended satellite and in situ sea-surface temperature for climate monitoring, modeling and environmental studies. *Earth System Science Data* **2016**, *8* (1), 165–176. https://doi.org/10.5194/essd-8-165-2016.

GLACIER MASS BALANCE DATA

Glacier mass balance data for the global network of reference glaciers are available from the World Glacier Monitoring Service (WGMS), https://www.wgms.ch. Data for the 2020–2021 mass balance year are preliminary, and are based on a subset of 32 (out of a total of ~42) WGMS reference glaciers. The glacier mass balance data for western Canada are based on multi-year, bi-annual (April and September) repeat LiDAR surveys conducted by Brian Menounos at the University of Northern British Columbia, Canada, as described in Pelto et al. (2019).

Pelto, B. M.; Menounos, B.; Marshall, S. J. Multi-year evaluation of airborne geodetic surveys to estimate seasonal mass balance, Columbia and Rocky Mountains, Canada. *The Cryosphere* **2019**, *13* (6), 1709–1727. https://doi.org/10.5194/tc-13-1709-2019.

Hugonnet, R.; McNabb, R.; Berthier, E. et al. Accelerated global glacier mass loss in the early twenty-first century. *Nature* **2021**, *592*, 726–731. https://doi.org/10.1038/s41586-021-03436-z.

GREENLAND AND ANTARCTIC ICE SHEET DATA

Greenland ice sheet mass balance data are reported from three sources. Modelled changes in surface mass balance and total mass balance from 1985 to 2021 are based on the average of three regional climate and mass balance models, described in Mankoff et al. (2021). An alternative estimate of 2021 mass balance is given in the NOAA Arctic Report Card (Moon et al., 2021), based on satellite observations of melt area and surface mass balance models driven by the PROMICE surface weather station network. Satellite gravity data of total ice sheet mass balance from the GRACE and GRACE-FO missions are available from Wiese et al. (2019, updated to 2021). These data are available for both the Greenland and Antarctic ice sheets.

Mankoff, K. D.; Fettweis, X.; Langen, P. L. et al. Greenland ice sheet mass balance from 1840 through next week. *Earth System Science Data* **2021**, 13 (10), 5001–5025. https://doi.org/10.5194/essd-13-5001-2021.

Moon, T. A.; Tedesco, M.; Box, J. E. et al. Greenland Ice Sheet. In *Arctic Report Card 2021*; Moon, T. A.; Druckenmiller, M. L.; Thoman, R. L., Eds.; National Oceanic and Atmospheric Administration, 2021. https://doi.org/10.25923/546g-ms61.

Wiese, D.N.; Yuan, D. -N; Boening, C. et al. 2019. JPL GRACE and GRACE-FO Mascon Ocean, Ice, and Hydrology Equivalent Water Height RL06M CRI Filtered Version 2.0, Ver. 2.0, PO.DAAC, CA, USA. http://dx.doi.org/10.5067/TEMSC-3MJ62.

SNOW DATA

Snow data and monthly anomaly time series charts are available at: https://climate.rutgers.edu/snowcover/files/wmo/rutgers-nh-sce-anomalies-2020-21-data.xlsx

SEA-ICE DATA

The sea ice section uses data from the EUMETSAT OSI SAF Sea Ice Index v2.1 (OSI-SAF, based on Lavergne et al., 2019) and the NSIDC v3 Sea Ice Index (Fetterer et al., 2017). Sea-ice concentrations are estimated from microwave radiances measured from satellites. Sea-ice extent is calculated as the area of ocean grid cells where the sea-ice concentration exceeds 15%. Although there are relatively large differences in the absolute extent between data sets, they agree well on the year-to-year changes and the trends. In this report, NSIDC data are reported for absolute extents (for example, "18.95 million km^2") for consistency with earlier reports, while rankings are reported for both data sets.

EUMETSAT Ocean and Sea Ice Satellite Application Facility, Sea ice index 1979-onwards (v2.1, 2020), OSI-420, Data extracted from OSI SAF FTP server: 1979–2020, Northern and Southern Hemisphere. https://osi-saf.eumetsat.int/products/osi-420.

Fetterer, F.; Knowles, K.; Meier, W. N. et al. 2017, updated daily. *Sea Ice Index, Version 3.* Boulder, Colorado USA. National Snow and Ice Data Center (NSIDC). https://doi.org/10.7265/N5K072F8.

Lavergne, T.; Sørensen, A. M.; Kern, S. et al. Version 2 of the EUMETSAT OSI SAF and ESA CCI sea-ice concentration climate data records. *The Cryosphere* **2019**, *13* (1), 49–78. https://doi.org/10.5194/tc-13-49-2019.

PERMAFROST DATA

Noetzli, J.; Christiansen, H. H.; Hrbáček, F. et al. Global Climate Permafrost Thermal State. In *State of the Climate in 2020*; Dunn, R. J., Aldred, H., F., Gobron, N. Eds.; *Bulletin of the American Meteorological Society* **2021**, *102* (8); S42–S44. https://doi.org/10.1175/BAMS-D-21-0098.1.

Smith, S. L.; Romanovsky, V. E.; Isaksen, K. et al. Permafrost. In *State of the Climate in 2020*; Druckenmiller, M. L., Moon, T., Thoman, R., Eds.; *Bulletin of the American Meteorological Society*, **2021**, *102* (8); S293–S297. https://doi.org/10.1175/BAMS-D-21-0086.1.

PRECIPITATION DATA

These Global Precipitation Climatology Centre (GPCC) data sets were used in the analysis:

- First Guess Monthly, doi: 10.5676/DWD_GPCC/FG_M_100.
- Monitoring Product (Version 2020), doi: 10.5676/DWD_GPCC/MP_M_V2020_100.
- Full Data Monthly (Version 2020), doi: 10.5676/DWD_GPCC/FD_M_V2020_100.
- First Guess Daily, doi: 10.5676/DWD_GPCC/FG_D_100.
- Full Data Daily (Version 2020), doi: 10.5676/DWD_GPCC/FD_D_V2020_100.

List of contributors

CONTRIBUTING MEMBERS AND TERRITORIES

Algeria, Andorra, Argentina, Armenia, Australia, Austria, Bahrain, Barbados, Belarus, Belgium, Belize, Bosnia and Herzegovina, Botswana, British Caribbean Territories, Bulgaria, Burkina Faso, Cameroon, Canada, Chile, China, Colombia, Croatia, Cyprus, Czech Republic, Denmark, Egypt, Estonia, Finland, France, Gambia, Georgia, Germany, Greece, Grenada, Guinea, Guinea-Bissau, Hong Kong, China; Hungary, India, Islamic Republic of Iran, Ireland, Israel, Italy, Japan, Jordan, Kazakhstan, Kenya, Latvia, Liberia, Libya, Lithuania, Luxembourg, Macao, China; Madagascar, Mali, Malta, Mauritius, Morocco, New Zealand, Niger, Nigeria, North Macedonia, Norway, Pakistan, Peru, Philippines, Poland, Portugal, Republic of Moldova, Romania, Russian Federation, Rwanda, Saint Vincent and the Grenadines, Saudi Arabia, Senegal, Serbia, Slovakia, Slovenia, South Africa, Spain, Saint Kitts and Nevis, Sudan, Sweden, Switzerland, Syrian Arab Republic, Thailand, Netherlands, Togo, Trinidad and Tobago, Tunisia, Turkey, Ukraine, United Kingdom, United Republic of Tanzania, United States of America, Uruguay, Uzbekistan, Zimbabwe

INSTITUTIONAL CONTRIBUTORS

ARC Centre of Excellence for Climate Extremes, University of Tasmania, Australia; Birmingham Institute of Forest Research, Birmingham University, UK; British Antarctic Survey (BAS); Bureau of Meteorology (BoM), Australia; Carbon Portal, Lund University, Sweden; Centre National d'Études Spatiales, CNES, France; Mercator Ocean international, France; Observatoire Midi-Pyrénées (OMP), France; IFREMER, France; University of Brest, France; Centre National de la Recherche Scientifique, (CNRS), France; Institut de Recherche pour le Développement (IRD), France; Laboratoire d'Océanographie Physique et Spatiale (LOPS), France; Laboratoire d'Etudes en Géophysique et Océanographie Spatiales (LEGOS), France; Institut Universitaire Européen de la Mer (IUEM), France; CELAD, France; Sorbonne Université, France; Laboratoire d'Océanographie de Villefranche, France; Center for Ocean Mega-Science, Chinese Academy of Sciences; Copernicus Climate Change Service (C3S); CSIRO Oceans and Atmosphere, Australia; Danmarks Meteorologiske Institut (DMI); Global Precipitation Climatology Centre, Deutscher Wetterdienst (GPCC, DWD); Environment and Climate Change Canada (ECCC); ETH Zürich, Switzerland; European Centre for Medium Range Weather Forecasts (ECMWF); George Washington University, USA; Hong Kong Observatory; Institute of Atmospheric Physics, Chinese Academy of Sciences (IAP, CAS); Japan Marine-Earth Science and Technology (JAMSTEC); Joint Institute for Marine and Atmospheric Research, University of Hawai'i (JIMAR), USA; Met Office Hadley Centre, UK; Department of Atmosphere, Ocean and Earth System Modeling Research, Meteorological Research Institute, Japan; National Environment Agency, Singapore (NEA); National Oceanographic and Atmosphere Administration, National Centers for Environmental Information (NOAA NCEI), USA; NOAA, Pacific Marine Environmental Laboratory (NOAA PMEL), USA; National Oceanography Centre (NOC), UK; Natural Resources Canada; Norwegian Meteorological Institute; Rutgers University, USA; Scripps Institution of Oceanography, USA; Tokyo Climate Center, Japan Meteorological Agency (TCC, JMA); Universidade Federal do Rio de Janeiro, Brazil; University of Exeter, UK; University of Victoria, Canada; Woods Hole Oceanographic Institution, USA; World Climate Research Programme (WCRP); World Data Centre for Greenhouse Gases (WDCGG)

UNITED NATIONS AGENCIES

United Nations Office for Disaster Risk Reduction (UNDRR), United Nations Environment Programme (UNEP), Food and Agriculture Organization of the United Nations (FAO), United Nations High Commissioner for Refugees (UNHCR), International Organization for Migration (IOM), World Food Programme (WFP), Intergovernmental Oceanographic Commission – United Nations (IOC-UNESCO)

INDIVIDUAL CONTRIBUTORS

Signe Aaboe (Norwegian Meteorological Institute), Jorge Alvar-Beltrán (FAO), Omar Baddour (WMO publication coordinator), Jessica Blunden (NOAA NCEI), Tim Boyer (NOAA NCEI), Anny Cazenave (LEGOS CNES and OMP), Lijing Cheng (IAP; Center for Ocean Mega-Science, Chinese Academy of Sciences), Louis Clement (National Oceanography Centre), Kyle Clem (University of Victoria), Estelle De Coning (WMO), Damien Desbruyères (IFREMER, CNRS, IRD, Laboratoire d'Océanographie Physique et Spatiale), Maxx Dilley (WMO), Robert Dunn (Met Office Hadley Centre), Simon Eggleston (WMO/GCOS), Thomas Estilow (Rutgers University), Florence Geoffroy (UNHCR), Donata Giglio (University of Colorado), Nathan Gillett (ECCC), John Gilson (Scripps Institution of Oceanography, University of California), Loretta Hieber Girardet (UNDRR), Atsushi Goto (TCC, JMA), Yvan Gouzenes (LEGOS and OMP), Stephan Gruber (Carleton University), Debbie Hemming (Met Office Hadley Centre, Birmingham Institute of Forest Research), Ana Heureux (FAO), Shigeki Hosoda (JAMSTEC), Matthias Huss (ETH Zürich), Kirsten Isensee (IOC UNESCO), Gregory C. Johnson (NOAA, PMEL), Ryan Kang (NEA), Maarten Kappelle (UNEP), John Kennedy (lead author, Met Office Hadley Centre), Valentina Khan (Hydrometeorological Research Center of the Russian Federation), Rachel Killick (Met Office Hadley Centre), Brian A. King (NOC), Animesh Kumar (UNDRR), Mikael Kuusela (Carnegie Mellon University), Gernot Laganda (WFP), Thomas Lavergne (Norwegian Meteorological Institute), Yuehua Li (University of New South Wales), Renata Libonati (Universidade Federal do Rio de Janeiro), Juerg Luterbacher (WMO), John Lyman (NOAA, PMEL), Shawn Marshall (ECCC and University of Calgary), Jesse Mason (WFP), Brian Menounos (University of Northern British Columbia), Audrey Minière (Mercator Ocean international), Maeva Monier (CELAD/Mercator Ocean international), Colin Morice (Met Office Hadley Centre), Lev Neretin (FAO), Stoyka Netcheva (WMO), Rodica Nitu (WMO), Jeannette Noetzli, (Institute for Snow and Avalanche Research), Ben Pelto (University of Northern British Columbia), Claire Ransom (WMO), Andrew Robertson (S2S co-chair, IRI), David Robinson (Rutgers University), Dean Roemmich (Scripps Institution of Oceanography), Kanako Sato (JAMSTEC), Katsunari Sato (JMA), Yousuke Sawa (JMA, WDCGG), Robert W. Schlegel (Sorbonne Université, CNRS, Laboratoire d'Océanographie de Villefranche), Katherina Schoo (IOC UNESCO), Karina von Schuckmann (Mercator Ocean international), Rahul Sengupta (UNDRR), Fumi Sezaki (TCC, JMA), José Álvaro Silva (WMO), Sharon Smith (Natural Resources Canada), Michael Sparrow (WCRP), Martin Stendel (DMI), Peter Stott (Met Office Hadley Centre, University of Exeter), Dmitry Streletskiy (George Washington University), Toshio Suga (JAMSTEC, Tohoku University), Tanguy Szekely (OceanScope), Wee Leng Tan (NEA), Oksana Tarasova (WMO), Blair Trewin (BoM), Thea Turkington (NEA, Singapore), John Turner (BAS), Freja Vamborg (ECMWF), Alex Vermeulen (Carbon Portal, Lund University), Frederic Vitart (S2S co-chair, ECMWF), Ying Wang (UNEP), Michelle Yonetani (UNHCR), Zhiwei Zhu (Nanjing University of Information Science and Technology), Markus Ziese (DWD)

UN environment programme

Food and Agriculture Organization of the United Nations

UNHCR The UN Refugee Agency

IOM UN MIGRATION

UNDRR UN Office for Disaster Risk Reduction

WFP World Food Programme

United Nations Educational, Scientific and Cultural Organization

Intergovernmental Oceanographic Commission

For more information, please contact:

World Meteorological Organization

7 bis, avenue de la Paix – P.O. Box 2300 – CH 1211 Geneva 2 – Switzerland

Strategic Communications Office
Cabinet Office of the Secretary-General

Tel: +41 (0) 22 730 83 14

Email: communications@wmo.int

public.wmo.int

JN 22229